space holder for signature page

A Search for
Chargino-Neutralino Production
at the Fermilab Tevatron Collider

by

Benn Tannenbaum

B.A., Physics, Grinnell College, 1990
M.S., Physics, Michigan State University, 1993

Doctor of Philosophy
Physics

December, 1997

List of Tables

Chapter 1

Introduction

phys·ics (fiz'iks) *n.* the science dealing with the properties, changes, interaction, etc. of matter and energy in which energy is considered to be continuous (**classical physics**), including electricity, heat, optics, mechanics, etc., and now also dealing with the atomic scale of nature in which energy is considered to be discrete (**quantum physics**), including such branches as atomic, nuclear, and solid-state physics [1]

Particle, or high energy, physics, is the study of quarks and leptons and their interactions. Just as cells compose living organisms, atoms compose molecules and protons, neutrons and electrons compose atoms, the various quarks compose neutrons and protons. The theory describing the quarks and leptons is known as the Standard Model. Just as Mendeleev's periodic table organizes the elements into columns and rows according to composition, the Standard Model groups the quarks and leptons into families by charge and mass. Tables 1.1 and 1.2 list the known particles. In addition to the quarks and leptons, there are particles which mediate the four known forces: the photon (γ) mediates the electromagnetic force, the $W^{\pm}$ and Z^0 mediate the the weak force, the gluon (g) mediates the strong force and the graviton mediates gravity[1].

The Standard Model is the combination of two other theories, the electroweak theory of Weinberg, Salam and Glashow (WSG) , and Quantum Chromodynamics (QCD). QED, the part of the electroweak theory that describes the interactions of electrons, muons and taus with photons, is one of the most successful theories in all of science. The remainder of the WSG theory describes the charged and neutral weak interactions. QCD describes the interaction of quarks via the strong force.

---

[1]The graviton is a postulated particle which has not yet been seen. Since gravity is significantly weaker than the other three forces, its mediator is much more difficult to detect.

Table 1.1: The fermionic particles of the Standard Model. The quarks in the top row have charge $+\frac{2}{3}$ times the electron charge, while the quarks in the second row have charge $-\frac{1}{3}$ times the electron charge. All of the leptons in the third row have charge -1 and all of the neutrinos are neutral. The quarks can interact via any of the four forces, the leptons via all but the strong force, and the neutrinos can interact via the weak and gravitational forces. All particles have been observed experimentally except the ν_τ.

quarks	up	u	charm	c	top	t
	down	d	strange	s	bottom	b
leptons	electron	e	muon	μ	tau	τ
	electron neutrino	ν_e	muon neutrino	ν_μ	tau neutrino	ν_τ

Table 1.2: The bosonic particles of the Standard Model. All bosons have been observed except the graviton (G).

Boson	Force Mediated
photon (γ)	Electromagnetic
$W^\pm$	Charged Weak
Z^0	Neutral Weak
gluon (g)	Strong
graviton (G)	Gravity

Overall, the Standard Model has been very successful. However, it leaves many questions unanswered. Many theories have been proposed to answer these questions. This dissertation is a search for evidence of physics beyond the Standard Model. Chapter 2 describes the theory examined, Chapter 3 the apparatus used, Chapter 4 the analysis techniques and Chapter 5 the limits reached. Chapter 6 draws some conclusions.

Chapter 2

Theory and Motivation

The Standard Model has proven to be a very effective low energy[1] theory– a theory that is accurate in the currently accessible energy spectrum. Its two major components, Quantum Chromodynamics (QCD) [2] and the electroweak theory of Weinberg, Salam and Glashow [3], predict the interaction of quarks, leptons and the gauge bosons well. The theory is so successful that the existence of the top quark was accepted long before its discovery. The production cross sections (σ) and decay branching ratios for the various interactions are accurately predicted. In fact, there is very little experimental evidence for any physics beyond the Standard Model.

There are, however, many unanswered questions about the Standard Model and the universe in which we live. Many of these questions deal with mass. For example,

- Depending on the parameterization used, either the masses of all of the quarks and leptons or the couplings of the leptons and quarks to the vacuum expectation value of the Higgs boson are free. Why? Why does the Standard Model not predict the masses of the particles? Why are there three generations?

- The mass of the top quark is 176 GeV/c^2 [4]. The mass of the other quark in its isospin doublet, the bottom quark, is $\simeq 4.5$ GeV/c^2. The ratio of the top to bottom mass is almost 40! The ratio of charm to strange mass is $\simeq 7.5$ and the ratio of up to down mass is $\simeq 0.5$ [5]. Why is the top quark so massive, and why is it so much more massive than its isospin partner?

- The mediator of the electromagnetic force, the photon, and the mediator of the strong force, the gluon, are both massless. Why are the mediators of the weak force, the $W^\pm$ and the Z^0,

---

[1] "Low energy", of course, depends on the beholder. For this dissertation low energy implies energies of the TeV (10^{12} eV) scale or less.
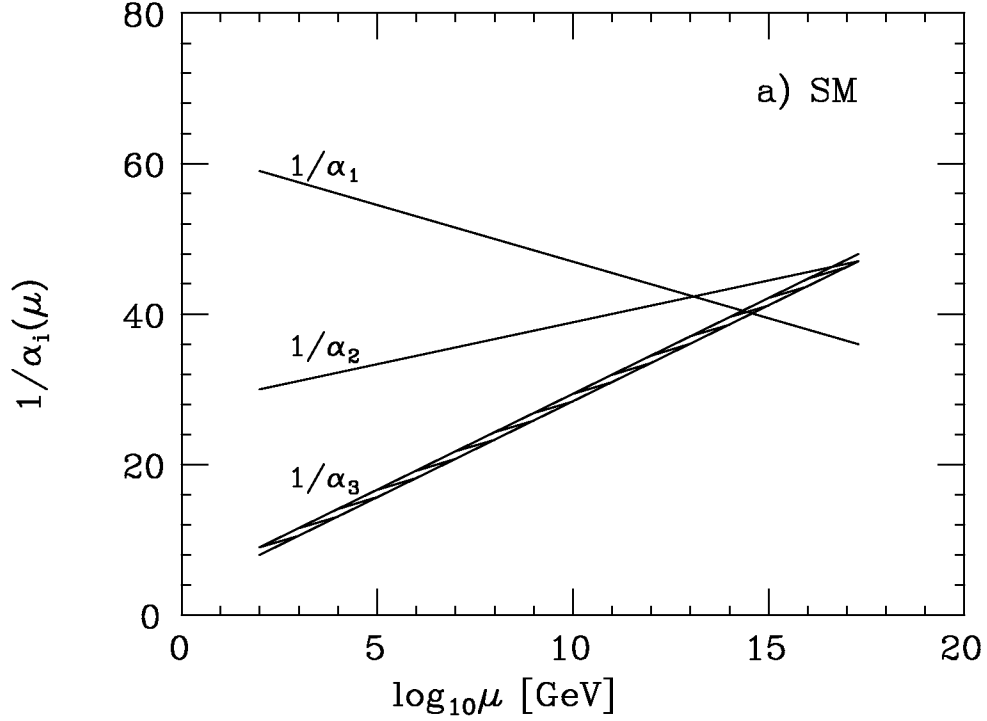
Figure 2.1: The extrapolation of the Standard Model gauge couplings to very high energies. α_1 is the $SU(1)_{\text{hypercharge}}$ coupling constant, α_2 is the $SU(2)_{\text{weak}}$ coupling constant and α_3 is the $SU(3)_{\text{strong}}$ coupling constant. Adapted from [6].

massive? Why are they so massive? What sets the scale for electroweak symmetry breaking?

- The Standard Model does not need to include the Higgs boson. The Higgs mechanism is inserted *ad hoc* to provide a mechanism for electroweak symmetry breaking and further gives masses to the quarks and leptons. It is a mechanism that works, but it may not be the right one.

- Early physics research led to the realization that electricity and magnetism are different aspects of the same force. The prediction and subsequent discovery of the $W^{\pm}$ and Z^0 led to the realization that, above certain energies, the electromagnetic and weak forces are different aspects of the same force. However, the SM-based extrapolation of precise measurements at LEP clearly show (Figure 2.1) that the strong, electromagnetic and weak forces do not unify at any energy. They do approach a common value, but do not meet at a point. We currently believe that there must exist a theory of everything in which all the forces unify: a Grand Unified Theory (GUT). This is not possible within the framework of the SM.

- Grand Unified Theories require a scalar particle to provide the mechanism for breaking the

symmetry at the Grand Unified scale. However, its mass (on the order of the GUT scale: 10^{16} GeV/c^2) must be specified to great accuracy to provide for the physics at the weak scale. This is known as the fine tuning or hierarchy problem.

- Current measurements of the rate of rotation of some distant galaxies do not match with the visible mass. This appears to imply that there must be some additional, unseen, mass that allows these galaxies to rotate as quickly as they do.

All of these facts lead us to believe that there must be a theory beyond the Standard Model. Many have been proposed, such as quark compositness (or technicolor), left-right symmetric models and SUperSYmmetry (SUSY). Each of these models solves some or all of the above problems and each has their own set of strengths and weaknesses. A weakness common to all of them is a total lack of experimental evidence for any of them. At present SUSY is a very popular theory and is generating interest in both the theoretical and experimental communities.

In the remainder of this Chapter, I will briefly describe the basic principles of SUSY and why SUSY is of interest, describe the particle spectrum, discuss signals and backgrounds germane to this analysis, and discuss naturalness.

2.1 Overview of Supersymmetry

The theory behind SUSY is complex and a complete introduction is beyond the scope of this dissertation. A quick search of the SPIRES data base [7] lists over 7,000 papers on the topic of SUSY. A good starting point for further reading can be found in Refs. [8, 9, 10] and the references within. However, an introduction is appropriate, especially as there are few references that are comprehensible to the experimentalist at first reading: the transition from the SUSY Lagrangian to the constrained model we use is difficult.

2.1.1 The Minimal Supersymmetric Model

In the SM, each particle is described by several quantum numbers: spin, charge, mass, isospin, etc. All quarks and leptons are fermions, meaning they have half-integral spin. The mediators of the various forces are all bosons and thus have integral spin. SUSY supposes that for each particle with an integral spin, there exists a particle with the same charge, isospin, etc., but with half-integral spin. Likewise, for each half-integral spin particle there exists an integral spin partner. The names of these new particles are related to the names of the original particles: the scalar partners to the fermions are the *s*fermions (such as *s*leptons and *s*quarks) and the partners to the gauge bosons gain an *-ino* (such as Higgs*ino*). The Minimal Supersymmetric Model (MSSM) gives each particle a superpartner and requires two Higgs doublets and their superpartners. This more than doubles the

particle spectrum and greatly increases the number of free parameters to over 100. A few reasonable assumptions (described in the following sections) reduce the number of free parameters to six[2].

The second Higgs doublet is necessary to cancel anomalies [8]. The second doublet also allows one to use one doublet to give masses to the up-type quarks and the neutrinos, and the other doublet to give masses to the down-type quarks and the charged leptons.

2.1.2 Reducing the parameter space

The MSSM in its purest form has over 100 free parameters. One of my complaints about the SM was that it had too many free parameters. By adding SUSY I seem to have made the problem worse! To reduce the number of free parameters we can make certain model assumptions that are either based on observed or desired physics. The resulting model is unfortunately also sometimes known as the MSSM. I shall refer to it as the SiMSSM (Supergravity-inspired MSSM).

Grand Unified Theories (GUTs)

If we require unification of the coupling constants at the GUT scale ("the GUT hypothesis" provided by supergravity [11]), we are led to the following relationships:

$$\left. \begin{array}{rcl} M_{\widetilde{W}} & = & \dfrac{\alpha_2}{\alpha_3} M_{\tilde{g}} \\[2mm] M_{\widetilde{B}} & = & \dfrac{5\alpha_1}{3\alpha_2} M_{\widetilde{W}} \end{array} \right\} \tag{2.1}$$

where $\widetilde{W}$ and $\widetilde{B}$ are the weak eigenstates of the SUSY partners to the SM electroweak gauge bosons and the α_i are the hypercharge, weak isospin, and strong coupling constants at the appropriate scale, respectively. At the Tevatron scale ($\sqrt{s} = 1.8$ TeV) $\alpha_1 = 0.00781$, $\alpha_2 = 0.03397$ and $\alpha_3 = 0.120$ [5]. The 5/3 arises from the use of SU(5) as the unifying group. SU(5) is the smallest group that can unify U(1)×SU(@)×SU(3) [12]. Equation 2.1 causes $M_{\widetilde{W}}$ and $M_{\widetilde{B}}$ to be functions of only $M_{\tilde{g}}$, since the α_i are well measured quantities.

Renormalization Group Equations

We relate the slepton ($\widetilde{\ell}$) and sneutrino ($\widetilde{\nu}$) masses to the squark ($\tilde{q}$) and gluino ($\tilde{g}$) masses through the Renormalization Group Equations as inspired by supergravity models [13]. These relations are made at the GUT scale and must be rescaled (or renormalized) to the TeV scale where we currently

---

[2]See *e.g.* Ref. [10] for more details.

work:

$$\begin{aligned}
M_{\tilde{\ell}_L}^2 &= M_{\tilde{q}}^2 - 0.73 M_{\tilde{g}}^2 - 0.27 M_Z^2 \cos 2\beta \\
M_{\tilde{\ell}_R}^2 &= M_{\tilde{q}}^2 - 0.78 M_{\tilde{g}}^2 - 0.23 M_Z^2 \cos 2\beta \\
M_{\tilde{\nu}_L}^2 &= M_{\tilde{q}}^2 - 0.73 M_{\tilde{g}}^2 + 0.5 M_Z^2 \cos 2\beta
\end{aligned} \right\} \tag{2.2}$$

We assume the masses of all generations of each type of slepton ($\widetilde{\ell}_L$, $\widetilde{\ell}_R$ and $\widetilde{\nu}_L$) to be degenerate. These relations are calculated by averaging similar equations which do not assume degenerate generations [14]. This is acceptable since this analysis is largely affected by the masses of only the first generation squarks. The masses of the $\widetilde{\ell}$s depend mainly on the difference in mass of the $\tilde{q}$s and $\tilde{g}$s.

R-parity and the Lightest Supersymmetric Partner

The MSSM allows the imposition of a global symmetry, so we assign each particle and superparticle a new multiplicative quantum number, $R \equiv (-)^{B+L+2S}$ where B is the baryon number, L is the lepton number and S is the spin of the particle. Thus, SM particles have $R = +1$ and SUSY particles have $R = -1$. If we require R-parity to be conserved, we then require the creation of SUSY particles in pairs. By requiring SUSY particles to be created in pairs, we must then have a lightest sparticle (LSP) that is stable. An electrically or color charged LSP causes many problems [15] so the LSP is generally assumed to be the lightest neutralino ($\tilde{\chi}_1^0$). Experimentally, the LSP can be thought of as a heavy neutrino: it will manifest itself as missing energy. The LSP is also an excellent candidate for cold dark matter [16].

Remaining free parameters

To continue reducing the number of free parameters, we further assume that the first and second generation squarks are degenerate in mass. This is an acceptable assumption, as this analysis is mainly affected by the masses of the first generation squarks. After making all the above assumptions, we are left with only a handful of free parameters: $\tan\beta$, μ, $M_{\tilde{g}}$, $M_{\tilde{q}}$, A_T, and M_{H_A}. $\tan\beta$ is the ratio of the vacuum expectation values for the two Higgs doublets:

$$\tan\beta = (\langle H_2 \rangle / \langle H_1 \rangle) \tag{2.3}$$

$$v^2 = \langle H_1 \rangle^2 + \langle H_2 \rangle^2 \tag{2.4}$$

where $v = 246$ GeV is fixed by the $W^\pm$ mass. $\tan\beta$ serves mainly to control the Higgsino vs gaugino content of the charginos ($\tilde{\chi}_i^\pm$) and neutralinos ($\tilde{\chi}_i^0$) (see Section 2.2 for explanations of these particles). μ is the un-mixed Higgsino mass (sometimes referred to as the supersymmetry-conserving Higgs mass parameter) and sets the scale for SUSY. It also has an effect on the Higgsino vs gaugino content of the charginos and neutralinos. $M_{\tilde{g}}$ is the gluino mass and $M_{\tilde{q}}$ is the common

squark mass. A_T is the Higgs-squark-squark trilinear interaction for the top squark, and M_{H_A} is the mass of the pseudoscalar Higgs boson.

This analysis, which is a search for $\tilde{\chi}_1^\pm \tilde{\chi}_2^0$ production, is obviously concerned with their masses and couplings. As will be seen below, once we know the masses and couplings of $\tilde{\chi}_1^\pm$, $\tilde{\chi}_1^0$, $\tilde{\chi}_2^0$ and sleptons (and to some degree, the squarks), we can begin to set limits on the production of SUSY particles.

In the regime where $M_{Z^0} \ll |M_i \pm \mu|$ the masses of $\tilde{\chi}_1^\pm$, $\tilde{\chi}_1^0$ and $\tilde{\chi}_2^0$ are functions solely of μ, $\tan\beta$ and the mass of the gluino [17]:

$$m_{\chi_1^\pm} = M_{\widetilde{W}} - \frac{M_W^2 \left(M_{\widetilde{W}} + \mu\sin 2\beta \right)}{\mu^2 - M_{\widetilde{W}}^2} \tag{2.5}$$

$$m_{\chi_1^0} = M_{\widetilde{B}} + \sin^2\theta_W \frac{m_Z^2 (M_{\widetilde{B}} + \mu\sin 2\beta)}{(M_{\widetilde{B}}^2 - \mu^2)}$$

$$m_{\chi_2^0} = M_{\widetilde{W}} + \cos^2\theta_W \frac{m_Z^2 (M_{\widetilde{W}} + \mu\sin 2\beta)}{(M_{\widetilde{W}}^2 - \mu^2)} \tag{2.6}$$

where $M_{\widetilde{B}}$ and $M_{\widetilde{W}}$ are determined using Equation 2.1, θ_W ($\sin^2\theta_W = 0.234$) is the Weinberg mixing angle, M_W ($= 80.33$ GeV/c^2) is the $W^\pm$ mass and M_Z ($= 91.187$ GeV/c^2) is the Z^0 mass. The slepton masses are determined by Equations 2.2 and are functions of the squark and gluino masses and $\tan\beta$. Figures 2.2-2.10 show $M_{\tilde{\chi}_1^\pm}$, $M_{\tilde{\chi}_1^0}$ and $M_{\tilde{\chi}_2^0}$ as functions of $\tan\beta$, μ and $M_{\tilde{g}}$. Note that the masses of each particle is primarily a function of $M_{\tilde{g}}$, and not of either $\tan\beta$ or μ.

The Higgsino and gaugino content of the neutralinos can be determined using [17]:

$$\begin{pmatrix} \tilde{\chi}_1^0 \\ \tilde{\chi}_2^0 \\ \tilde{\chi}_3^0 \\ \tilde{\chi}_4^0 \end{pmatrix} = \begin{pmatrix} 1 & 0 & \frac{s_\theta(s_\beta+c_\beta)m_Z}{\sqrt{2}(\mu-M_{\widetilde{B}})} & \frac{s_\theta(s_\beta-c_\beta)m_Z}{\sqrt{2}(\mu+M_{\widetilde{B}})} \\ 0 & 1 & -\frac{c_\theta(s_\beta+c_\beta)m_Z}{\sqrt{2}(\mu-M_{\widetilde{W}})} & -\frac{c_\theta(s_\beta-c_\beta)m_Z}{\sqrt{2}(\mu+M_{\widetilde{W}})} \\ -\frac{s_\theta(s_\beta+c_\beta)m_Z}{\sqrt{2}(\mu-M_{\widetilde{B}})} & \frac{c_\theta(s_\beta+c_\beta)m_Z}{\sqrt{2}(\mu-M_{\widetilde{W}})} & 1 & 0 \\ -\frac{s_\theta(s_\beta-c_\beta)m_Z}{\sqrt{2}(\mu+M_{\widetilde{B}})} & \frac{c_\theta(s_\beta-c_\beta)m_Z}{\sqrt{2}(\mu+M_{\widetilde{W}})} & 0 & 1 \end{pmatrix} \begin{pmatrix} \widetilde{B} \\ \widetilde{W}_3 \\ \widetilde{H}_A \\ \widetilde{H}_S \end{pmatrix} \tag{2.7}$$

where s_x (c_x) is the sine (cosine) of the appropriate angle. It is immediately obvious that the $\tilde{\chi}_1^0$ is mainly $\widetilde{B}$ with some Higgsino content and the $\tilde{\chi}_2^0$ is mainly $\widetilde{W}_3$ with some Higgsino content. Figures 2.11-2.15 show the Higgsino fraction of $\tilde{\chi}_2^0$ as a function of $\tan\beta$, μ and $M_{\tilde{g}}$.
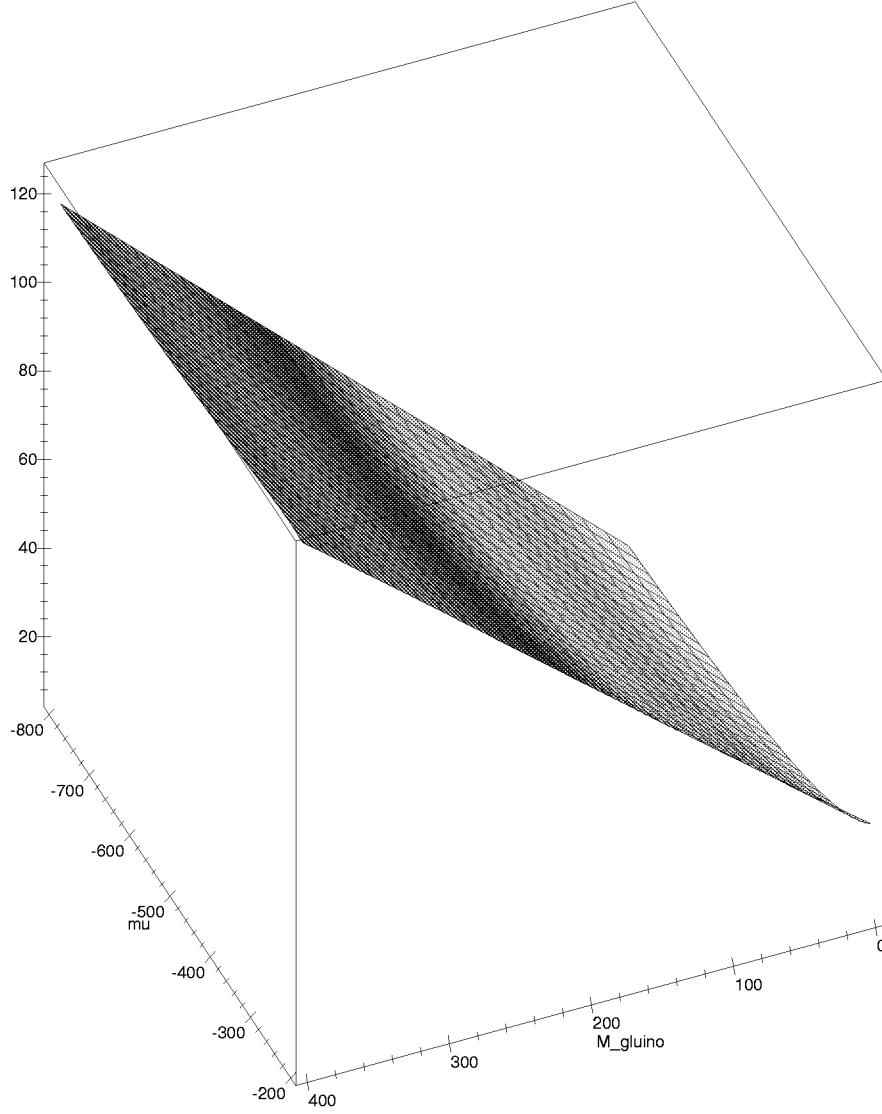
Figure 2.2: $M_{\tilde{\chi}_1^{\pm}}$ (vertical axis; in GeV/c^2) as a function of μ (left axis; in GeV/c^2) and $M_{\tilde{g}}$ (right axis; in GeV/c^2) for $\tan\beta = 2$. Note that the $\tilde{\chi}_1^{\pm}$ mass has little μ dependence. The shading in this and the following figures is an artifact of the program used to generate the plots.
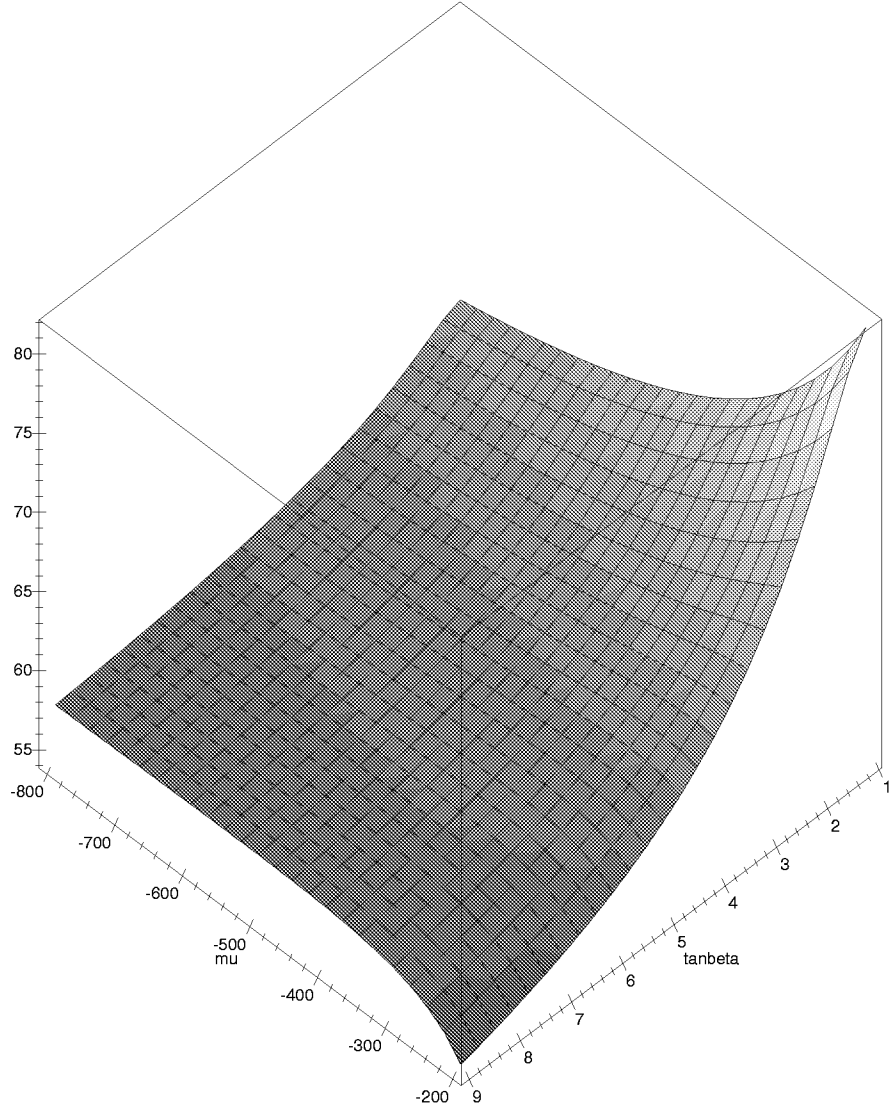
Figure 2.3: $M_{\tilde{\chi}_1^\pm}$ (vertical axis; in GeV/c^2) as a function of μ (left axis; in GeV/c^2) and $\tan\beta$ (right axis) for $M_{\tilde{g}} = 200$ GeV/c^2. Note that the vertical axis has a range of only 15 GeV/c^2; the $\tilde{\chi}_1^\pm$ mass has much smaller dependence on μ and $\tan\beta$ than on $M_{\tilde{g}}$.
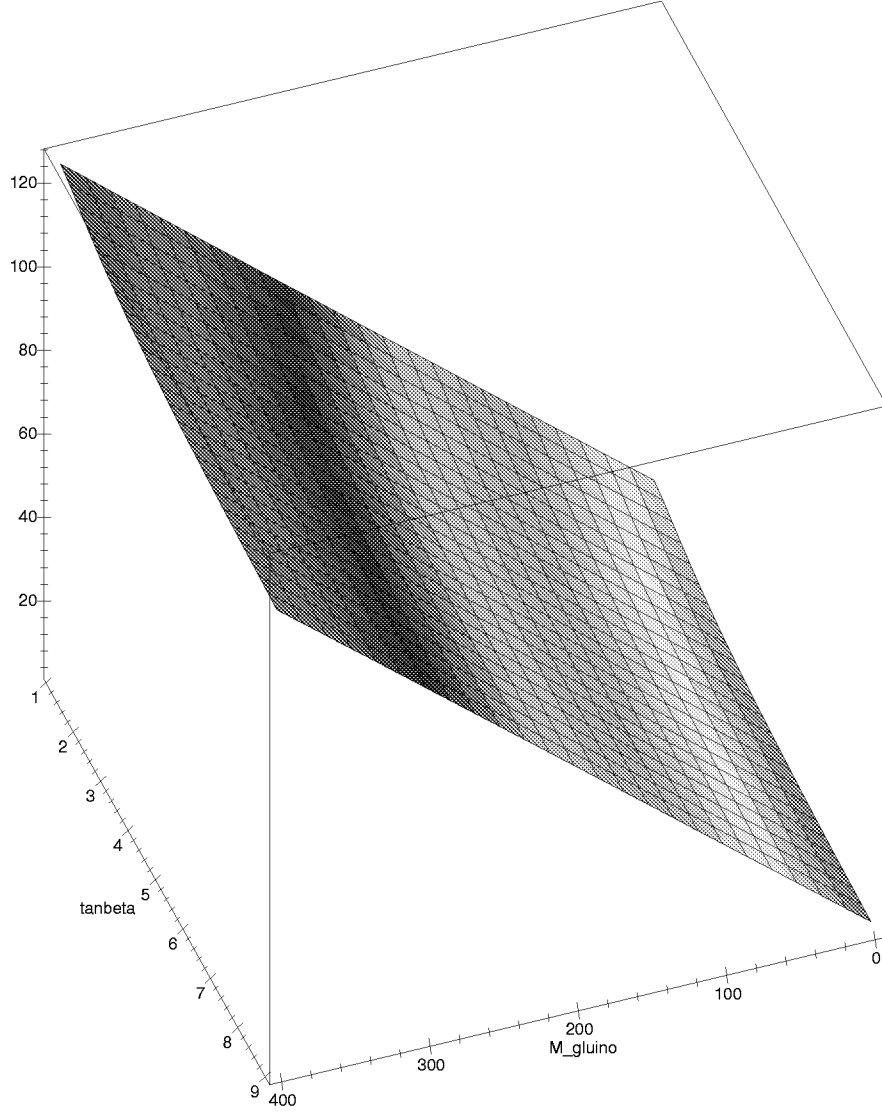
Figure 2.4: $M_{\tilde{\chi}_1^{\pm}}$ (vertical axis; in GeV/c^2) as a function of $\tan\beta$ (left axis) and $M_{\tilde{g}}$ (right axis; in GeV/c^2) for $\mu = -400$ GeV/c^2. Note that the mass has little $\tan\beta$ dependence.
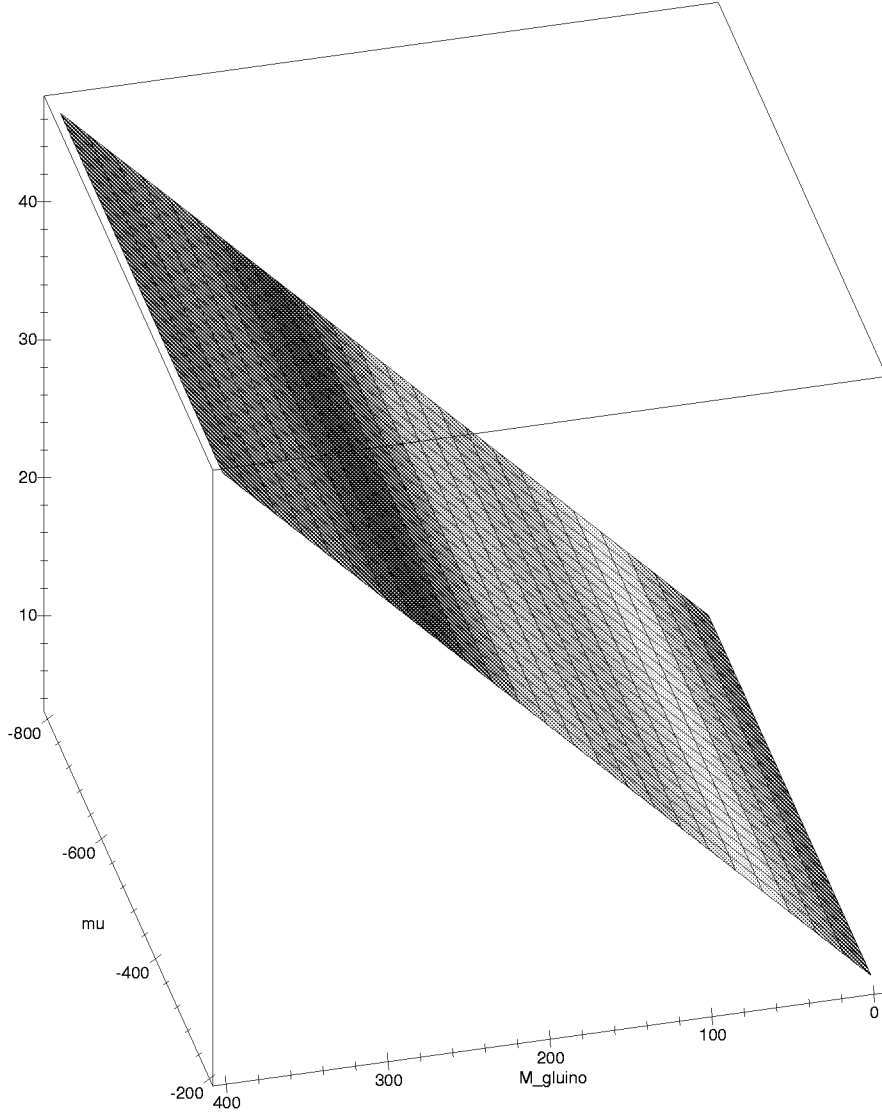
Figure 2.5: $M_{\tilde{\chi}_1^0}$ (vertical axis; in GeV/c^2) as a function of μ (left axis; in GeV/c^2) and $M_{\tilde{g}}$ (right axis; in GeV/c^2) for $\tan\beta = 2$. Note that the mass is largely independent of μ.
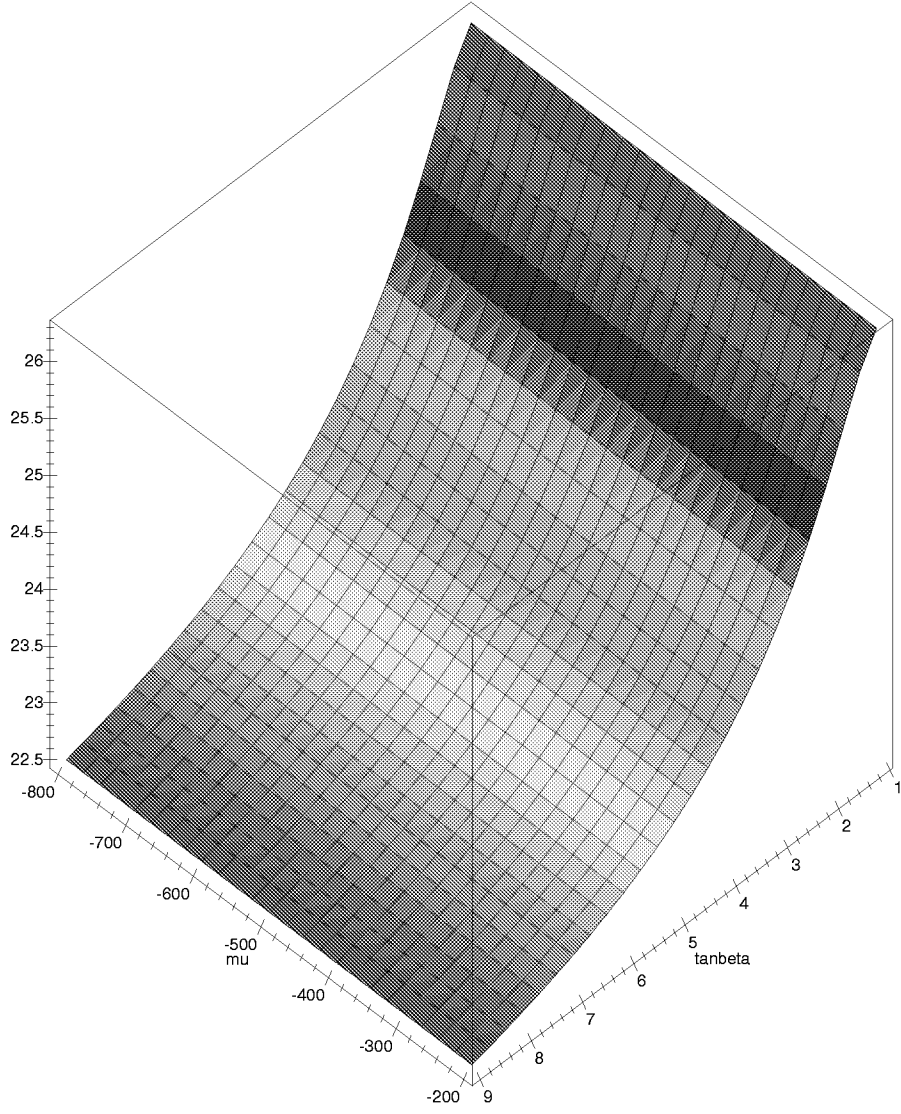
Figure 2.6: $M_{\tilde{\chi}_1^0}$ (vertical axis; in GeV/c^2) as a function of μ (left axis; in GeV/c^2) and $\tan\beta$ (right axis) for $M_{\tilde{g}} = 200$ GeV/c^2. Note that the mass is independent of μ and only weakly depends on $\tan\beta$ (the vertical scale only spans 4 GeV/c^2).
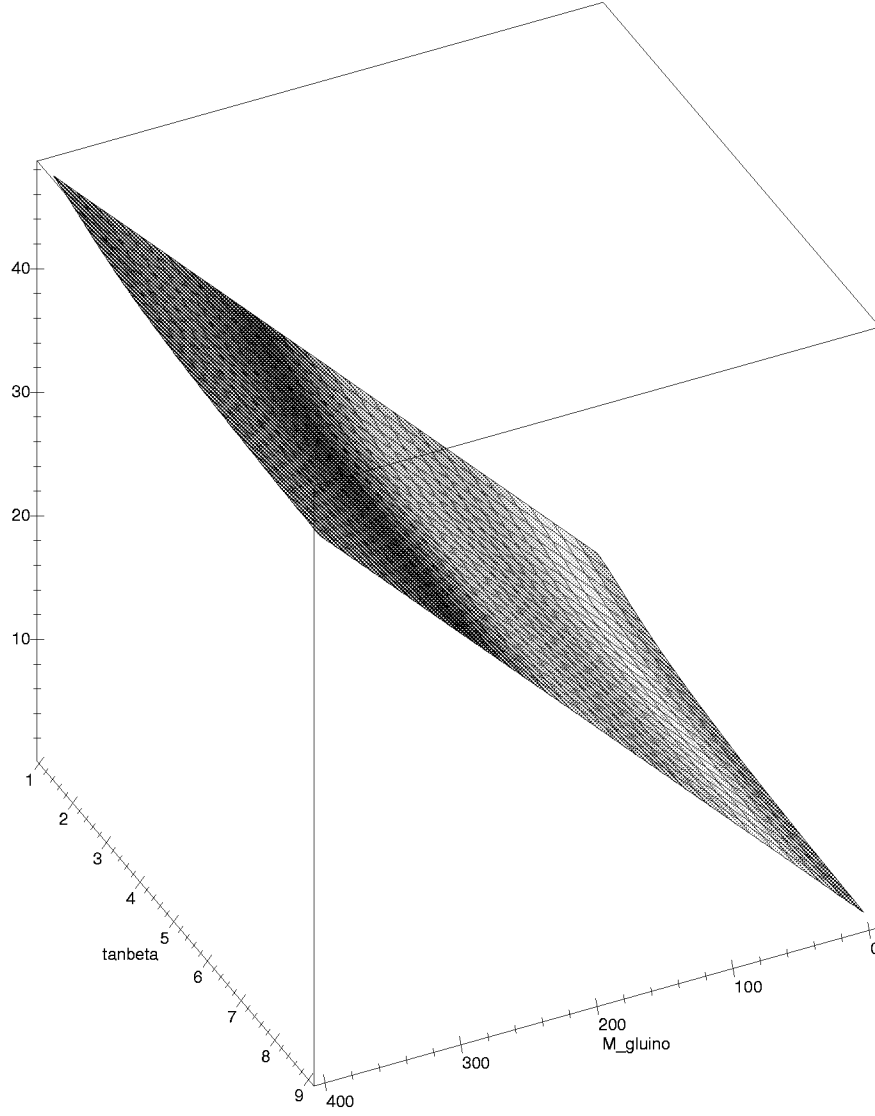
Figure 2.7: $M_{\tilde{\chi}_1^0}$ (vertical axis; in GeV/c^2) as a function of $\tan\beta$ (left axis) and $M_{\tilde{g}}$ (right axis; in GeV/c^2) for $\mu = -400$ GeV/c^2.
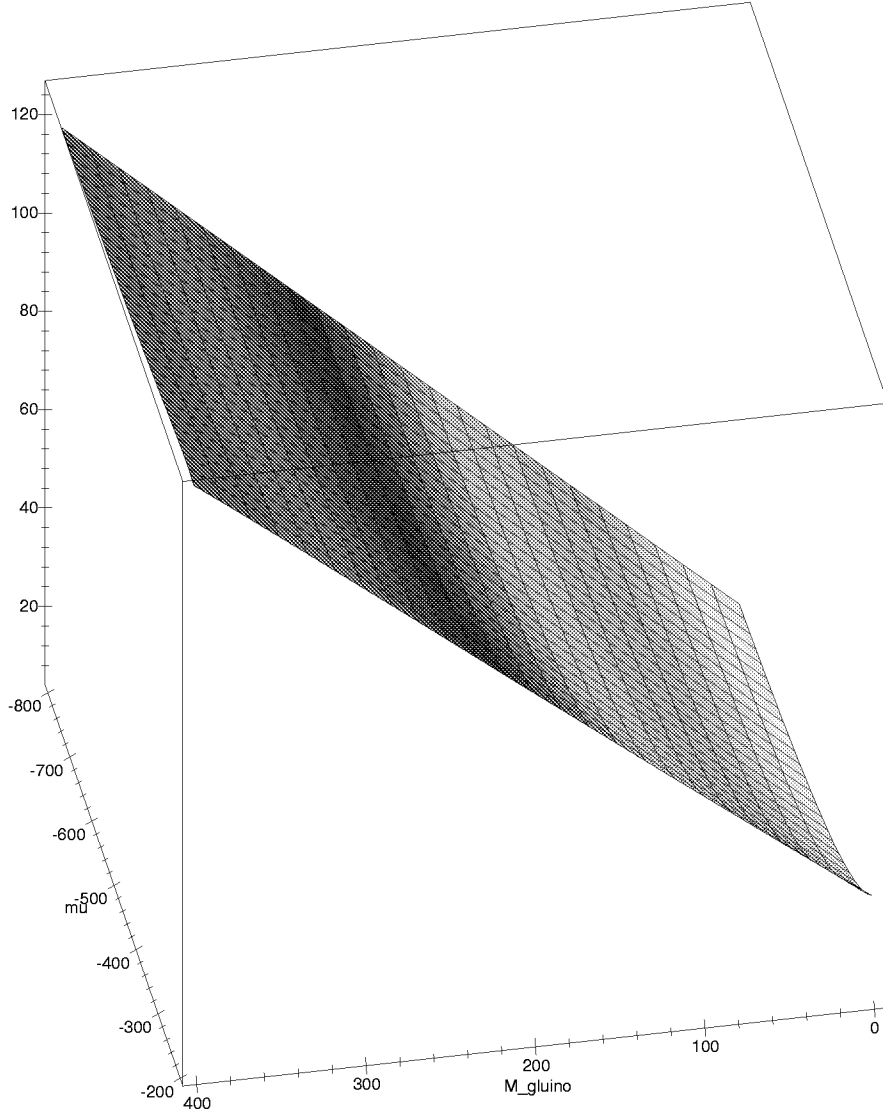
Figure 2.8: $M_{\tilde{\chi}_2^0}$ (vertical axis; in GeV/c^2) as a function of μ (left axis; in GeV/c^2) and $M_{\tilde{g}}$ (right axis; in GeV/c^2) for $\tan\beta = 2$.
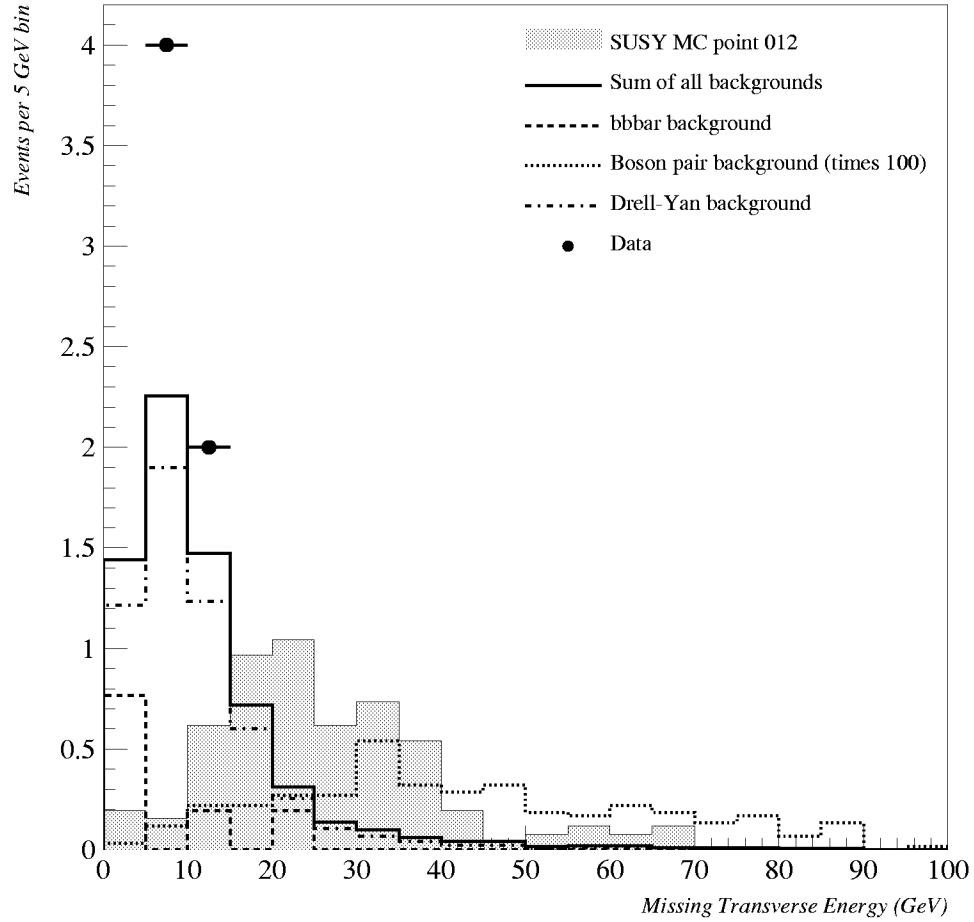
Figure 4.28: Missing transverse energy for each of the types of background and a sample signal point (012). The dashed line is $b\bar{b}$, the dot-dash line is Drell-Yan, the dotted line is boson pair production and the solid line is the sum. The filled histogram is MC signal point 012. Each histogram is normalized such that the area of the histogram is equal to the number of events expected after all cuts but before the $\not{E}_T$ cut. The boson pair histogram is multiplied by 100 so it is visible. The data are indicated by circles (•).

Table 4.9: Number of expected background events after each cut, for contributions from $b\bar{b}/c\bar{c}$, boson pair, Drell-Yan and $t\bar{t}$. All numbers are scaled by the Monte Carlo correction factor discussed in Chapter 3. The fake lepton rate (0.00289/event) is applied to all dilepton backgrounds. As can be seen, the isolation and ΔR cuts reduce the heavy flavor contribution, the Z^0 mass cut removes the boson pair and Drell-Yan contributions, and the $\Delta\phi_{\ell\ell}$ cut further reduces the Drell-Yan contribution. The $\not{E}_T$ cut reduces the total expected background to 0.99 events.

| | Events remaining after each cut | | | | |
Cut	$b\bar{b}/c\bar{c}$	Boson pair	Drell-Yan	$t\bar{t}$	Sum
3 lepton requirement	14.83	0.58	20.46	0.05	35.92
good run requirement	14.83	0.58	20.46	0.05	35.92
cosmic removal	14.83	0.58	20.46	0.05	35.92
$|z_{vertex}| < 60$ cm	14.60	0.52	19.57	0.04	34.73
Vertex Requirements	14.22	0.52	19.57	0.04	34.35
$ISO < 2$	3.17	0.48	18.77	0.02	22.44
$|Q_1+Q_2+Q_3| < 3$	3.17	0.48	18.77	0.02	22.44
Require e^+e^- or $\mu^+\mu^-$	2.71	0.46	18.30	0.02	21.49
$\Delta R_{\ell\ell} > 0.4$	1.70	0.45	18.21	0.01	20.37
$\Delta\phi_{\ell_1\ell_2} < 170°$	1.70	0.38	7.86	0.00	9.94
Z^0 removal (75-105 GeV/c^2)	1.70	0.04	5.81	0.00	7.55
Υ removal (9-11 GeV/c^2)	1.70	0.04	5.49	0.00	7.23
J/ψ removal (2.9-3.1 GeV/c^2)	1.15	0.04	5.49	0.00	6.68
$\not{E}_T > 15$ GeV	0.00	0.02	0.97	0.00	0.99

4.6.4 Estimate of Expected Background

We generate a large quantity of Monte Carlo background for each type of event: at least 60 pb^{-1} for $b\bar{b}/c\bar{c}$, 100-400 pb^{-1} for each of the Drell-Yan types, 5,000 pb^{-1} for $t\bar{t}$and 2,000-7,000 pb^{-1} for boson pair. We examine each type of background with our analysis code and apply the lepton ID cuts and additional cuts described above. Table 4.9 lists the number of events expected after each cut from each type of background. Table 4.10 compares the sum from background to the number of data events and a sample MC signal point. As can be seen, the data and the MC background agree quite well. After all cuts, we expect to see 0.99±0.2 events and see none.

After all cuts, no events remain in the data and the number of events before the final cuts are applied agree well with the expected background. We see no evidence for Supersymmetry.

Table 4.10: Number of expected background, data and signal Monte Carlo events left after each cut. Below the line the data and background predictions agree quite well. Above the line the cuts remove both predictable background and unpredictable background (such as cosmic rays and multiple interactions). This is especially true for the ΔR cut– we expect to remove 1 event and instead remove 14. Examination of these events shows they are clearly cosmic rays. After all cuts, we expect 0.99 events from background and see none. For the sample Monte Carlo signal point 012, we expect 4.47 events after all cuts.

Cut	Background	Data	Signal MC
3 lepton requirement	35.92	247	8.44
good run requirement	35.92	232	8.44
cosmic removal	35.92	70	8.44
$|z_{vertex}| < 60$ cm	34.73	66	8.01
Vertex Requirements	34.35	59	8.01
$ISO < 2$	22.44	23	6.89
$|Q_1 + Q_2 + Q_3| < 3$	22.44	23	6.89
Require $e^+ e^-$ or $\mu^+ \mu^-$	21.49	23	6.89
$\Delta R_{\ell\ell} > 0.4$	20.37	9	6.81
$\Delta \phi_{\ell_1 \ell_2} < 170°$	9.94	8	6.19
Z^0 removal (75-105 GeV/c^2)	7.55	7	5.95
Υ removal (9-11 GeV/c^2)	7.23	7	5.49
J/ψ removal (2.9-3.1 GeV/c^2)	6.68	6	5.49
$\not{E}_T > 15$ GeV	0.99	0	4.47

Chapter 5

Limits on the SiMSSM parameter space

We see no evidence for Supersymmetry. However, it is instructive to examine a few models and set limits on the production of $\tilde{\chi}_1^{\pm}$ and $\tilde{\chi}_2^0$. We can then find the naturalness of SUSY with our limits, and can also compare our sensitivity to that of other experiments. I will describe the Monte Carlo simulation techniques, the limit setting method, and the limits on the SUGRA-inspired MSSM, the SU(5)×U(1) Supergravity model, and SUGRA.

5.1 Monte Carlo Simulation techniques

Simulating both background and SUSY signal events is a two stage process. First, we use a Monte Carlo program to generate the events. For this analysis, we use ISAJET v7.06 (for much of the background calculation) and ISAJET v7.20 (for all of the signal calculation) [36]. There are no substantial differences between the versions; v7.20 contains bug fixes which were corrected manually in v7.06. ISAJET is a general Monte Carlo program that can be used to generate events for any Standard Model process as well as many different SM extensions. We use it for all the background processes (see Section 4.6) and to generate a wide variety of points in SiMSSM space.

A generated event cannot be examined using the analysis code. The information is limited to the P_T, η and ϕ for each particle and the decay chains. We use QFL (see Section 3.2.7) to include detector effects (such as resolution and smearing). As mentioned in Section 3.2.7, QFL is over-efficient for lepton identification so we apply an overall correction factor of 0.864/event. After the events generated with ISAJET are simulated with QFL, they are identical in structure to data taken with the detector.

The simulated events are examined with the analysis program, with one addition. Data that is recorded must pass through the trigger system. QFL simulation does not include a simulation of

the trigger. We use a trigger simulation program written specifically for SUSY analyses, MC_WGT.

5.1.1 Trigger Simulation

There is no specific trigger path which events must follow to enter our data set. This has both advantages and disadvantages. Since this is a search for new physics, allowing all possible signal events into the data is the proper technique. However, this means events can follow any one of many trigger paths. For the dilepton data set on which this analysis is based, many different triggers contribute to the data set. To properly simulate a trigger, we must include several effects: the actual trigger efficiency and both static and dynamic prescales.

The trigger efficiency for each trigger is taken from a variety of CDF Notes [38]. This information is coded (in either 500 MeV or 1 GeV lepton E_T (P_T) bins) into the trigger simulation routine MC_WGT. Each event is passed to this routine. The E_T (P_T) and η for each lepton in the event is examined to see which possible Level 1, Level 2 and Level 3 triggers it could have passed. For many detector regions, there are several possible triggers which could be used. The trigger which returns the highest probability at each level is the probability that that lepton would pass that trigger level. The values for different detector regions and lepton species are ORed together[1] and this number is the probability that this event would pass that trigger level. The values returned from each trigger level are multiplied and the total is the probability that this particular event would have entered the data set.

To calculate the static and dynamic prescales, we use SIGMON [39]. SIGMON examines the online LUMMON[2] data files to find the actual luminosity recorded for each trigger on a run-by-run basis. This can be compared to the luminosity recorded for each run to determine the effective prescale of each trigger for each run. We divide the Run IB data into three bins according to the average instantaneous luminosity for each run ($\mathcal{L} < 1.7 \times 10^{30}$ s^{-1}cm^{-2}, $1.7 < \mathcal{L} < 4 \times 10^{30}$ s^{-1}cm^{-2} and $\mathcal{L} > 4 \times 10^{30}$ s^{-1}cm^{-2}) and find the effective prescale for each trigger in each $\mathcal{L}$ bin (Table 5.1[3]). We then calculate a weighted average of each of the prescale bins as a function of the percent of the total integrated luminosity from Run IB in each bin. The low instantaneous $\mathcal{L}$ bin has 43%

---

[1]If trigger a has efficiency ϵ_a and trigger b has efficiency ϵ_b the total efficiency is

$$\epsilon_{a+b} = \epsilon_a + \epsilon_b(1 - \epsilon_a).$$

[2]LUMMON is an online program that monitors the amount of data recorded by each trigger during a run. It also controls the dynamic prescales.

[3]The names of the triggers can easily be converted to a meaningful statement. For example, the trigger CEM_8_CFT_7_5_XCES requires at least 8 GeV in the CEM, a CFT track with P_T above 7.5 GeV/c and a good hit in the CES. Numbers written as words ('TWO') indicate the number of objects required in a particular detector. 5DEG indicates how close a muon stub must be to matching the extrapolation of a CTC track.

Table 5.1: The Level 2 triggers used in this analysis and the effective prescale as a function of instantaneous luminosity. For this analysis, low $\mathcal{L}$ means $\mathcal{L} < 1.7 \times 10^{30}$ s^{-1}cm^{-2} (43% of the data), middle is $1.7 < \mathcal{L} < 4 \times 10^{30}$ s^{-1}cm^{-2} (41% of the data) and high is $\mathcal{L} > 4 \times 10^{30}$ s^{-1}cm^{-2} (16% of the data).

Trigger	Low $\mathcal{L}$	Middle $\mathcal{L}$	High $\mathcal{L}$	Average
CEM_8_CFT_7_5_XCES	1.11	1.29	1.55	1.21
TWO_CMU_TWO_CFT_2_2	1.00	1.00	1.00	1.00
CMUP_CFT_12_5DEG	1.00	1.00	1.00	1.00
CEM_5_CFT_4_7_CMU_2_7	1.72	2.19	3.35	2.14
CMX_CMU_TWO_CFT_2_2	1.05	1.39	3.02	1.50
TWO_CMU_ONE_CFT_2_2_6TOW	1.11	1.26	1.56	1.24
CMNP_CFT_12_5DEG	1.35	7.58	31.27	8.69
CMUP_CFT_7_5_5DEG	1.18	2.52	6.16	2.53
CEM_16_CFT_12	1.00	1.00	1.00	1.00
CMX_CFT_12_5DEG	5.25	5.70	16.67	7.26

of the data, the middle instantaneous $\mathcal{L}$ bin 41%, and the high instantaneous $\mathcal{L}$ bin 16%. This final number is the effective prescale for the entire IB data set for each trigger. It is entered in the MC_WGT routine and applied to each event, depending on which trigger that event passes.

This technique for including the prescale effect as a part of the trigger efficiency simplifies several calculations. This also automatically applies the prescale to both background and signal Monte Carlo studies.

To minimize the statistical uncertainty in our Monte Carlo studies, we generate numbers of events corresponding to large $\int \mathcal{L}dt$. We maintain a database listing the $\int \mathcal{L}dt$ for each sample and use this normalize to the amount of data present in Run IB. This constant is also included as part of the trigger efficiency.

The final trigger efficiency returned for each event is a product of four numbers: a weighting factor for the $\int \mathcal{L}dt$, the Level 1 trigger efficiency, the Level 2 trigger efficiency (including the prescale) and the Level 3 trigger efficiency.

5.2 Limit setting method

We generate and analyze a statistically significant number of events for a particular point in SiMSSM space to determine if we should see evidence for $\tilde{\chi}_1^\pm \tilde{\chi}_2^0$ production at that point. We use the formula

$$\sigma_{\tilde{\chi}_1^{\pm} \tilde{\chi}_2^0} \cdot \mathrm{BR}(\tilde{\chi}_1^{\pm} \tilde{\chi}_2^0 \to 3\ell + X) \quad > \quad \frac{N_{exp}}{\epsilon^{tot} \cdot \int \mathcal{L} dt} \tag{5.1}$$

to compare the predicted production cross section ($\sigma_{\tilde{\chi}_1^{\pm} \tilde{\chi}_2^0}$) times branching ratio to trileptons ($\mathrm{BR}(\tilde{\chi}_1^{\pm} \tilde{\chi}_2^0 \to 3\ell + X)$) with the number of expected events (N_{exp}) divided by the total event acceptance (ϵ^{tot}) times the integrated luminosity.

5.2.1 N_{exp}: Systematic Uncertainty

The number of expected events is calculated by taking a Poisson distribution for having seen 0 events and convolving it with a Gaussian[4] whose width is determined by the total systematic uncertainty. The systematic uncertainty has several components:

- Uncertainty in the total integrated luminosity: 8% [40].

- Uncertainty in the trigger efficiency [41]. We determine the trigger efficiency for a particular trigger by studying electron or muon events which pass triggers other than the one we are examining. We then impose the trigger conditions and count the number of events passing. We find that the total trigger efficiencies for electrons and muons are [42, 43]

$$\epsilon_e^{trig} = (87.3 \,{}^{+3.8}_{-4.9})\%,$$
$$\epsilon_\mu^{trig} = (87.1 \pm 2.9)\%.$$

In a multi-lepton event analysis, we must take into account the possibility of events with multiple trigger-leptons: (a) one trigger lepton and (b) two trigger leptons. [Note that there were no three lepton triggers available in Run IB, so we do not have to worry about that case.]

We obtain a conservative estimate of the trigger efficiency uncertainty by assuming all dilepton events are in case (a). The electron trigger has the largest uncertainty and so we use that value. This situation gives a trigger efficiency uncertainty of ±5.6%.

- Uncertainty in the trilepton finding efficiency:

---

[4]The number of expected events for having seen 0 using a Poisson distribution at a 95% Confidence Level is 3.0. A Poisson distribution can only take integer values. However, we can be more precise if we combine the information from the Poisson distribution with a Gaussian distribution. A Gaussian distribution is continuous. For more details see pg. 166 of Ref. [5].

- Uncertainty in the degradation of the Isolation cut: ±8% [44]. This is important as we combine Run IA and IB data sets to increase the integrated luminosity (see Section 5.2.3). Run IB had much higher instantaneous luminosity, which degraded the efficiency of the isolation cut.

- Uncertainty in the Monte Carlo correction factor from Section 3.2.7: ±2%. We calculate this by taking the combination of three leptons (one tight and two loose) that give us the largest correction factor using the information in Table 3.2. For this analysis that combination is a tight CEM electron and two loose CMX muons (0.864±0.017: 0.017/0.864 = 2%).

- Uncertainty in the trilepton finding efficiency: ±2%. This is calculated by taking the combination of lepton finding efficiencies from Table 3.2 that results in the largest uncertainty. For this analysis that combination is a tight CEM electron and two loose CMIO muons.

• Uncertainty in the structure functions: ±7%. We used CTEQ-3L for all of the signal Monte Carlo generation and compared the results from it and an average of CTEQ-3L, GRV-94lo and MRS-D0′. The largest deviation between the two is our systematic uncertainty.

• Uncertainty in the fit for the detection efficiency (see Section 5.2.2): ±13%.

The uncertainties combine in quadrature for a total systematic uncertainty of ±20%. This yields N_{exp} = 3.2 at a Confidence Level of 95%.

5.2.2 ϵ^{tot}: Detection Efficiency

The detection efficiency is a combination of geometric acceptance, trigger efficiency and kinematic acceptance. Naïvely, one would expect the detection efficiency to be mainly a function of the $\tilde{\chi}_1^\pm$, $\tilde{\chi}_1^0$ and $\tilde{\chi}_2^0$ masses: since $M_{\tilde{\chi}_1^\pm} \approx M_{\tilde{\chi}_2^0} \approx 2M_{\tilde{\chi}_1^0}$, higher $\tilde{\chi}_1^\pm$ and $\tilde{\chi}_2^0$ masses result in stiffer (more energetic), easier to detect leptons. Figure 5.1 shows the detection efficiency as a function of $M_{\tilde{\chi}_1^\pm}$ for $\mu = -200$ GeV/c^2, $\tan\beta = 2$ and $M_{\tilde{q}} = M_{\tilde{g}}$. The detection efficiency clearly rises as a function of $M_{\tilde{\chi}_1^\pm}$. Figure 5.2 shows the detection efficiency for a variety of points in SiMSSM space where we varied μ, $M_{\tilde{q}}/M_{\tilde{g}}$ and $\tan\beta$. We fit a straight line to these points to get a function for the detection efficiency as a function of $M_{\tilde{\chi}_1^\pm}$. Figure 5.3 is a comparison between the fit to all points and a variety of subsets.

We found that the detection efficiency was not completely model independent: changing $\tan\beta$ changes the acceptance. Figure 5.4 shows the fit for points where we constrained $\tan\beta$ to be 2. The quality of the fit clearly improves. Because of this, we use the fit for SiMSSM points where $\tan\beta = 2$ and the individual acceptances for other points.

MINUIT χ^2 Fit to Plot   7&0

mu=-200, m_sq=m_gl
File: noteplots.dat   26-SEP-97 15:29
Plot Area Total/Fit   71.960 / 71.960   Fit Status 3
Func Area Total/Fit   336.18 / 336.18   E.D.M. 5.667E-21

χ^2=   0.8 for   8 - 2 d.o.f.,   C.L.= 99.1%

Errors   Parabolic   Minos
Function 1: Polynomial of Order 1
NORM   -4.6157   ±   2.322   - 0.0000E+00   + 0.0000E+00
POLY01   0.17005   ±   3.0748E-02   - 0.0000E+00   + 0.0000E+00
* OFFSET   0.00000E+00   ±   0.0000E+00   - 0.0000E+00   + 0.0000E+00
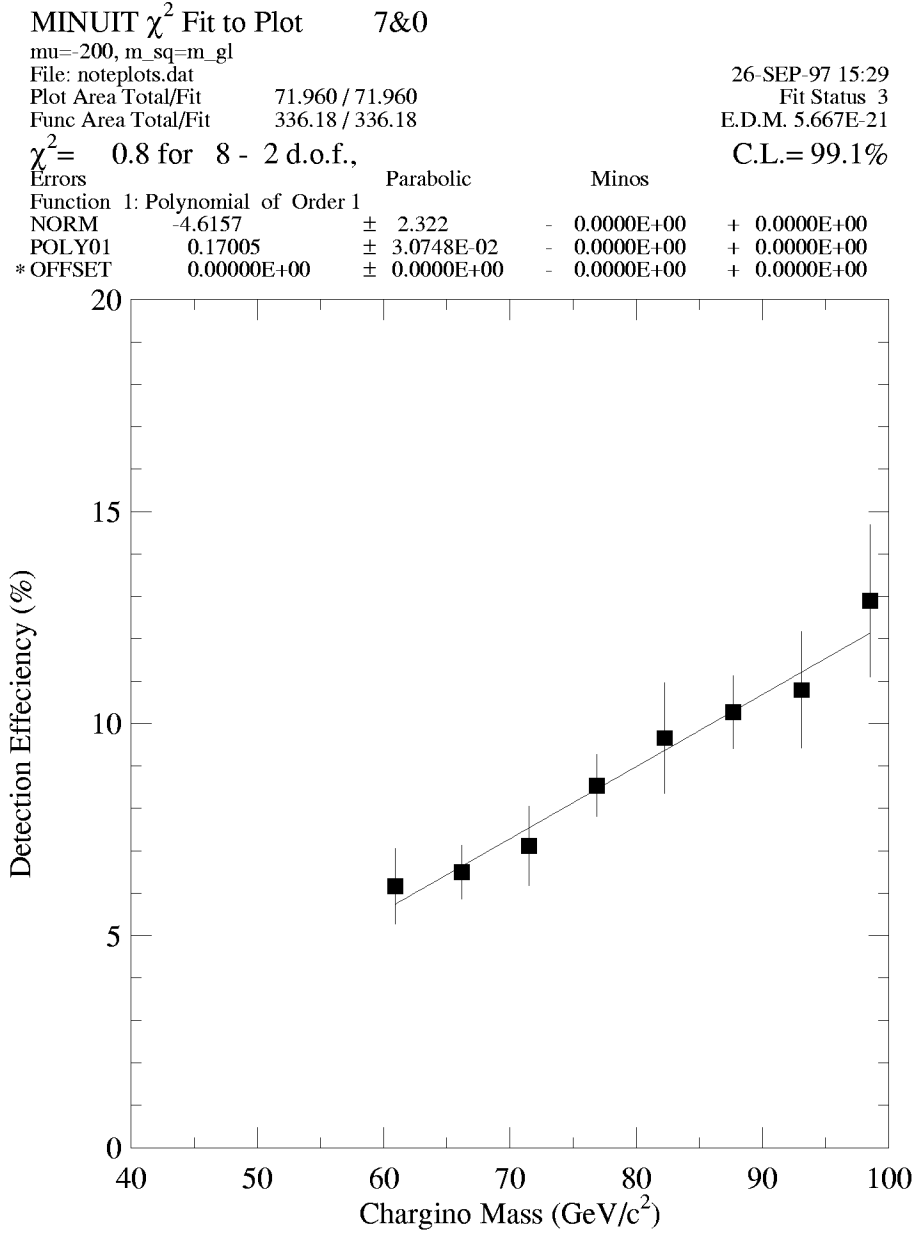
Figure 5.1: The detection efficiency as a function of $M_{\tilde{\chi}_1^\pm}$. For this plot we set $\mu = -200$ GeV/c^2, $\tan\beta = 2$ and $M_{\tilde{q}} = M_{\tilde{g}}$. The detection efficiency is clearly a function of the chargino mass.

94

MINUIT χ^2 Fit to Plot   2&0

All Points
File: noteplots.dat   26-SEP-97 15:29
Plot Area Total/Fit   484.25 / 484.25   Fit Status 3
Func Area Total/Fit   423.16 / 423.16   E.D.M. 1.960E-20

$\chi^2 =$ 84.1 for 61 - 2 d.o.f.,   C.L.= 1.8%

Errors   Parabolic   Minos
Function 1: Polynomial of Order 1
NORM   -5.0341   ± 0.6528   - 0.0000E+00   + 0.0000E+00
POLY01   0.17007   ± 9.3581E-03   - 0.0000E+00   + 0.0000E+00
*OFFSET   0.00000E+00   ± 0.0000E+00   - 0.0000E+00   + 0.0000E+00
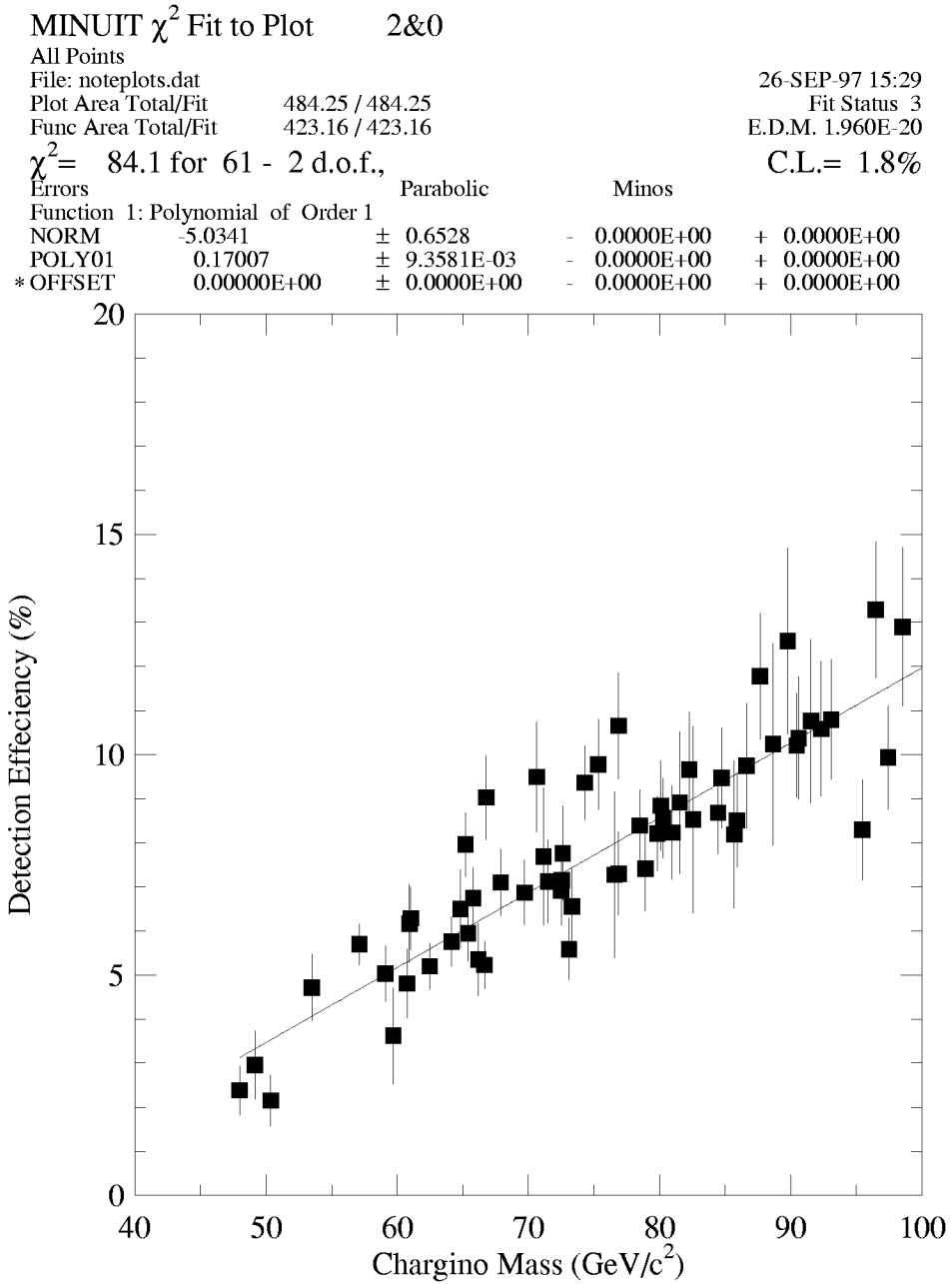
Figure 5.2: The detection efficiency as a function of $M_{\tilde{\chi}_1^\pm}$ for a variety of points in SiMSSM space.

ID	IDB	Symb	Date/Time	Area	Mean	R.M.S.
4	0	-32	000000/0000	54.35	82.10	12.00
4	981	-1	970926/1529	299.9	81.07	10.90
2	981	-2	970926/1529	424.6	80.71	14.81
5	0	-32	000000/0000	58.32	78.91	9.128
5	981	-1	970926/1529	243.8	79.56	8.252
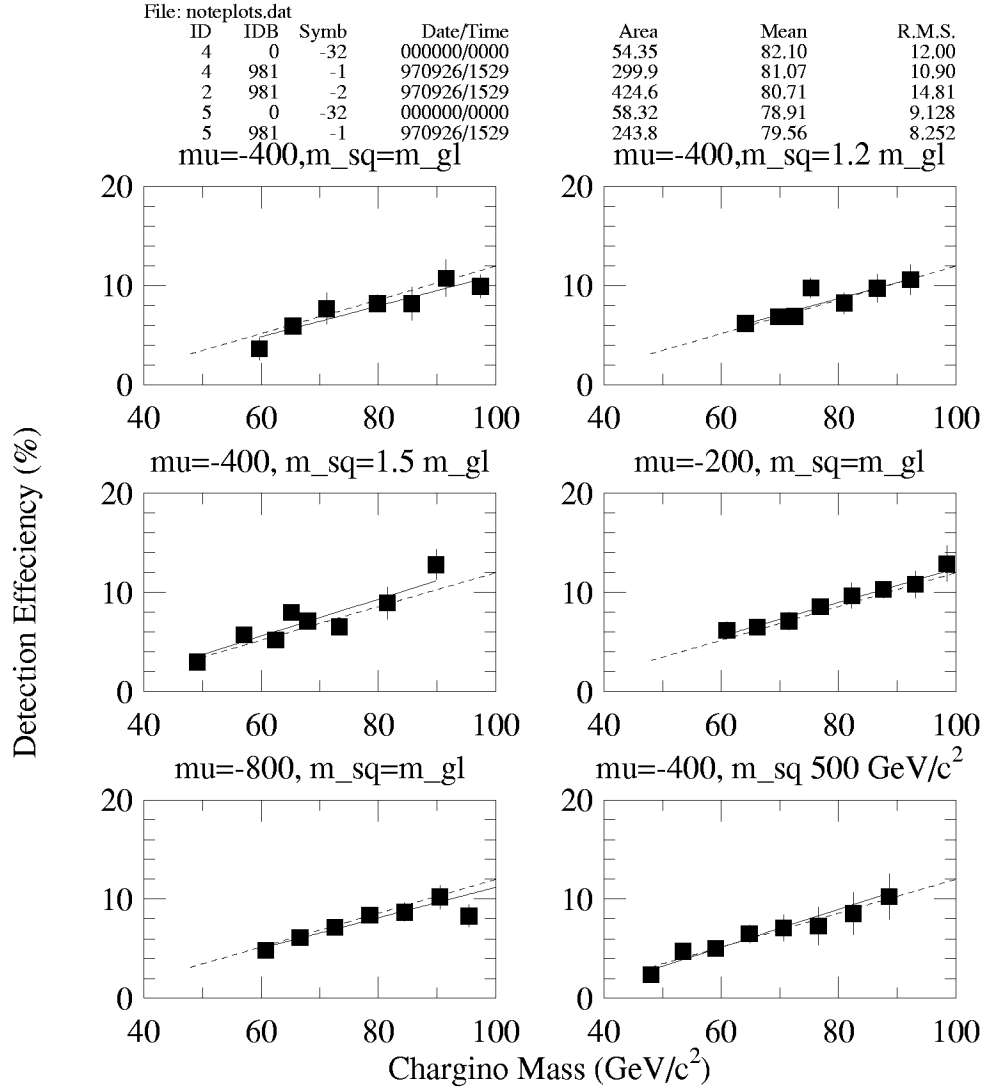
Figure 5.3: The detection efficiency as a function of $M_{\tilde{\chi}_1^\pm}$ comparing individual SiMSSM points to an overall fit. The fit agrees well with the individual points, so we use the overall fit for each of these points. In each plot the solid line is the fit to that particular set of points and the dashed line is a fit to all points with $\tan \beta = 2$.

MINUIT χ^2 Fit to Plot   3&0

tan B=2

File: noteplots.dat   26-SEP-97 15:29
Plot Area Total/Fit   360.20 / 360.20   Fit Status 3
Func Area Total/Fit   418.43 / 418.43   E.D.M. 1.364E-20

$\chi^2=$ 47.6 for 46 - 2 d.o.f.,   C.L.= 32.7%

Errors   Parabolic   Minos

Function 1: Polynomial of Order 1

NORM   -4.5587   ± 0.7424   - 0.0000E+00   + 0.0000E+00
POLY01   0.16260   ± 1.0731E-02   - 0.0000E+00   + 0.0000E+00
*OFFSET   0.00000E+00   ± 0.0000E+00   - 0.0000E+00   + 0.0000E+00
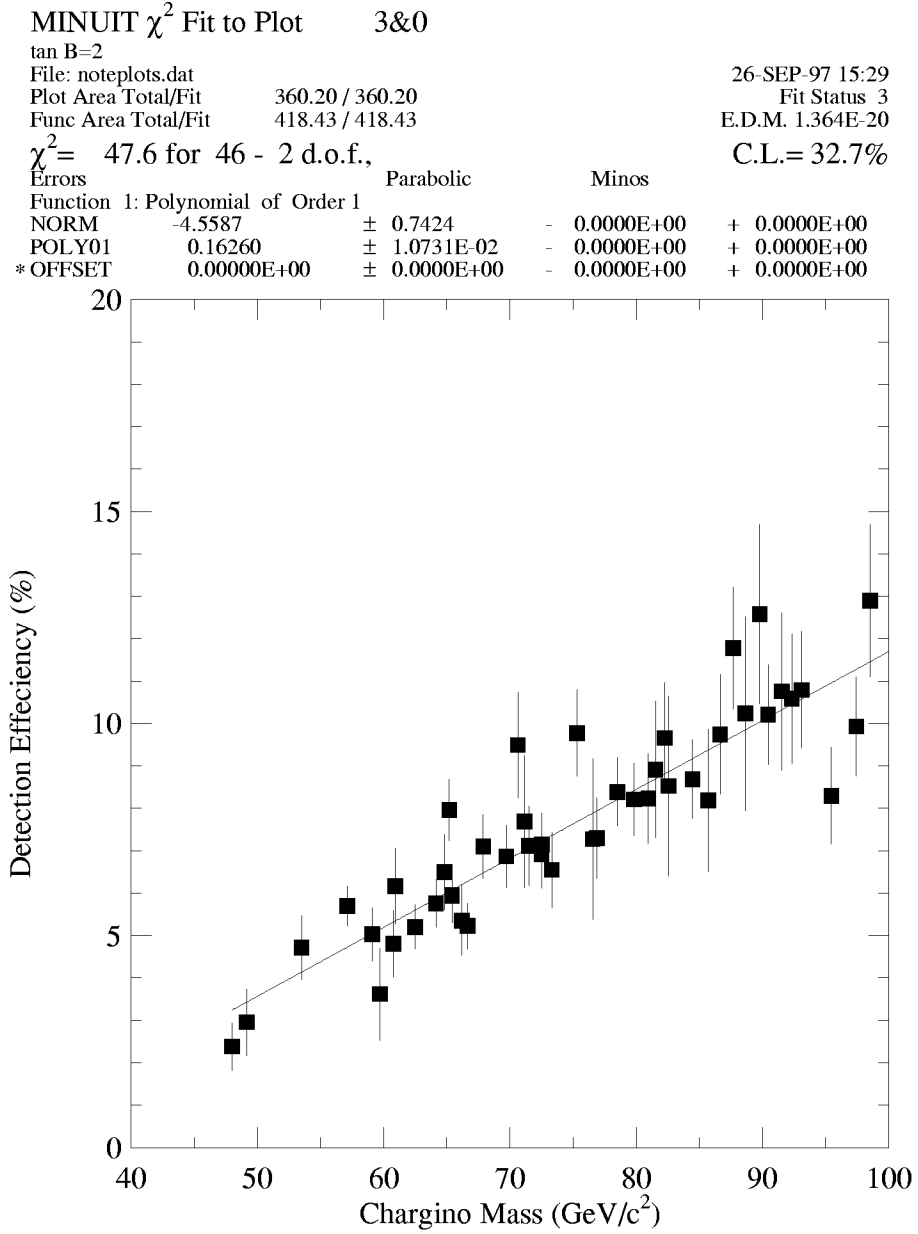
Figure 5.4: The detection efficiency as a function of $M_{\tilde{\chi}_1^\pm}$ for a variety of points in SiMSSM space, constraining $\tan\beta = 2$. The quality of the fit is better than when $\tan\beta$ is unconstrained.

97

It is appropriate to wonder why we want a functional form for the detection efficiency. To determine the detection efficiency, we must generate and simulate at least 20,000 events. This can take some time. If the detection efficiency is independent of the model parameters, than we need only calculate the cross section and branching ratio for a particular SiMSSM point. This is a much less time consuming process. For points where $\tan \beta = 2$, we use (see Figure 5.4)

$$\epsilon_{tot} = -4.56 + 0.16 M_{\tilde{\chi}_1^\pm}.$$

For all other points we use the ϵ_{tot} determined from Monte Carlo for that particular point. If we determine ϵ_{tot} for each SiMSSM point, the total systematic uncertainty drops from 20% to 15%. However, this only reduces N_{exp} from 3.2 to 3.1. The increased analysis speed is a great benefit, with only a small decrease in our limit.

5.2.3 $\int \mathcal{L} dt$: Integrated Luminosity

This analysis is primarily concerned with the Run IB data. However, a similar analysis was done using the Run IA data [45]. That analysis used identical cuts (but did not apply the $\not{E}_T$ cut) and had no events remaining. Thus, we can combine the 87.7 pb^{-1} Run IB data with the 19.1 pb^{-1} of Run IA data for a total of 107 pb^{-1}. We have no candidate events in the entire sample.

5.3 Limits on the SiMSSM

It is impractical for us to try to examine the entire SiMSSM parameter space, even after reducing to the six free parameters discussed in Chapter 2. We can further reduce the number of free parameters to four by noting that this analysis is insensitive to the top trilinear coupling (A_T) and the mass of the pseudoscalar Higgs boson (H_A). We set $A_T = \mu / \tan \beta$[5] and $M_{H_A} = 500$ GeV/c^2.[6] The remaining parameters are μ, $\tan \beta$, M$_{\tilde{q}}$ and M$_{\tilde{g}}$. Since the $\tilde{\ell}$ mass is mainly a function of $\Delta(M_{\tilde{q}}, M_{\tilde{g}})$ we replace M$_{\tilde{q}}$ with M$_{\tilde{q}}$/M$_{\tilde{g}}$. However, we still need guidance to determine which regions of parameter space we should examine.

This analysis yields the strongest limits when the leptonic branching ratios of the $\tilde{\chi}_1^\pm$ and $\tilde{\chi}_2^0$ are maximized. This occurs for two reasons: small Higgsino content of the $\tilde{\chi}_1^\pm$ and $\tilde{\chi}_2^0$ (as Higgsino-like $\tilde{\chi}_1^\pm$ and $\tilde{\chi}_2^0$ prefer to decay to quarks), and small $\tilde{\ell}$ masses (as light, but still virtual, sleptons can enhance the leptonic branching ratio). A quick look at Figures 2.12 and 2.15 reveals gaugino-like $\tilde{\chi}_1^\pm$ and $\tilde{\chi}_2^0$ for $|\mu| \gtrsim 200$ GeV/c^2 or $1 \lesssim \tan \beta \lesssim 10$. The $\tilde{\chi}_1^\pm$ and $\tilde{\chi}_2^0$ masses increase

---

[5]We use $A_T = \mu / \tan \beta$ as it gives the smallest stop splitting. This is not relevant to this analysis (as we ignore all but the first generation of squarks) but is used for consistency with other CDF analyses.

[6]We use $M_{H_A} = 500$ GeV/c^2 to remove any possibility of decay to Higgs. Any value > 100 GeV/c^2 would be acceptable.

with $|\mu|$, resulting in small production cross sections. We thus only study $|\mu| < 1000$ GeV/c^2. As discussed in Section 2.3, large $\tilde{q}$ masses reduce the t-channel production mechanism, thus increasing the overall $\tilde{\chi}_1^\pm \tilde{\chi}_2^0$ production cross section. However, since the $\tilde{\ell}$ masses are determined mainly by the difference in $\tilde{q}$ and $\tilde{g}$ masses (Equation 2.2), increasing the $\tilde{q}$ mass yields heavier $\tilde{\ell}$. That in turn reduces the branching ratio to leptons. The reduction in branching ratio is a larger effect than the increase of production cross section. We thus want to keep the $\tilde{q}$ to $\tilde{g}$ mass ratio less than 2. Finally, if the squarks are too much lighter than the gluinos, the renormalization group equations (Equation 2.2) break down. These formulae are useful for $M_{\tilde{q}}/M_{\tilde{g}} > 0.90$. When the squarks are lighter than the gluinos, the sleptons are lighter than the $\tilde{\chi}_1^\pm$ and $\tilde{\chi}_2^0$. This results in two-body decays of the $\tilde{\chi}_1^\pm$ and $\tilde{\chi}_2^0$. However, for $0.90 < M_{\tilde{q}}/M_{\tilde{g}} \lesssim 0.95$ the lightest slepton is a sneutrino and invisible decays of the $\tilde{\chi}_1^\pm$ and $\tilde{\chi}_2^0$ dominate. $M_{\tilde{\chi}_1^\pm}$ and $M_{\tilde{\chi}_2^0}$ are mainly functions of $M_{\tilde{g}}$ so we set $M_{\tilde{g}}$ to values that yield 45 GeV/c$^2 \lesssim M_{\tilde{\chi}_1^\pm} \lesssim 100$ GeV/c^2.

To summarize, we search the SiMSSM parameter space in the regions

- -200 GeV/c$^2 \leq \mu \leq$ -1000 GeV/c^2,

- $1.1 \leq \tan\beta \leq 8$,

- $0.95 \leq M_{\tilde{q}}/M_{\tilde{g}} \leq 2$, and

- 150 GeV/c$^2 \leq M_{\tilde{g}} \leq 340$ GeV/c^2.

Our limits for the SiMSSM parameter space outside these regions are weaker and thus less interesting. For all points we examine we find $M_{\tilde{\chi}_1^\pm} \approx M_{\tilde{\chi}_2^0} \approx 2\, M_{\tilde{\chi}_1^0}$.

In Figures 5.5-5.16 we present the 95% Confidence Level (C.L.) upper limit curve and compare it to the predicted cross section times branching ratio for a variety of points in SiMSSM space. The 95% C.L. upper limit curve is a line indicating the minimum cross section times branching ratio we can detect as a function of $\tilde{\chi}_1^\pm$ mass[7]. Above the line enough events would be produced so we could detect them; below it we cannot. This line is the right hand side of Equation 5.1. The cross section times branching ratio lines are calculated using ISAJET 7.20 and are the production cross section for $p\bar{p}\rightarrow \tilde{\chi}_1^\pm \tilde{\chi}_2^0$ times the branching ratio $\tilde{\chi}_1^\pm \tilde{\chi}_2^0 \rightarrow 3\ell + X$, where ℓ is either e or μ. It is important to realize the branching ratio is the sum of all four possible e or μ combinations (eee, $ee\mu$, $e\mu\mu$, $\mu\mu\mu$). Figure 5.5 shows the 95% C.L. upper limit curve (solid line) in comparison to cross section times branch ratio curves (dashed lines) for $M_{\tilde{q}}/M_{\tilde{g}} = 1$, 1.2, 1.5 and 2.0. The mass lower limit and $\sigma_{\tilde{\chi}_1^\pm \tilde{\chi}_2^0}\cdot\text{BR}(\tilde{\chi}_1^\pm \tilde{\chi}_2^0 \rightarrow 3\ell + X)$ upper limit can be read off the graph where the dashed and solid lines intersect. Clearly, as the squarks become heavier than the gluinos, the limit degrades.

---

[7]The 95% indicates we would detect events in 95 experiments out of 100 performed; it does not mean we are 95% sure about our result.

For the case where $M_{\tilde{q}}/M_{\tilde{g}} = 0.95$ we have two-body decays of the $\tilde{\chi}_1^\pm$ and $\tilde{\chi}_2^0$, so the acceptances are somewhat different. Figure 5.6 shows we set no limit for $M_{\tilde{q}}/M_{\tilde{g}} = 0.95$. Figure 5.7 is the lower limit on $M_{\tilde{\chi}_1^\pm}$ as a function of $M_{\tilde{q}}/M_{\tilde{g}}$. For all of these points we hold both $\tan\beta$ and μ constant and set them to 2 and -400 GeV/c^2, respectively. We also compare our $\sigma_{\tilde{\chi}_1^\pm \tilde{\chi}_2^0} \cdot \mathrm{BR}(\tilde{\chi}_1^\pm \tilde{\chi}_2^0 \to 3\ell + X)$ limit to that of D0 [46][8]. Their limit is weaker than ours for two reasons: they have somewhat poorer muon detection abilities, and use a higher P_T threshold for all of their leptons. It is very important to realize that every experiment makes slightly different assumptions about models and so limits cannot always be easily compared. D0 only examines SUGRA models (see below for that comparison).

Figure 5.8 compares the 95 % C.L. line to a variety of μ values: -200, -400 and -800 GeV/c^2. For this plot we set $\tan\beta = 2$ and $M_{\tilde{q}}/M_{\tilde{g}} = 2$. Recall that $|\mu|$ is the unmixed Higgsino mass, so as μ increases the Higgsino content of the $\tilde{\chi}_1^\pm$ and $\tilde{\chi}_2^0$ will decrease. However, as $|\mu|$ gets large, the masses of the $\tilde{\chi}_1^\pm$ and $\tilde{\chi}_2^0$ tends to increase. This decreases the production cross section, reducing our limit. This can be seen in Figure 5.8. Figure 5.9 is the lower limit on $M_{\tilde{\chi}_1^\pm}$ as a function of μ. For comparison, we indicate the ALEPH limit [47]. It is important to note that the ALEPH limit includes searches for hadronic final states of the $\tilde{\chi}_1^\pm$ and $\tilde{\chi}_2^0$, as well as the leptonic signature we use. Also, the LEP experiments (since LEP in an e^+e^- machine) are more sensitive to low values of $|\mu|$ while Tevatron experiments are more sensitive to high values of $|\mu|$. As with the D0 limit, ALEPH makes somewhat different model assumptions. They examine only SUGRA, which (see below) favors low $|\mu|$ values. However, their kinematic limit is quite model independent and can be compared with our limit.

Having varied both $M_{\tilde{q}}/M_{\tilde{g}}$ and μ, we now vary $\tan\beta$. Since the acceptance changes with $\tan\beta$, each 95% C.L. curve is on a separate plot. We show plots for $\tan\beta = 1.1$, 1.5, 2, 4 and 8. For these points we set $M_{\tilde{q}}/M_{\tilde{g}}$ and μ to 1 and -400 GeV/c^2, respectively. Figures 5.10-5.14 show the individual $\sigma \cdot BR$ plots for each $\tan\beta$ point and Figure 5.15 summarizes the lower limit on $M_{\tilde{\chi}_1^\pm}$ as a function of $\tan\beta$. As expected, the limit decreases as $\tan\beta$ increases.

We have also examined the $\tilde{\chi}_1^\pm$ mass limit for high $\tilde{q}$ mass. This region is interesting since, as mentioned above, the t-channel virtual $\tilde{q}$ exchange interferes destructively with the s-channel $W^\pm$ exchange. Regions of high $\tilde{q}$ mass effectively turn off t-channel production. Figure 5.16 shows the limit on $M_{\tilde{\chi}_1^\pm}$ for $M_{\tilde{q}} = 500$ GeV/c^2. For this plot we fix $M_{\tilde{q}}$ and allow $M_{\tilde{g}}$ to vary freely. Again, high $\tilde{q}$ masses lead to high $\tilde{\ell}$ masses, which lead to somewhat degraded limits.

Tables 5.2-5.6 list the input ($M_{\tilde{q}}$, $M_{\tilde{g}}$, $\tan\beta$ and μ) and the relevant output parameters ($M_{\tilde{\chi}_1^0}$, $M_{\tilde{\chi}_2^0}$, $M_{\tilde{\chi}_1^\pm}$, $M_{\tilde{\ell}_L}$, $M_{\tilde{\nu}_L}$, $M_{\tilde{\ell}_R}$ and the branching ratios to leptons) for each point examined in SiMSSM

---

[8]D0 plots their limit for an average branching ratio to leptons; we use a sum of branching ratios to e or μ. Thus, their result is scaled by a factor of 4 for comparison with ours.
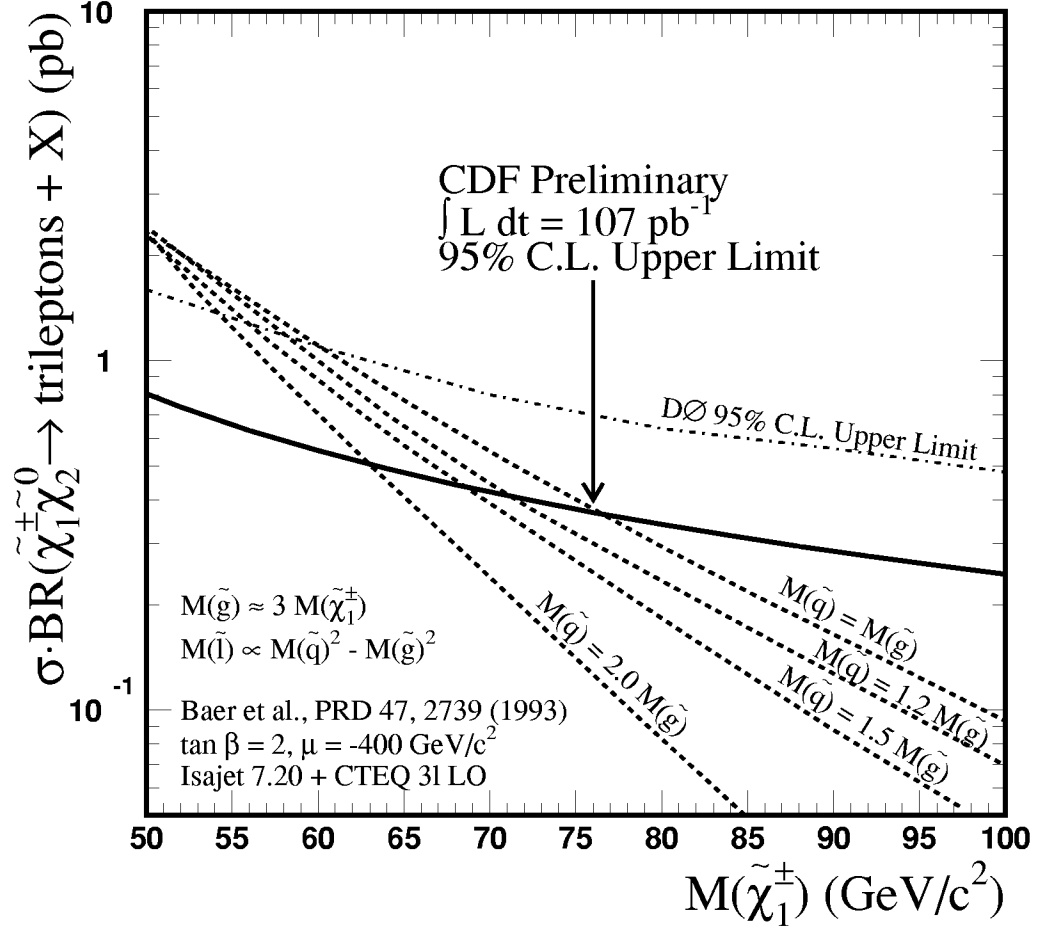
Figure 5.5: Production cross section times branching ratio to leptons (e or μ) for $\tilde{\chi}_1^{\pm} \tilde{\chi}_2^0$ production as a function of $\tilde{\chi}_1^{\pm}$ mass for $\tan \beta = 2$, and $\mu = -400$ GeV/c^2. The dashed lines are the theoretical prediction and the solid line is the 95% Confidence Level limit (using the fit to all $\tan \beta = 2$ points). We use ISAJET 7.20 with the CTEQ 3L structure functions to generate the Monte Carlo. As expected, the limit worsens as the squarks become much heavier than the gluinos. For comparison, we indicate the D0 95% C.L. limit [46].
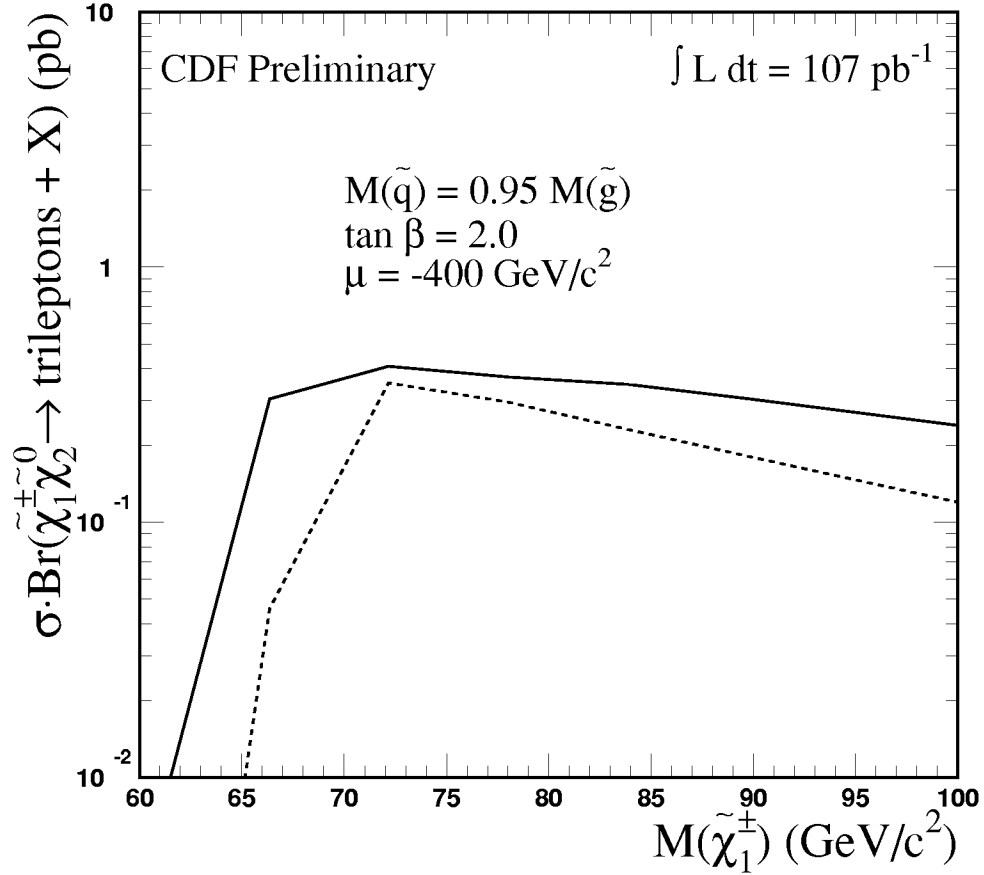
Figure 5.6: Production cross section times branching ratio to leptons (e or μ) for $\tilde{\chi}_1^{\pm}\tilde{\chi}_2^0$ production as a function of $\tilde{\chi}_1^{\pm}$ mass for $\tan\beta = 2$, $M_{\tilde{q}}/M_{\tilde{g}} = 0.95$ and $\mu = -400$ GeV/c^2. The dashed line is the theoretical prediction and the solid line is the 95% Confidence Level limit. We use ISAJET 7.20 with the CTEQ 3L structure functions to generate the Monte Carlo. We do not set a mass limit at this point; at low chargino masses the sneutrino is lighter than the sleptons so invisible decays dominate.
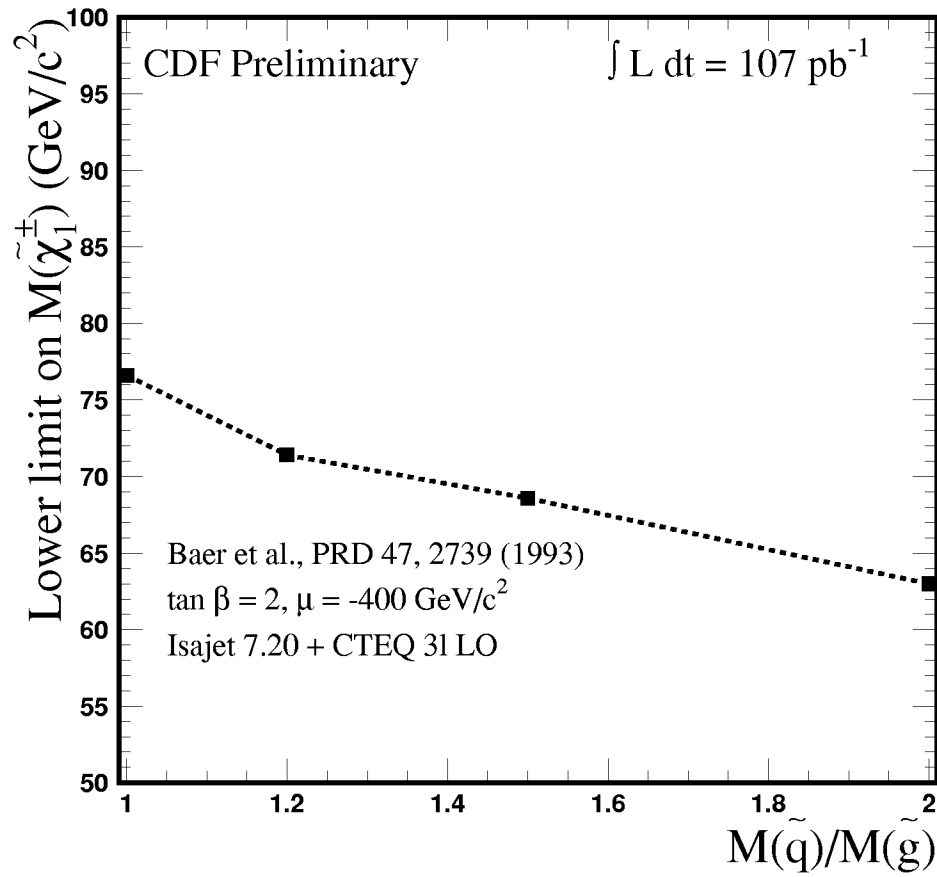
Figure 5.7: Limit on $M_{\tilde{\chi}_1^{\pm}}$ as a function of $M_{\tilde{q}}/M_{\tilde{g}}$. The limit decreases as the $\tilde{q}$s become much more

massive than the $\tilde{g}$s since the $\tilde{\ell}$ masses depend on the difference between them. Heavier $\tilde{\ell}$s lead to fewer decays via virtual $\tilde{\ell}$s and thus a smaller branching ratio to leptons.
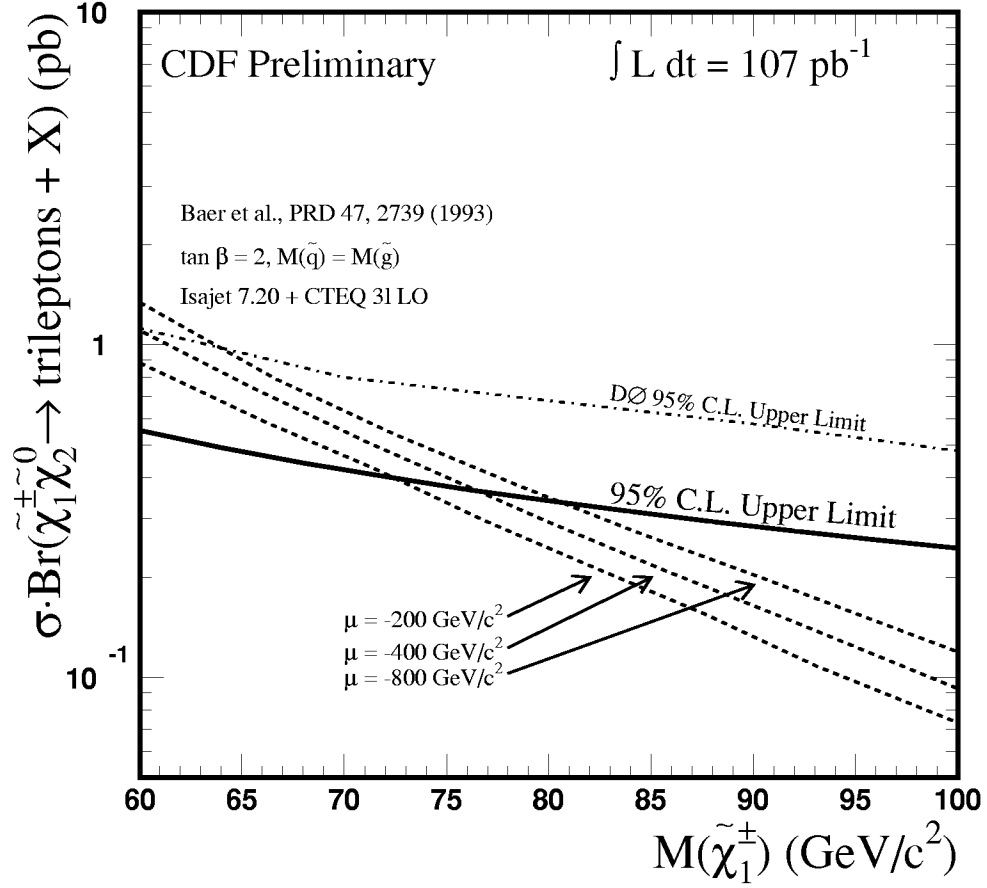
Figure 5.8: Production cross section times branching ratio to leptons (e or μ) for $\tilde{\chi}_1^{\pm}\tilde{\chi}_2^0$ production as a function of $\tilde{\chi}_1^{\pm}$ mass for $\tan\beta = 2$, and $M_{\tilde{q}} = M_{\tilde{g}}$. The dashed lines are the theoretical prediction and the solid line is the 95% Confidence Level limit (using the fit to all $\tan\beta = 2$ points). We use ISAJET 7.20 with the CTEQ 3L structure functions to generate the Monte Carlo. For comparison, we indicate the D0 95% C.L. limit [46].

Search for SUSY using p̄p → eee, eeμ, eμμ, μμμ
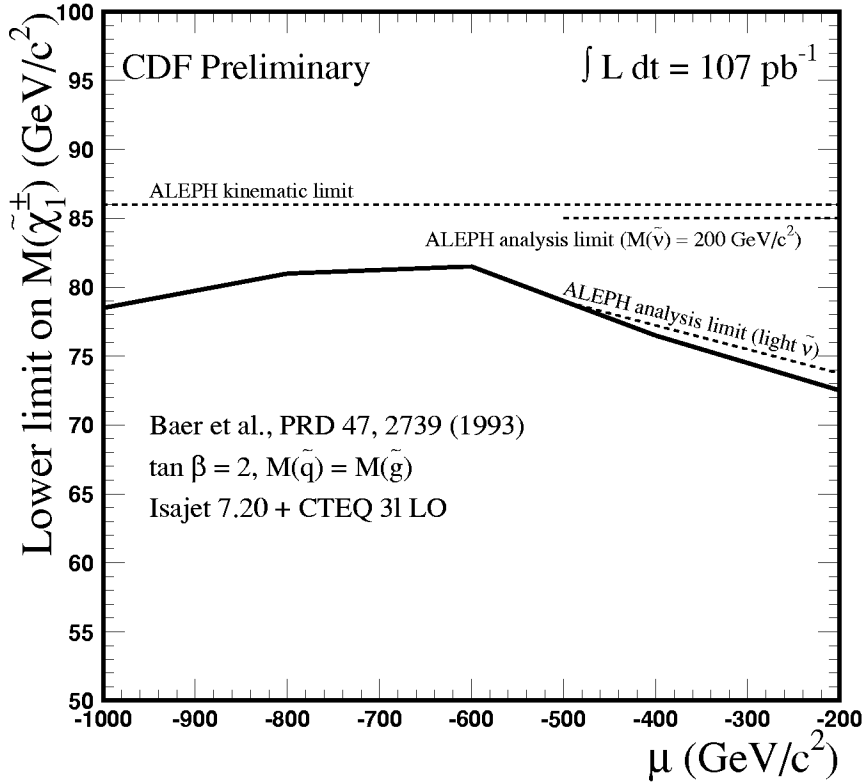
Figure 5.9: The solid curve is the limit on $M_{\tilde{\chi}_1^\pm}$ as a function of μ. The maximum limit is 81.5 GeV/c^2, for μ = -600 GeV/c^2. For comparison, we show the ALEPH limit (dashed lines) [47]. The kinematic limit is half the LEP-II center-of-mass energy. It is important to realize that ALEPH searches for several final states, not only the trilepton state searched for in this analysis. Just as the s- and t-channels interfere at the Tevatron, so do they at LEP (where the production mechanism is via virtual sneutrino exchange). Thus, higher $\tilde{\nu}$ masses result in higher production cross sections, but since ALEPH searches for all possible final states, they do not have the degradation in branching ratio we do. For the best comparison, we include the ALEPH limit for light $\tilde{\nu}$. Also, ALEPH only examines SUGRA, which tends to keep $|\mu| < 500$ GeV/c^2.
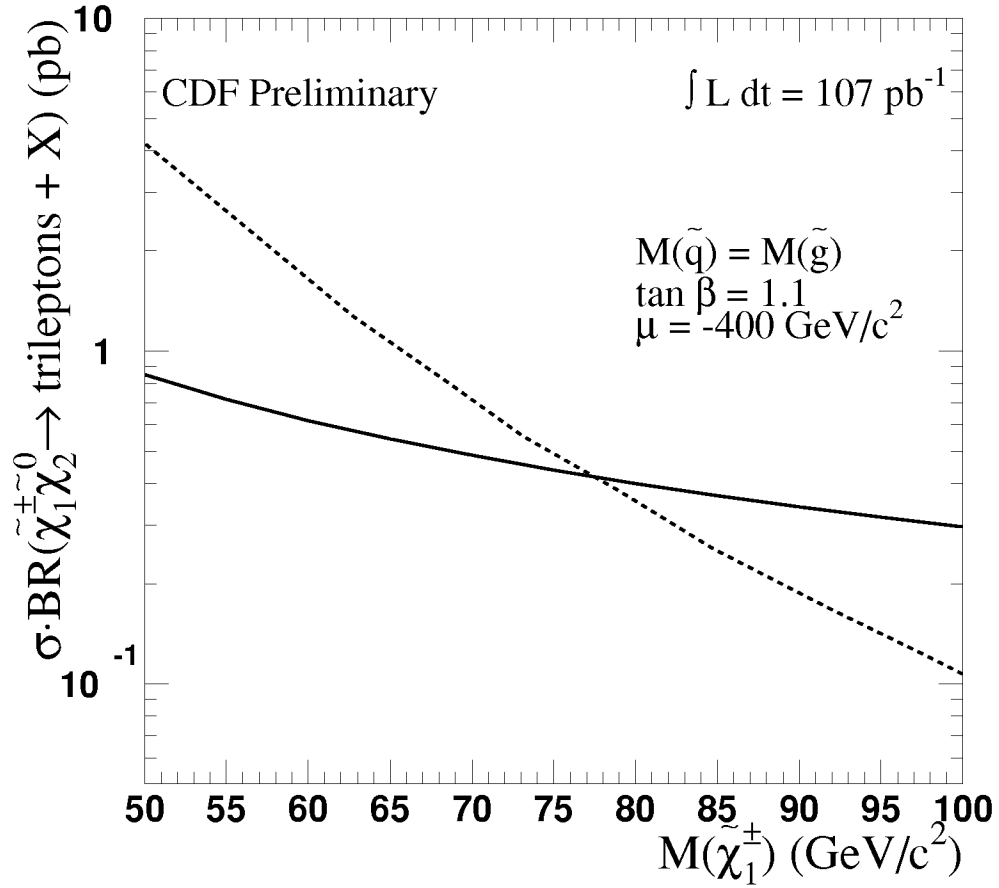
Figure 5.10: Production cross section times branching ratio to leptons (e or μ) for $\tilde{\chi}_1^\pm \tilde{\chi}_2^0$ production as a function of $\tilde{\chi}_1^\pm$ mass for $\tan\beta = 1.1$, $M(\tilde{q}) = M(\tilde{g})$ and $\mu = -400$ GeV/c^2. The dashed line is the theoretical prediction and the solid line is the 95% Confidence Level limit. We use ISAJET 7.20 with the CTEQ 3L structure functions to generate the Monte Carlo.
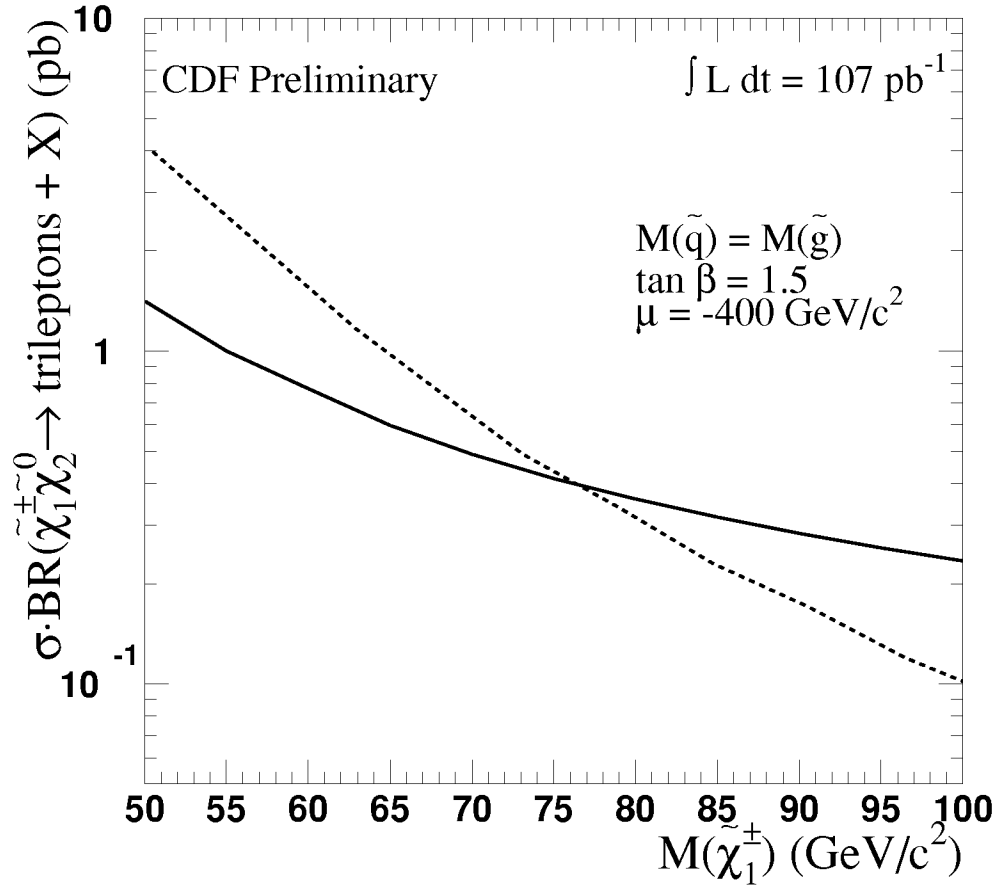
Figure 5.11: Production cross section times branching ratio to leptons (e or μ) for $\tilde{\chi}_1^{\pm}\tilde{\chi}_2^0$ production as a function of $\tilde{\chi}_1^{\pm}$ mass for $\tan\beta = 1.5$, $M(\tilde{q}) = M(\tilde{g})$ and $\mu = -400$ GeV/c^2. The dashed line is the theoretical prediction and the solid line is the 95% Confidence Level limit. We use ISAJET 7.20 with the CTEQ 3L structure functions to generate the Monte Carlo.
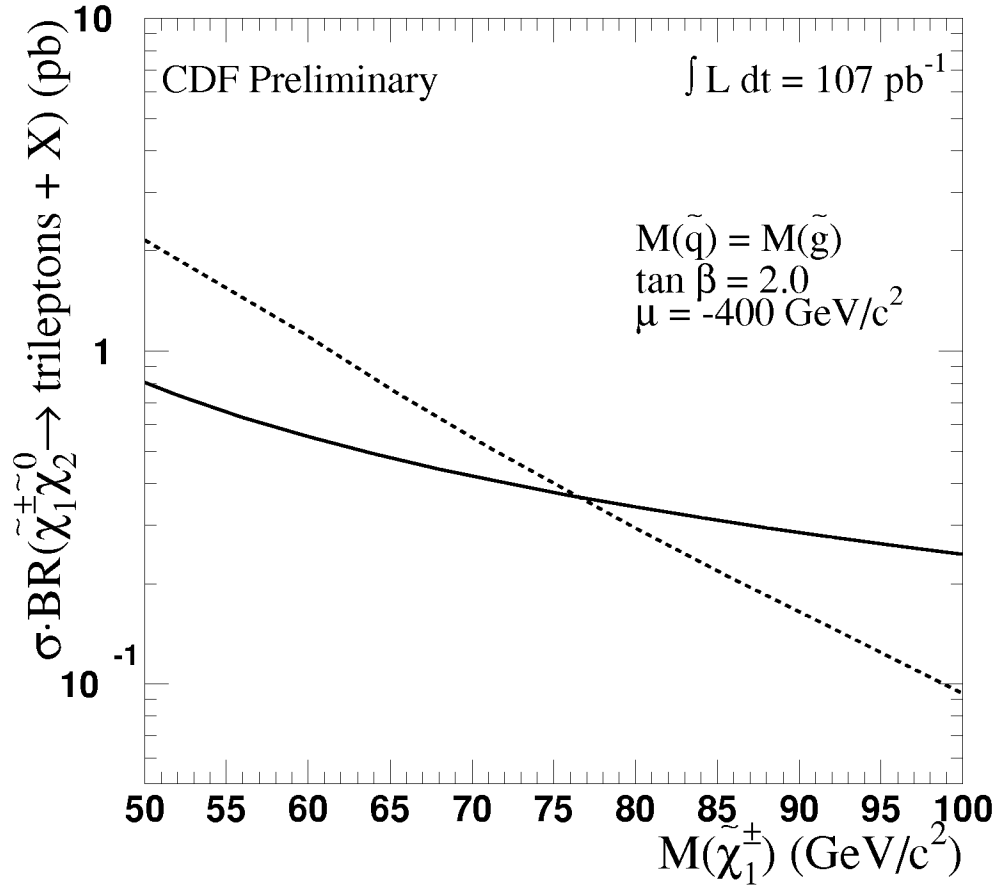
Figure 5.12: Production cross section times branching ratio to leptons (e or μ) for $\tilde{\chi}_1^{\pm}\tilde{\chi}_2^0$ production as a function of $\tilde{\chi}_1^{\pm}$ mass for $\tan\beta = 2$, $M(\tilde{q}) = M(\tilde{g})$ and $\mu = -400\ \mathrm{GeV}/c^2$. The dashed line is the theoretical prediction and the solid line is the 95% Confidence Level limit. We use ISAJET 7.20 with the CTEQ 3L structure functions to generate the Monte Carlo.
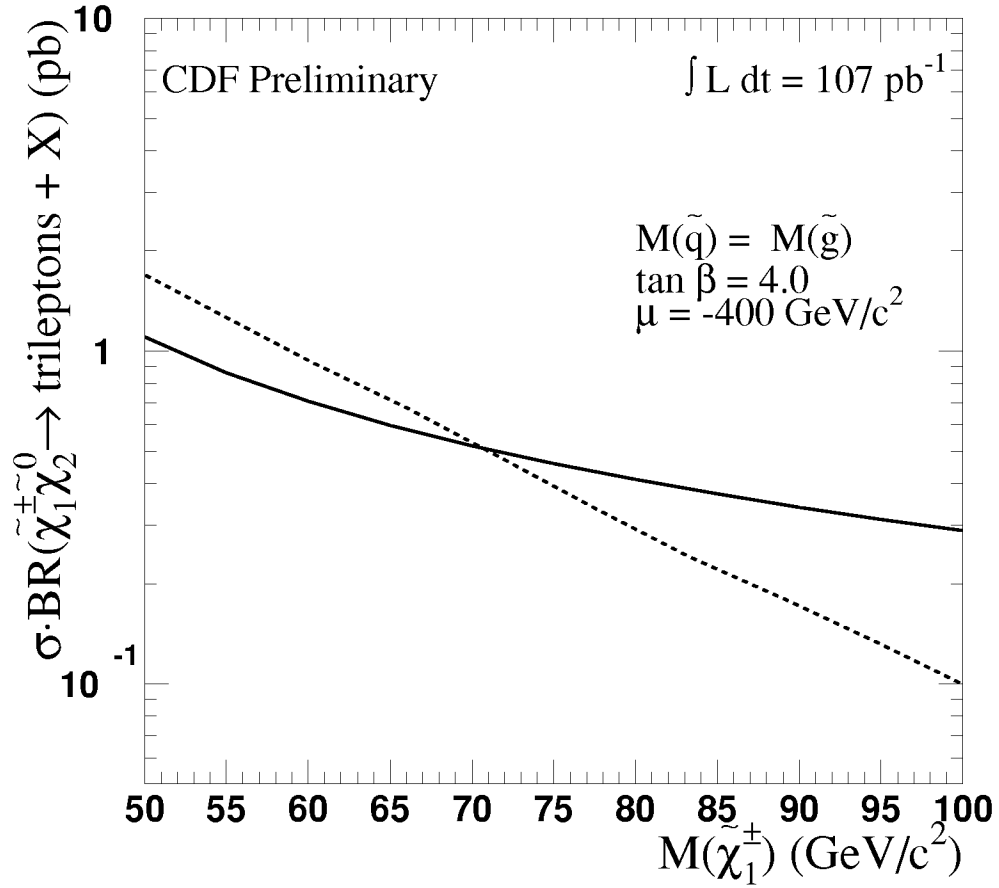
Figure 5.13: Production cross section times branching ratio to leptons (e or μ) for $\tilde{\chi}_1^{\pm}\tilde{\chi}_2^0$ production as a function of $\tilde{\chi}_1^{\pm}$ mass for $\tan\beta = 4$, $M(\tilde{q}) = M(\tilde{g})$ and $\mu = -400$ GeV/c^2. The dashed line is the theoretical prediction and the solid line is the 95% Confidence Level limit. We use ISAJET 7.20 with the CTEQ 3L structure functions to generate the Monte Carlo.
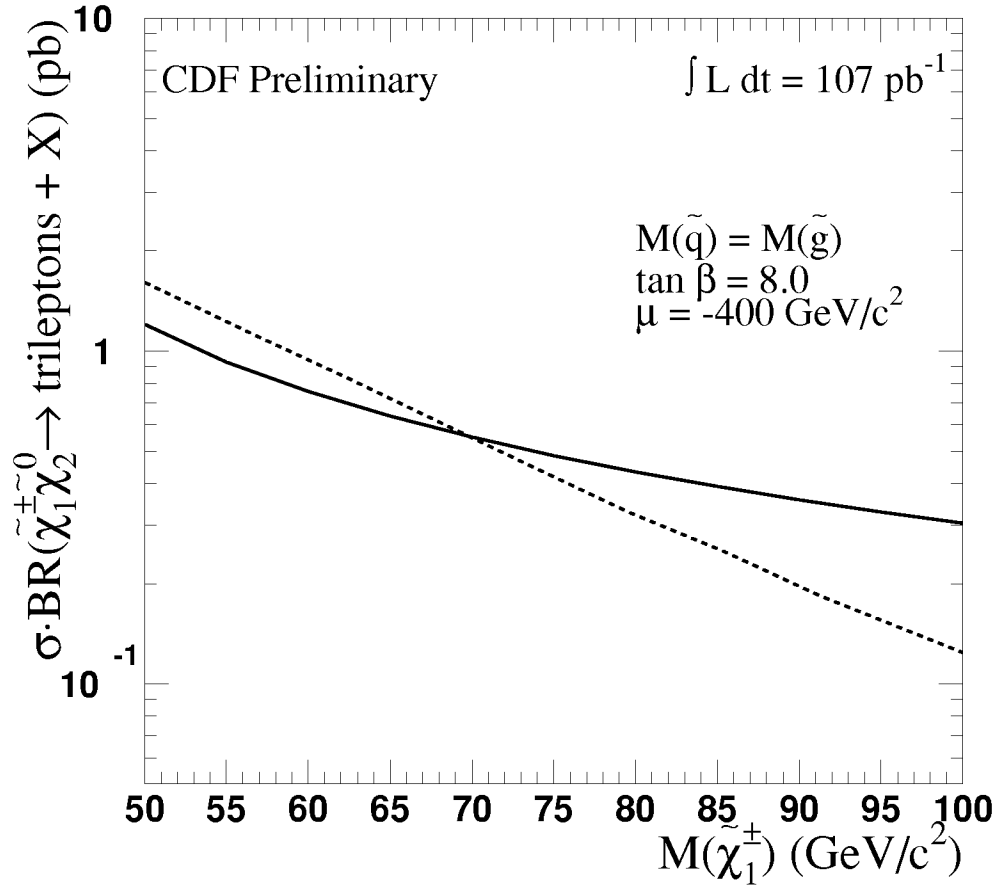
Figure 5.14: Production cross section times branching ratio to leptons (e or μ) for $\tilde{\chi}_1^\pm \tilde{\chi}_2^0$ production as a function of $\tilde{\chi}_1^\pm$ mass for $\tan\beta = 8$, $M(\tilde{q}) = M(\tilde{g})$ and $\mu = -400$ GeV/c^2. The dashed line is the theoretical prediction and the solid line is the 95% Confidence Level limit. We use ISAJET 7.20 with the CTEQ 3L structure functions to generate the Monte Carlo.
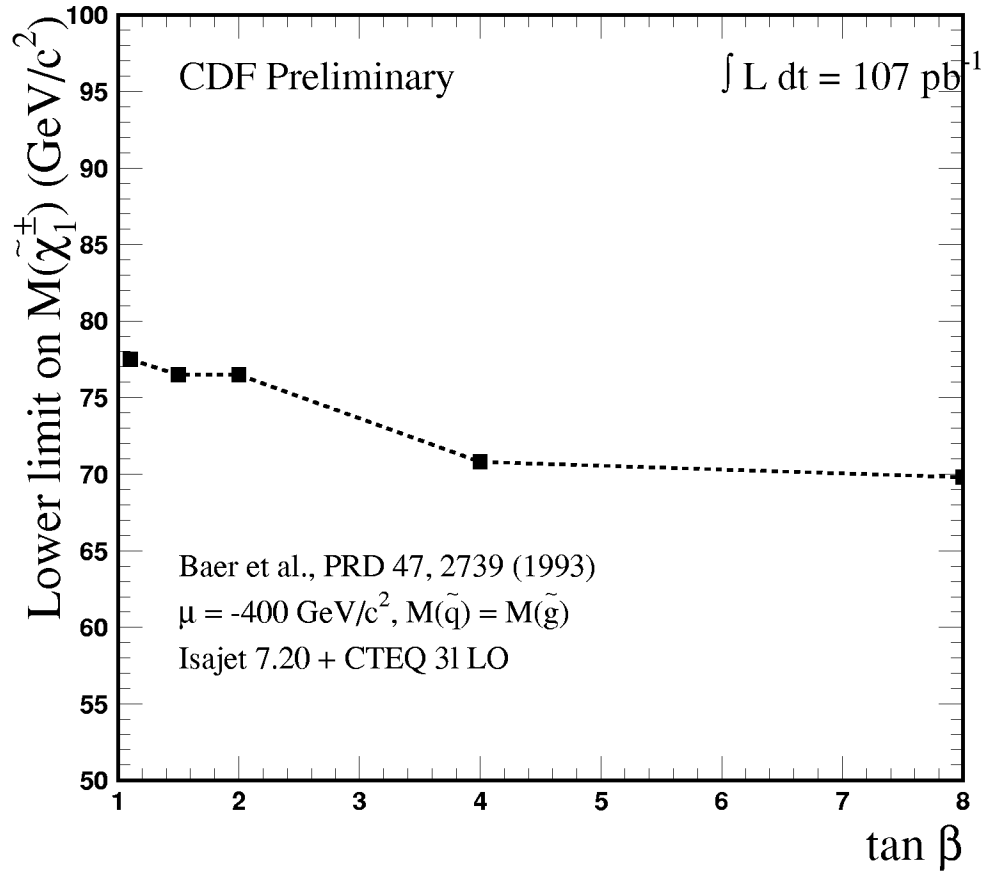
Figure 5.15: Lower limit on $M(\tilde{\chi}_1^{\pm})$ as a function of $\tan\beta$ for, $M(\tilde{q}) = M(\tilde{g})$ and $\mu = -400$ GeV/c^2. As expected, the limit decreases as $\tan\beta$ increases.
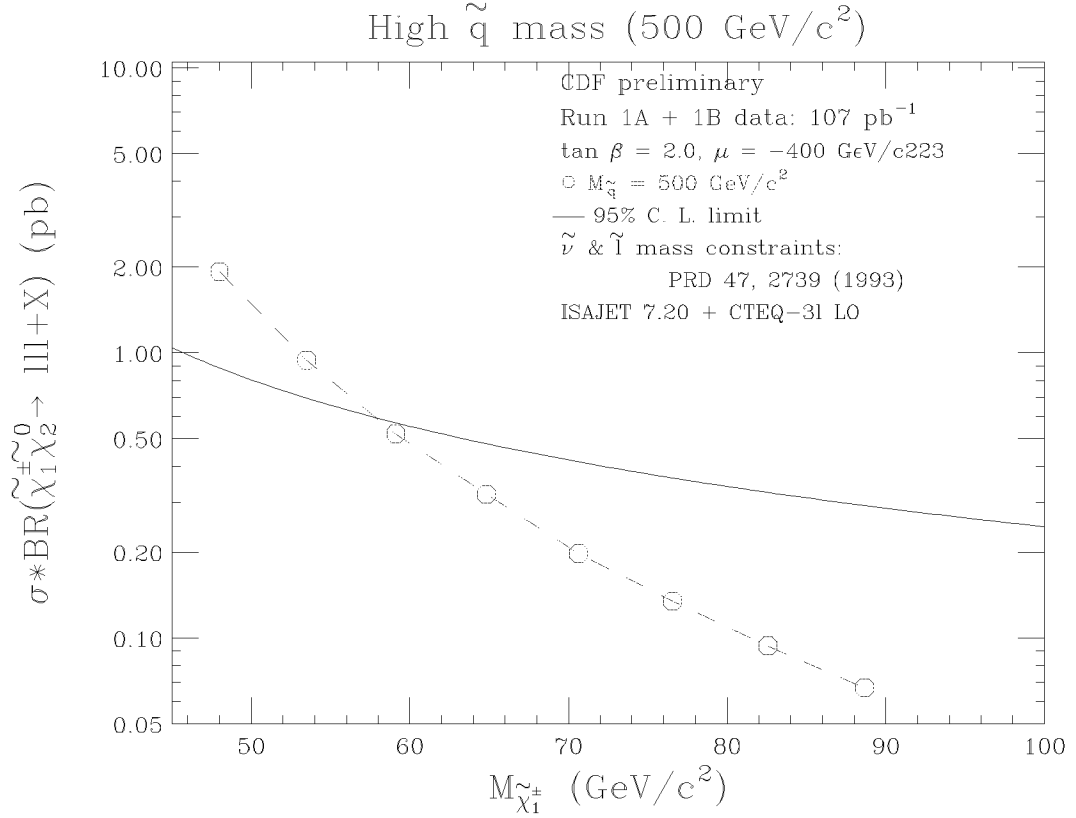
Figure 5.16: Production cross section times branching ratio to leptons (e or μ) for $\tilde{\chi}_1^{\pm}\tilde{\chi}_2^0$ production as a function of $\tilde{\chi}_1^{\pm}$ mass for $\tan\beta = 2$ and $\mu = -400$ GeV/c^2 and $M_{\tilde{q}} = 500$ GeV/c^2. The dashed line is the theoretical prediction and the solid line is the 95% Confidence Level limit (using the fit to all $\tan\beta = 2$ points). We use ISAJET 7.20 with the CTEQ 3L structure functions to generate the Monte Carlo.

112

Table 5.2: Input and output parameters for the SiMSSM points scanned. All masses are in GeV/c^2 and all σ are in picobarns.

	Input		Output										
Set	$\tilde{q}$	$\tilde{g}$	$\tilde{\chi}_1^0$	$\tilde{\chi}_2^0$	$\tilde{\chi}_1^\pm$	$\tilde{\ell}_L$	$\tilde{\nu}$	$\tilde{\ell}_R$	BR$\to\ell\ell$	BR$\to\ell\nu$	BR$\to 3\ell$	σ	$\sigma\cdot$BR
	(GeV/c^2)		(GeV/c^2)						$\tilde{\chi}_2^0$	$\tilde{\chi}_1^\pm$	Total		
$\mathrm{M}_{\tilde{q}}\simeq\mathrm{M}_{\tilde{g}}$, $\mu=-400$ GeV/c^2, $\tan\beta=2.0$													
14.1	180	179	26.7	60.7	59.7	101.8	80.7	92.6	0.321	0.461	0.148	7.66	1.13
11	200	199	29.7	66.3	65.4	111.5	92.7	101.3	0.348	0.433	0.151	4.98	0.75
12	199	200	29.9	66.7	65.8	108.4	88.9	97.7	0.331	0.455	0.151	4.80	0.72
14.2	220	219	32.7	71.9	71.1	121.4	104.4	110.2	0.364	0.409	0.149	3.42	0.51
13	250	249	37.3	80.5	79.8	136.3	121.4	123.6	0.377	0.377	0.142	2.09	0.30
14	249	250	37.5	80.9	80.2	133.1	117.8	120.0	0.370	0.393	0.145	2.03	0.30
14.3	270	269	40.3	86.3	85.7	146.4	132.6	132.7	0.381	0.359	0.137	1.53	0.21
14.4	290	289	43.3	92.1	91.5	156.4	143.6	141.8	0.384	0.342	0.131	1.15	0.15
14.5	310	309	46.4	97.9	97.4	166.6	154.6	150.9	0.384	0.326	0.125	0.88	0.11
High $\mathrm{M}_{\tilde{q}}$ ($\mathrm{M}_{\tilde{q}}=500$ GeV/c^2), $\mu=-400$ GeV/c^2, $\tan\beta=2.0$													
15	500	160	20.5	49.2	48.0	482.4	478.4	480.8	0.212	0.222	0.047	41.08	1.93
16	500	180	23.4	54.6	53.5	477.2	473.1	475.3	0.198	0.222	0.044	21.50	0.94
17	500	200	26.4	60.1	59.1	471.3	467.2	469.0	0.187	0.222	0.041	12.58	0.52
18	500	220	29.4	65.7	64.8	464.8	460.6	462.0	0.178	0.222	0.039	8.11	0.32
19	500	240	32.5	71.4	70.6	457.5	453.3	454.1	0.171	0.221	0.038	5.23	0.20
19.1	500	260	35.6	77.2	76.6	449.4	445.1	445.4	0.166	0.221	0.037	2.61	0.09
19.2	500	280	38.7	83.2	82.6	440.6	436.2	435.9	0.163	0.221	0.036	3.67	0.13
19.3	500	300	41.8	89.2	88.6	430.9	426.4	425.4	0.162	0.221	0.036	1.87	0.07
$\mathrm{M}_{\tilde{q}}=1.2\mathrm{M}_{\tilde{g}}$, $\mu=-400$ GeV/c^2, $\tan\beta=2.0$													
34.1	180	150	21.7	51.5	50.3	131.6	116.1	126.5	0.421	0.292	0.122	23.96	2.94
30	240	200	29.1	65.0	64.1	172.5	161.0	166.0	0.418	0.261	0.109	6.40	0.70
31	264	220	32.0	70.5	69.7	189.0	178.5	181.9	0.411	0.253	0.104	4.37	0.45
32	276	230	33.5	73.3	72.5	197.3	187.3	189.9	0.407	0.249	0.102	3.68	0.37
33	288	240	34.9	76.0	75.3	205.5	196.0	197.9	0.403	0.246	0.099	3.16	0.31
34	312	260	37.9	81.6	81.0	222.1	213.3	213.9	0.392	0.241	0.094	2.34	0.22
34.2	336	280	40.8	87.2	86.6	238.8	230.6	230.0	0.379	0.237	0.090	1.85	0.17
34.3	360	300	43.7	92.8	92.3	255.4	247.8	246.1	0.363	0.233	0.084	1.31	0.11

space.

5.4 Limits on other models

The limits we set above are rather general. We can also examine somewhat more specific models and set limits on them. We examine two models: a SU(5)×U(1) Supergravity model and a somewhat more general supergravity model known simply as SUGRA.

5.4.1 SU(5)×U(1) Supergravity model

The string-derived SU(5) × U(1) one parameter supergravity model [48] predicts

Table 5.3: Input and output parameters for the SiMSSM points scanned. All masses are in GeV/c² and all σ are in picobarns.

Set	$\tilde{q}$	$\tilde{g}$	$\tilde{\chi}_1^0$	$\tilde{\chi}_2^0$	$\tilde{\chi}_1^\pm$	$\tilde{\ell}_L$	$\tilde{\nu}$	$\tilde{\ell}_R$	BR→$\ell\ell$ $\tilde{\chi}_2^0$	BR→$\ell\nu$ $\tilde{\chi}_1^\pm$	BR→3ℓ Total	σ	σ·BR
	(GeV/c²)				(GeV/c²)								
$M_{\tilde{q}} = 1.5 M_{\tilde{g}}$, $\mu = -400$ GeV/c², $\tan\beta = 2.0$													
39.1	225	150	21.1	50.4	49.1	188.5	178.1	185.0	0.407	0.237	0.096	31.04	3.00
35	270	180	25.3	58.1	57.1	224.9	216.2	220.9	0.394	0.231	0.091	12.52	1.14
36	300	200	28.2	63.4	62.5	249.3	241.5	244.8	0.379	0.228	0.086	8.19	0.71
37	315	210	29.6	66.1	65.2	261.5	254.0	256.9	0.369	0.227	0.084	6.73	0.56
38	330	220	31.0	68.7	67.9	273.7	266.6	268.9	0.359	0.226	0.081	5.68	0.46
39	360	240	33.9	74.1	73.3	298.2	291.7	293.0	0.332	0.225	0.075	4.08	0.30
39.2	405	270	38.1	82.1	81.5	334.9	329.1	329.1	0.283	0.223	0.063	2.75	0.17
39.3	450	300	42.4	90.3	89.8	371.7	366.5	365.3	0.227	0.222	0.050	1.57	0.08
$M_{\tilde{q}} \simeq M_{\tilde{g}}$, $\mu = -200$ GeV/c², $\tan\beta = 2.0$													
214.1	160	159	24.5	62.8	60.9	92.1	68.2	83.8	0.355	0.401	0.142	5.51	0.78
214.2	180	179	27.6	67.8	66.2	101.8	80.7	92.5	0.419	0.364	0.152	3.83	0.58
214.3	200	199	30.7	72.9	71.5	111.5	92.7	101.3	0.444	0.336	0.149	2.83	0.42
214.4	220	219	33.8	78.0	76.9	121.4	104.4	110.2	0.455	0.313	0.142	2.08	0.30
211	240	239	36.9	83.1	82.3	131.3	115.8	119.1	0.456	0.292	0.133	1.61	0.21
212	260	259	40.0	88.3	87.7	141.3	127.0	128.2	0.450	0.274	0.123	1.26	0.16
213	280	279	43.0	93.5	93.1	151.4	138.1	137.2	0.435	0.258	0.112	0.97	0.11
214	300	299	46.1	98.8	98.5	161.5	149.1	146.3	0.411	0.243	0.100	0.77	0.08
$M_{\tilde{q}} \simeq M_{\tilde{g}}$, $\mu = -800$ GeV/c², $\tan\beta = 2.0$													
234.1	200	199	28.8	61.1	60.7	111.5	92.7	101.3	0.275	0.540	0.149	9.03	1.34
230	220	219	31.8	66.9	66.6	121.4	104.4	110.2	0.295	0.521	0.153	5.15	0.79
231	240	239	34.8	72.8	72.5	131.3	115.8	119.1	0.308	0.503	0.155	3.47	0.54
232	260	259	37.8	78.7	78.5	141.3	127.0	128.2	0.317	0.485	0.154	2.47	0.38
233	280	279	40.8	84.7	84.5	151.4	138.1	137.2	0.324	0.467	0.151	1.79	0.27
234	300	299	43.8	90.6	90.4	161.5	149.1	146.3	0.329	0.450	0.148	1.35	0.20
234.2	340	319	46.3	95.6	95.5	206.5	197.0	193.3	0.348	0.336	0.117	1.13	0.13
234.3	340	339	49.9	102.1	102.5	181.8	170.9	164.6	0.336	0.416	0.134	0.75	0.10
$M_{\tilde{q}} \simeq M_{\tilde{g}}$, $\mu = -400$ GeV/c², $\tan\beta = 1.5$													
15.3	160	159	23.9	57.4	55.9	89.5	74.5	81.3	0.405	0.471	0.191	10.36	1.97
15.2	180	179	26.9	62.9	61.6	99.4	86.1	90.2	0.420	0.443	0.186	6.26	1.16
270	220	219	33.0	74.2	73.1	119.4	108.6	108.3	0.429	0.395	0.169	2.88	0.49
271	240	239	36.1	79.9	78.9	129.5	119.6	117.4	0.429	0.374	0.160	2.13	0.34
272	260	259	39.1	85.6	84.7	139.6	130.5	126.5	0.427	0.356	0.152	1.52	0.23
273	280	279	42.1	91.4	90.6	149.8	141.3	135.7	0.424	0.339	0.144	1.18	0.17
274	300	299	45.2	97.2	96.5	160.0	152.1	144.9	0.421	0.325	0.137	0.91	0.12
15.1	320	319	48.3	103.1	102.4	170.2	162.8	154.1	0.418	0.311	0.130	0.68	0.09

Table 5.4: Input and output parameters for the SiMSSM points scanned. All masses are in GeV/c^2 and all σ are in picobarns.

Set	Input $\tilde{q}$ $\tilde{g}$ (GeV/c^2)		$\tilde\chi^0_1$	$\tilde\chi^0_2$	$\tilde\chi^\pm_1$	$\tilde\ell_L$	$\tilde\nu$	$\tilde\ell_R$	BR$\to\ell\ell$ $\tilde\chi^0_2$	BR$\to\ell\nu$ $\tilde\chi^\pm_1$	BR$\to3\ell$ Total	σ	$\sigma\cdot$BR
					(GeV/c^2)								
High M$_{\tilde{q}}$ (M$_{\tilde{q}}=500$) GeV/c^2, $\mu=-400$ GeV/c^2, $\tan\beta=1.5$													
277	500	200	26.6	62.4	61.0	471.3	467.2	469.0	0.261	0.222	0.058	10.47	0.61
278	500	220	29.7	68.0	66.8	464.2	461.6	461.5	0.255	0.222	0.057	6.79	0.39
279	500	240	32.7	73.7	72.6	457.0	454.3	453.7	0.250	0.222	0.056	4.57	0.25
M$_{\tilde{q}}\simeq$M$_{\tilde{g}}$, $\mu=-400$ GeV/c^2, $\tan\beta=1.1$													
11.4	160	159	24.0	58.8	57.1	85.8	82.2	77.9	0.517	0.476	0.246	8.89	2.19
11.3	180	179	27.0	64.3	62.8	96.0	92.8	87.1	0.507	0.448	0.227	5.58	1.27
11.2	200	199	30.1	69.9	68.5	106.3	103.4	96.4	0.496	0.422	0.209	3.85	0.81
280	220	219	33.1	75.5	74.3	116.6	114.0	105.7	0.488	0.398	0.194	2.86	0.56
281	240	239	36.2	81.2	80.1	126.9	124.5	115.0	0.478	0.377	0.180	2.12	0.38
282	260	259	39.3	87.0	85.9	137.3	135.1	124.3	0.469	0.359	0.168	1.51	0.25
283	280	279	42.3	92.7	91.8	147.6	145.5	133.7	0.457	0.342	0.156	1.08	0.17
284	300	299	45.4	98.6	97.7	158.0	156.0	143.0	0.446	0.328	0.146	0.83	0.12
11.1	320	319	48.4	104.4	103.6	168.3	166.5	152.3	0.434	0.315	0.137	0.64	0.09
M$_{\tilde{q}}\simeq$M$_{\tilde{g}}$, $\mu=-1000$ GeV/c^2, $\tan\beta=2$													
1k.2	220	219	31.5	65.7	65.5	121.3	104.3	110.1	0.278	0.554	0.154	5.72	0.88
1k.3	240	239	34.5	71.6	71.5	131.3	115.7	119.1	0.293	0.538	0.157	3.87	0.61
1k.4	260	259	37.5	77.6	77.4	141.3	127.0	128.1	0.303	0.522	0.158	2.64	0.41
1k.5	280	279	40.5	83.6	83.4	151.4	138.1	137.2	0.311	0.506	0.157	1.85	0.29
1k.6	300	299	43.5	89.6	89.4	161.5	149.1	146.3	0.316	0.490	0.155	1.41	0.21
1k.7	320	319	46.5	95.6	95.4	171.6	160.0	155.4	0.321	0.474	0.152	1.05	0.16
1k.8	340	339	49.6	101.6	101.5	181.8	170.9	164.6	0.324	0.458	0.148	0.77	0.11
M$_{\tilde{q}}\simeq$M$_{\tilde{g}}$, $\mu=-600$ GeV/c^2, $\tan\beta=2$													
600.1	200	199	29.1	62.9	62.4	111.5	92.7	101.2	0.301	0.496	0.149	6.79	1.02
600.2	220	219	32.1	68.7	68.2	121.3	104.3	110.1	0.319	0.474	0.151	4.54	0.68
600.3	240	239	35.1	74.5	74.1	131.3	115.7	119.1	0.331	0.453	0.150	3.10	0.46
600.4	260	259	38.1	80.4	80.0	141.3	127.0	128.1	0.339	0.433	0.147	2.16	0.31
600.5	280	279	41.1	86.3	85.9	151.4	138.1	137.2	0.345	0.415	0.143	1.56	0.22
600.6	300	299	44.2	92.2	91.9	161.5	149.1	146.3	0.348	0.397	0.138	1.19	0.16
600.7	320	319	47.2	98.2	97.9	171.6	160.0	155.4	0.351	0.380	0.133	0.90	0.12
600.8	340	339	50.3	104.1	103.9	181.8	170.9	164.6	0.353	0.364	0.128	0.68	0.08

Table 5.5: Input and output parameters for the SiMSSM points scanned. All masses are in GeV/c^2 and all σ are in picobarns. Note that the $\tilde{\chi}_2^0$ branching ratio is quite small for the cases where the $\tilde{q}$ is lighter than the $\tilde{g}$.

Set	Input $\tilde{q}$ (GeV/c^2)	$\tilde{g}$	Output $\tilde{\chi}_1^0$	$\tilde{\chi}_2^0$	$\tilde{\chi}_1^\pm$	$\tilde{\ell}_L$ (GeV/c^2)	$\tilde{\nu}$	$\tilde{\ell}_R$	BR→$\ell\ell$ $\tilde{\chi}_2^0$	BR→$\ell\nu$ $\tilde{\chi}_1^\pm$	BR→3ℓ Total	σ	σ·BR
M$_{\tilde{q}} = 2$M$_{\tilde{g}}$, $\mu = -400$ GeV/c^2, $\tan\beta = 2$												
20.1	300	150	20.3	48.9	47.7	273.7	266.6	271.2	0.359	0.224	0.080	39.52	3.18
20.2	340	170	23.0	53.9	52.8	309.5	303.3	306.9	0.336	0.223	0.074	21.38	1.60
20.3	380	190	25.7	58.9	57.9	345.5	339.9	342.6	0.302	0.222	0.067	13.15	0.88
20.4	420	210	28.5	64.0	63.1	381.5	376.4	378.3	0.259	0.222	0.057	8.63	0.49
20.5	460	230	31.2	69.1	68.3	417.5	412.9	414.1	0.213	0.221	0.047	6.04	0.28
20.6	500	250	34.0	74.3	73.5	453.5	449.3	449.8	0.168	0.221	0.037	4.39	0.16
20.7	540	270	36.7	79.5	78.8	489.6	485.6	485.6	0.128	0.221	0.028	3.27	0.09
M$_{\tilde{q}} \sim$ M$_{\tilde{g}}$, $\mu = -400$ GeV/c^2, $\tan\beta = 4$												
4.8	160	159	23.0	49.2	48.9	95.5	59.0	87.0	0.090	0.606	0.055	29.56	1.62
4.2	200	199	28.9	60.4	60.2	114.3	86.2	103.9	0.204	0.539	0.110	8.44	0.93
4.3	220	219	31.8	66.1	65.9	123.9	98.6	112.6	0.237	0.514	0.122	5.56	0.68
4.4	240	239	34.8	71.8	71.7	133.7	110.6	121.4	0.261	0.492	0.128	3.74	0.48
4.5	260	259	37.8	77.6	77.5	143.6	122.3	130.2	0.278	0.471	0.131	2.58	0.34
4.6	280	279	40.8	83.4	83.3	153.5	133.8	139.2	0.290	0.450	0.131	1.84	0.24
4.7	300	299	43.8	89.2	89.1	163.5	145.1	148.2	0.298	0.429	0.128	1.40	0.18
4.10	320	319	46.8	95.0	955.0	173.5	156.3	157.2	0.304	0.408	0.124	1.06	0.13
4.11	340	339	49.8	100.9	100.9	183.5	167.4	166.3	0.306	0.387	0.118	0.80	0.10
M$_{\tilde{q}} \sim$ M$_{\tilde{g}}$, $\mu = -400$ GeV/c^2, $\tan\beta = 8$												
8.1	180	179	25.9	51.0	51.0	105.8	70.6	96.2	0.100	0.637	0.064	23.54	1.51
8.2	200	199	28.1	56.7	56.7	115.2	84.0	104.7	0.144	0.627	0.090	12.45	1.12
8.3	220	219	31.0	62.4	62.4	124.8	96.7	113.3	0.178	0.616	0.110	7.58	0.83
8.5	260	259	36.9	73.8	73.9	144.2	120.8	130.9	0.224	0.596	0.133	3.34	0.45
8.6	280	279	39.9	79.6	79.7	154.1	132.5	139.8	0.238	0.584	0.139	2.34	0.33
8.7	300	299	42.9	85.4	85.5	164.0	143.9	148.7	0.249	0.570	0.142	1.75	0.25
8.9	320	319	45.9	91.3	91.3	174.0	155.2	157.7	0.256	0.552	0.141	1.30	0.18
8.10	340	339	48.9	97.1	97.1	184.1	166.4	166.8	0.260	0.530	0.138	0.97	0.13
M$_{\tilde{q}} = 0.9$ M$_{\tilde{g}}$, $\mu = -400$ GeV/c^2, $\tan\beta = 2$												
2	180	200	30.6	67.8	67.0	67.4	26.6	48.5	0.006	0.667	0.004	4.03	0.01
3	198	220	33.6	73.6	72.9	72.2	37.1	51.0	0.008	0.667	0.005	2.80	0.01
4	216	240	36.7	79.5	78.8	77.2	46.0	53.6	0.011	0.667	0.007	1.93	0.01
5	234	260	39.8	85.3	84.7	82.2	54.0	56.3	0.016	0.667	0.010	1.38	0.01
6	252	280	42.9	91.3	90.7	87.3	61.5	59.2	0.022	0.667	0.014	1.05	0.02
7	270	300	46.0	97.2	96.7	92.4	68.6	62.0	0.028	0.667	0.019	0.80	0.02

Table 5.6: Input and output parameters for the SiMSSM points scanned. All masses are in GeV/c^2 and all σ are in picobarns.

	Input		Output										
Set	$\tilde{q}$	$\tilde{g}$	$\tilde{\chi}_1^0$	$\tilde{\chi}_2^0$	$\tilde{\chi}_1^\pm$	$\tilde{\ell}_L$	$\tilde{\nu}$	$\tilde{\ell}_R$	BR→$\ell\ell$ $\tilde{\chi}_2^0$	BR→$\ell\nu$ $\tilde{\chi}_1^\pm$	BR→3ℓ Total	σ	σ·BR
	(GeV/c^2)		(GeV/c^2)										
$M_{\tilde{q}} = 0.95\,M_{\tilde{g}}$, $\mu = -400$ GeV/c^2, $\tan\beta = 2$													
2	190	200	30.2	67.2	66.3	90.8	66.4	77.8	0.017	0.620	0.010	4.49	0.05
3	209	220	33.3	72.9	72.2	98.5	76.5	84.1	0.197	0.576	0.114	3.09	0.35
4	228	240	36.3	78.7	78.0	106.2	86.2	90.6	0.250	0.549	0.137	2.16	0.30
5	247	260	39.4	84.5	83.9	114.0	95.7	97.1	0.283	0.525	0.149	1.56	0.23
6	266	280	42.5	90.4	89.8	121.9	105.0	103.7	0.305	0.503	0.154	1.18	0.18
7	285	300	45.5	96.2	95.7	129.9	114.1	110.3	0.321	0.482	0.155	0.89	0.14

1. a top quark mass of ≈ 175 GeV/c^2;

2. light $\tilde{\chi}_1^\pm$ and $\tilde{\chi}_2^0$: $M_{\tilde{\chi}_1^\pm} \approx M_{\tilde{\chi}_2^0} \leq 90$ GeV/c^2;

3. light $\tilde{\ell}_R$: $M_{\tilde{\ell}_R} \approx 45\text{-}50$ GeV/c$^2 < M_{\tilde{\chi}_2^0} < M_{\tilde{\ell}_L}$;

4. $M_{\tilde{q}} \approx 0.98\,M_{\tilde{g}}$.

In this model, the trilepton signal is nearly maximized because the $\tilde{\chi}_2^0$ decays exclusively to dileptons with dominant two-body decay modes $\tilde{\chi}_2^0 \rightarrow \ell^\pm \tilde{\ell}_R^\mp$ ($BR = 66\%$ for e and μ) and $\tilde{\ell}_R \rightarrow \ell \tilde{\chi}_1^0$ ($BR = 100\%$). This results in a final state with three leptons and $\not{E}_T$ (Figures 2.18 and 2.20). Since we observe zero trilepton events, we set limits on this model using ISAJET[9] with parameters supplied by J. Lopez (as listed in Table 5.7) [48].

Figure 5.17 shows the acceptance for this model as a function of $\tilde{\chi}_1^\pm$ mass. The acceptance decreases for large $\tilde{\chi}_1^\pm$ masses as the $\tilde{\chi}_1^0$ mass approaches the $\tilde{\ell}_R$ mass (see Table 5.8) and carries away much of the energy, resulting in soft leptons. As shown in Figure 5.18, we exclude

$$M_{\tilde{\chi}_1^\pm} < 80.5 \text{ GeV/c}^2 \tag{5.2}$$

$$\sigma_{\tilde{\chi}_1^\pm \tilde{\chi}_2^0} \cdot BR(\tilde{\chi}_1^\pm \tilde{\chi}_2^0 \rightarrow 3\ell + X) > 0.4 \text{ pb}. \tag{5.3}$$

This is comparable to the ALEPH limit of 83 GeV/c^2 [47]. We do not entirely exclude the SU(5)×U(1) Supergravity model. However, our analysis excludes the model for small and moderate $\tilde{\chi}_1^\pm$ masses and leaves only a small window for $\tilde{\chi}_1^\pm$s heavier than 80.5 GeV/c^2.

---

[9]We use ISAJET 7.06 for this section of this analysis. It does not have explicit Supergravity input parameters. However, J. Lopez calculated the necessary input parameters for use with ISAJET 7.06.

Search for SUSY using p$\bar{\text{p}}$ → eee, eeμ, eμμ, μμμ

CDF Preliminary

Increasing $\tilde{\chi}_1^{\pm}\,\tilde{\chi}_2^0$ masses
increase lepton P_T

Small mass difference
between $\tilde{\chi}_1^0$ and $\tilde{l}_R$
gives soft leptons

SU(5) × U(1) Model

Lopez, et al, PRD 52, 4178 (1995)

Isajet 7.06 + CTEQ 31 LO

Detection Effeciency (%)

$M(\tilde{\chi}_1^{\pm})$ (GeV/c^2)
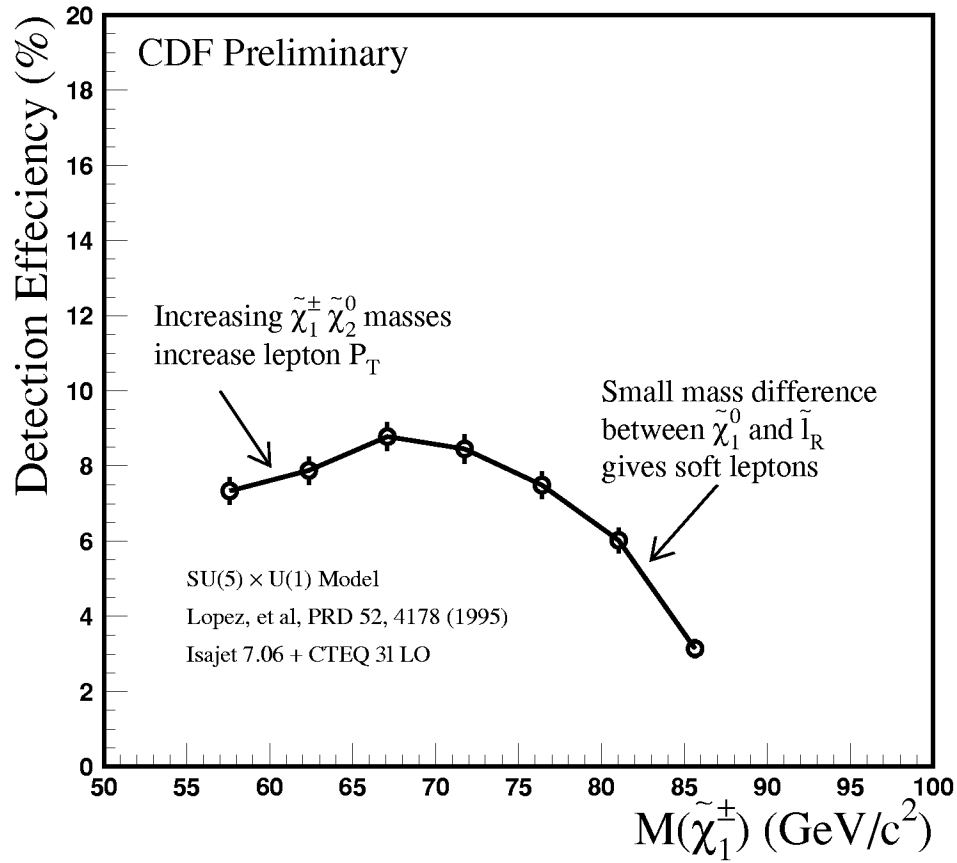
Figure 5.17: The acceptance for all four trilepton modes for SU(5) × U(1) model production of trileptons. The acceptance decreases for large $\tilde{\chi}_1^{\pm}$ masses as the $\tilde{\chi}_1^0$ mass approaches the $\tilde{\ell}_R$ mass and carries away much of the energy, resulting in soft leptons. The error bars indicate the statistical uncertainty.

Search for SUSY using $\mathrm{p\bar{p}} \to$ **eee, ee**μ**, e**$\mu\mu$**,** $\mu\mu\mu$
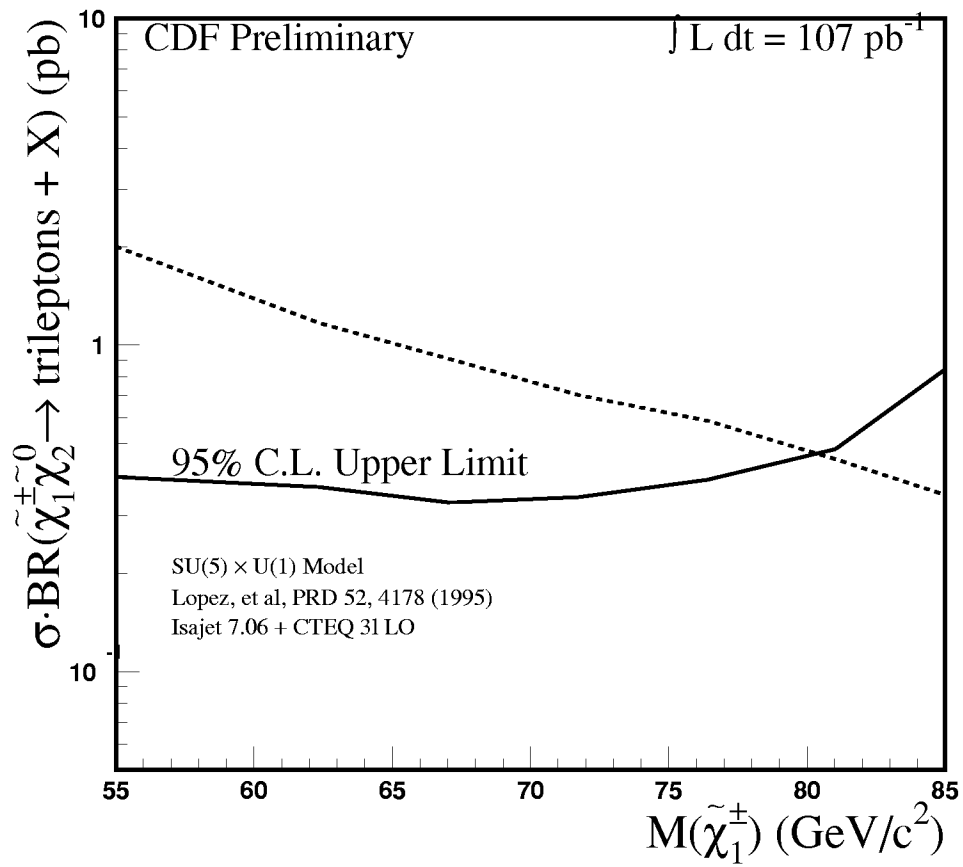
Figure 5.18: $\sigma \cdot BR$ versus $\tilde{\chi}_1^{\pm}$ mass for SU(5) $\times$ U(1) model production of trileptons. This sets a mass limit of 80.5 GeV/c^2 and a cross section times branching ratio limit of 0.4 pb.

Table 5.7: The input and output parameters used to examine the SU(5)×U(1) model. These values are courtesy of Jorge Lopez. Note that $\tan\beta = 1.4$ for the entire set and all masses are in GeV/c^2.

$M_{\tilde{g}}$	$M_{\tilde{q}}$	$M_{\tilde{\ell}_L}$	$M_{\tilde{\ell}_R}$	$M_{\tilde{\nu}_L}$	$M_{\tilde{t}_L}$	$M_{\tilde{t}_R}$	A_t	$M_{\tilde{b}_L}$	$M_{\tilde{b}_R}$	μ	M_{H_A}
310.2	302.9	107.1	44.4	85.2	197.0	394.6	-211.7	328.7	308.9	242.3	295.0
322.9	315.6	111.0	45.1	89.9	205.0	405.5	-220.4	342.0	321.4	252.2	306.6
335.7	328.3	114.8	45.8	94.6	213.1	416.5	-229.1	355.4	333.9	262.1	318.3
348.4	341.0	118.7	46.6	99.2	221.4	427.5	-237.8	368.7	346.5	271.9	329.8
361.2	353.6	122.7	47.3	103.8	229.7	438.5	-246.5	382.1	359.0	281.7	341.5
373.9	366.3	126.6	48.1	108.3	238.3	449.6	-255.2	395.5	371.5	291.3	352.8
386.6	378.9	130.5	48.8	112.9	246.8	460.7	-263.9	408.9	384.1	301.0	364.3

Table 5.8: Masses of the $\tilde{\chi}_1^{\pm}$, $\tilde{\chi}_2^0$, $\tilde{\chi}_1^0$ for the points examined in the SU(5)×U(1) model. For comparison, the difference in masses between the $\tilde{\chi}_1^{\pm}$ and the $\tilde{\ell}_R$ and the detection efficiency are shown. We have reasonable efficiency as long as the mass difference is ≥ 5 GeV/c^2. All masses are in GeV/c^2 and the efficiency is in %.

$M_{\tilde{g}}$	$M_{\tilde{\chi}_1^{\pm}}$	$M_{\tilde{\chi}_2^0}$	$M_{\tilde{\chi}_1^0}$	$M_{\tilde{\ell}_R}-M_{\tilde{\chi}_1^0}$	efficiency
310.2	57.5	67.0	29.1	15.2	7.3
322.9	62.3	70.8	32.1	12.9	7.9
335.7	67.0	74.7	35.0	10.7	8.8
348.4	71.7	78.6	37.8	8.7	8.5
361.2	76.4	82.6	40.6	6.7	7.5
373.9	81.0	86.7	43.2	4.8	6.0
386.6	85.6	90.8	45.8	3.0	3.1

5.4.2 SUGRA

The SiMSSM as we have examined it only unifies the electromagnetic, weak and strong forces. Supergravity (or SUGRA) [49] also unifies gravity with the other three forces [13, 14]. SUGRA has a nice feature in that gauge symmetry-breaking is induced at the weak scale as a requirement of the model. However, it is a more constrained model than the SiMSSM so limits set using SUGRA are not as general. It has four and one-half free parameters: m_0, the common scalar mass; $m_{1/2}$, the common gaugino mass; the *sign* of μ; $\tan\beta$; and A_t. As seen in Section 5.3, the trilepton analysis strongly depends on the squark to gluino mass ratio and μ. These parameters are not free in the context of SUGRA which makes it more difficult to understand a limit at a particular point in SUGRA space.

SUGRA is currently quite popular, so, despite its limitations, we have examined several

points in SUGRA space. Figure 5.19 shows the detection efficiency as a function of $M_{\tilde{\chi}_1^\pm}$. Since the squark to gluino mass ratio and μ are now set inside the model, it is impossible to plot limits as a function of them. Therefore, we plot many different theoretical $\sigma_{\tilde{\chi}_1^\pm \tilde{\chi}_2^0} \cdot \mathrm{BR}(\tilde{\chi}_1^\pm \tilde{\chi}_2^0 \to 3\ell + X)$ points on the same plot for comparison with a single 95% C.L. limit curve in Figure 5.20. As before, we use ISAJET 7.20 with the CTEQ3l parton distribution function. The values of μ tend to be rather low, and as seen in Figure 5.9 that degrades our limit setting ability. We set $\tan\beta = 2$, A = 0 and require $\mu < 0$. We exclude

$$M_{\tilde{\chi}_1^\pm} \quad < \quad 62\ \mathrm{GeV/c^2} \tag{5.4}$$
$$\sigma_{\tilde{\chi}_1^\pm \tilde{\chi}_2^0} \cdot BR(\tilde{\chi}_1^\pm \tilde{\chi}_2^0 \to 3\ell + X) \quad > \quad 0.5\ \mathrm{pb}. \tag{5.5}$$

Tables 5.9-5.13 list the input and output parameters used.

Sugra acceptance
File: data.dat   22-OCT-97 10:43
Plot Area Total/Fit   270.52 / 270.52   Fit Status 3
Func Area Total/Fit   552.25 / 552.25   E.D.M. 3.750E-22

$\chi^2 = $ 28.5 for 30 - 2 d.o.f.,   C.L.= 43.6%

Errors   Parabolic   Minos
Function 1: Polynomial of Order 1
NORM   -3.1468   ± 0.6381   - 0.0000E+00   + 0.0000E+00
POLY01   0.14805   ± 8.7479E-03   - 0.0000E+00   + 0.0000E+00
*OFFSET   0.00000E+00   ± 0.0000E+00   - 0.0000E+00   + 0.0000E+00
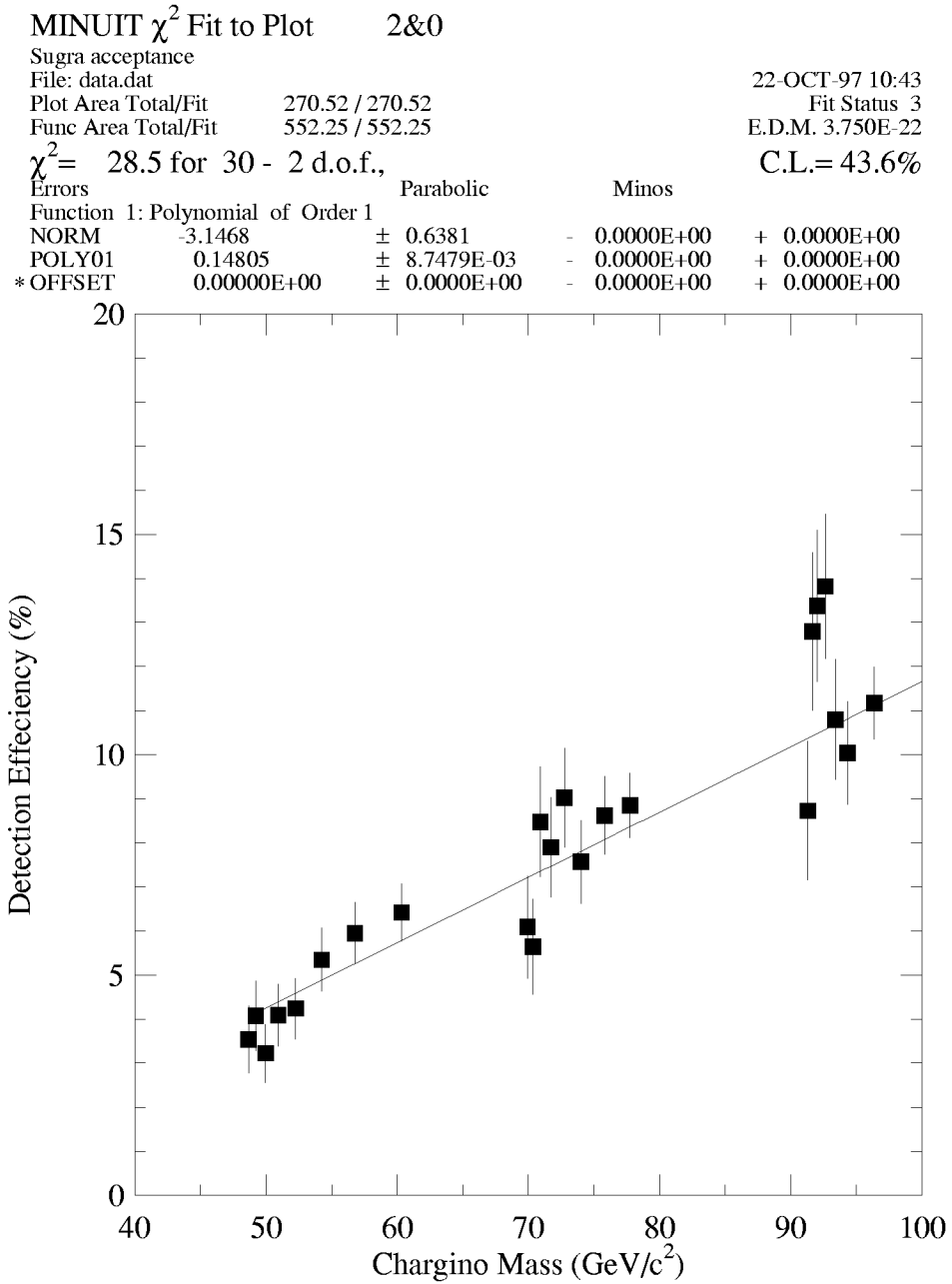
Figure 5.19: Detection efficiency as a function of $M_{\tilde{\chi}_1^\pm}$ in the framework of the SUGRA model.

122
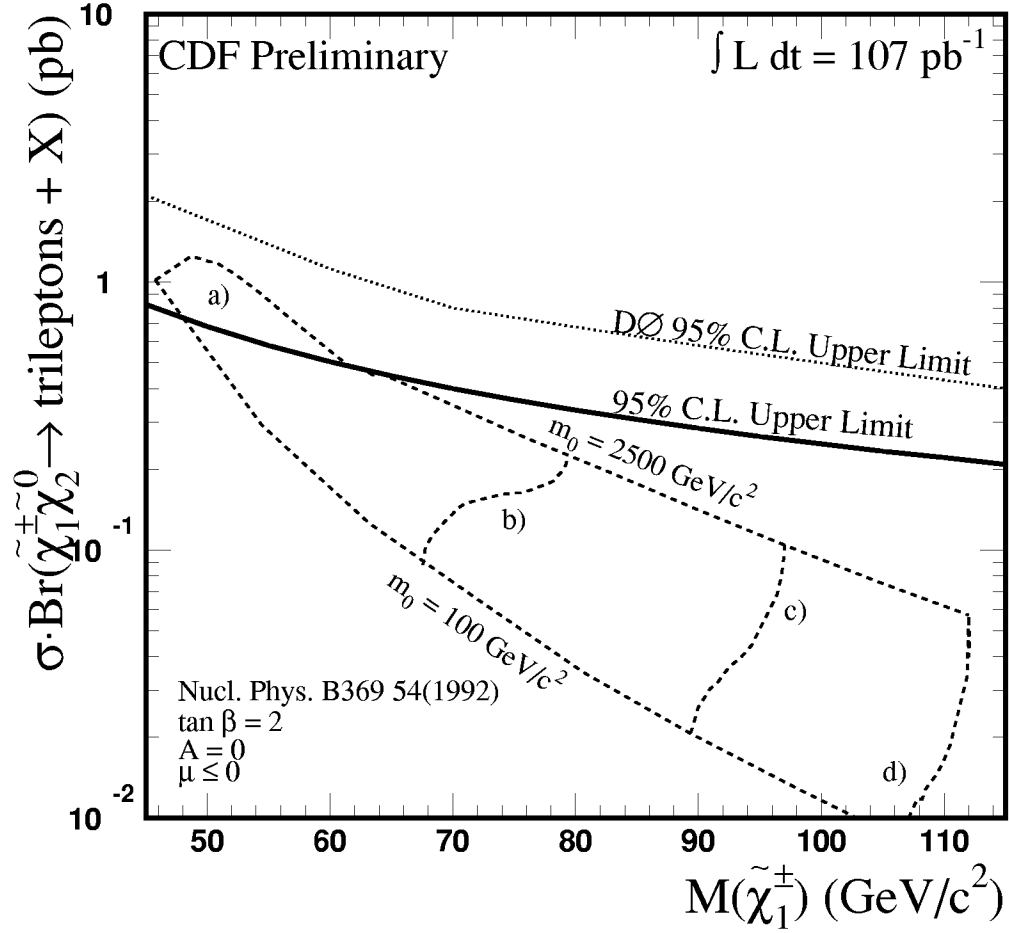
Figure 5.20: Production cross section times branching ratio to leptons for $\tilde{\chi}_1^\pm \tilde{\chi}_2^0$ production as a function of $\tilde{\chi}_1^\pm$ mass within the SUGRA framework (dashed lines). The solid line is the 95% C.L. limit curve; all points above it are excluded. We set $\tan\beta = 2$, A = 0 and require $\mu \leq 0$. For lines a)-d) we set 100 GeV/c^2 $\leq$ m$_0$ $\leq$ 2500 GeV/c^2 and (a) m$_{1/2}$ = 50 GeV/c^2, (b) m$_{1/2}$ = 75 GeV/c^2, (c) m$_{1/2}$ = 100 GeV/c^2 and (d) m$_{1/2}$ = 120 GeV/c^2 . For the lines m$_0$ = 100 GeV/c^2 and 2500 GeV/c^2 we set 50 $\leq$ m$_{1/2}$ $\leq$ 120 GeV/c^2. For comparison we show the D0 95% C.L. limit curve (dotted line).

Table 5.9: Input and output parameters for the SUGRA points scanned. All masses are in GeV/c^2. m_0 and $m_{1/2}$ are input parameters and μ is an output parameter.

Set	m_0	$m_{1/2}$	μ	Set	m_0	$m_{1/2}$	μ
1	200	50	-186.069	b1	100	75	-163.662
2	300	50	-266.678	b2	120	75	-172.144
3	400	50	-350.862	b3	140	75	-183.200
4	500	50	-444.768	b4	160	75	-194.698
5	600	50	-536.425	b5	180	75	-205.839
6	700	50	-623.811	b6	1000	75	-893.558
7	800	50	-714.489	b7	1500	75	-1345.179
8	900	50	-805.791	b8	2000	75	-1813.768
9	200	75	-219.498	b9	2500	75	-2240.462
10	300	75	-291.085	c1	100	100	-207.422
11	400	75	-371.920	c2	120	100	-214.530
12	500	75	-456.418	c3	140	100	-222.741
13	600	75	-542.042	c4	160	100	-231.186
14	700	75	-630.116	c5	180	100	-241.346
15	800	75	-716.663	c6	1000	100	-880.959
16	900	75	-803.768	c7	1500	100	-1315.166
17	200	100	-252.082	c8	2000	100	-1750.734
19	400	100	-386.463	c9	2500	100	-2216.317
20	500	100	-464.421	d1	100	120	-241.032
21	600	100	-545.403	d2	120	120	-246.732
22	700	100	-627.902	d3	140	120	-253.473
23	800	100	-709.089	d4	160	120	-261.335
24	900	100	-794.251	d5	180	120	-269.867
25	200	120	-279.473	d6	1000	120	-886.271
26	300	120	-335.698	d7	1500	120	-1313.595
27	400	120	-404.963	d8	2000	120	-1760.341
28	500	120	-476.957	d9	2500	120	-2198.631
29	600	120	-552.079	e1	2500	40	-2273.547
30	700	120	-633.072	e2	2500	50	-2274.281
31	800	120	-714.718	e3	2500	60	-2271.083
32	900	120	-794.095	e4	2500	70	-2244.072
a1	180	50	-170.656	e5	2500	80	-2259.290
a2	160	50	-156.111	e6	2500	90	-2209.621
a3	140	50	-144.023	e7	2500	100	-2216.317
a4	120	50	-129.635	e8	2500	110	-2213.630
a5	100	50	-117.714	e9	2500	120	-2198.631

Table 5.10: Input and output parameters for the SUGRA points scanned. All masses are in GeV/c^2. m_0 and $m_{1/2}$ are input parameters and μ is an output parameter.

Set	m_0	$m_{1/2}$	μ	Set	m_0	$m_{1/2}$	μ
f1	100	40	-99.201	f6	100	90	-189.670
f2	100	50	-117.714	f7	100	100	-207.422
f3	100	60	-135.514	f8	100	110	-224.225
f4	100	70	-153.708	f9	100	120	-241.032
f5	100	80	-172.995				

Table 5.11: Output parameters for the SUGRA points scanned. All σ are in picobarns.

Set	$\tilde{q}$	$\tilde{g}$	$\tilde{\chi}_1^0$	$\tilde{\chi}_2^0$	$\tilde{\chi}_1^\pm$	$\tilde{\ell}_L$	$\tilde{\nu}$	$\tilde{\ell}_R$	BR→$\ell\ell$ $\tilde{\chi}_2^0$	BR→$\ell\nu$ $\tilde{\chi}_1^\pm$	BR→3ℓ Total	σ	σ·BR
					(GeV/c^2)								
1	237.3	168.0	23.5	62.3	60.3	206.5	197.0	203.8	0.33	0.22	0.07	7.55	0.54
2	324.3	173.1	23.2	58.5	56.8	304.4	298.0	302.5	0.26	0.22	0.06	12.85	0.73
3	417.8	177.1	23.0	55.5	54.2	403.3	398.5	401.9	0.22	0.22	0.05	18.87	0.92
4	513.6	179.2	22.8	53.2	52.3	502.6	498.8	501.5	0.19	0.22	0.04	24.78	1.07
5	611.0	181.3	22.7	51.7	50.9	602.2	599.0	601.3	0.17	0.22	0.04	30.26	1.17
6	709.2	183.5	22.6	50.6	50.0	701.8	699.1	701.1	0.16	0.22	0.03	34.66	1.20
7	807.9	185.5	22.5	49.7	49.2	801.6	799.2	801.0	0.14	0.22	0.03	38.88	1.23
8	906.9	188.0	22.4	49.0	48.6	901.4	899.3	900.8	0.13	0.22	0.03	42.84	1.24
9	275.0	236.5	34.1	78.9	77.8	210.4	201.1	204.9	0.34	0.22	0.07	2.37	0.18
10	351.0	240.6	33.9	76.8	75.8	307.0	300.7	303.3	0.23	0.22	0.05	3.24	0.16
11	438.6	246.8	33.6	74.8	74.0	405.2	400.5	402.5	0.18	0.22	0.04	4.09	0.16
12	530.2	252.0	33.4	73.3	72.7	504.2	500.4	502.0	0.15	0.22	0.03	4.77	0.16
13	624.8	255.9	33.2	72.2	71.7	603.5	600.3	601.7	0.13	0.22	0.03	5.36	0.15
14	720.7	258.9	33.1	71.3	70.9	703.0	700.2	701.4	0.11	0.22	0.03	5.84	0.15
15	817.9	262.0	33.0	70.7	70.3	802.6	800.2	801.2	0.10	0.22	0.02	6.19	0.14
16	915.3	261.6	33.0	70.2	69.9	902.3	900.2	901.1	0.10	0.22	0.02	6.39	0.14
17	316.7	298.4	44.5	97.0	96.4	215.7	206.6	206.5	0.33	0.22	0.07	0.92	0.07
19	465.9	314.2	44.0	94.8	94.3	408.0	403.2	403.3	0.15	0.22	0.03	1.34	0.04
20	552.4	319.1	43.9	93.8	93.4	506.4	502.6	502.6	0.12	0.22	0.03	1.52	0.04
21	642.9	323.4	43.7	93.0	92.6	605.3	602.1	602.2	0.10	0.22	0.02	1.67	0.04
22	736.4	327.7	43.6	92.3	92.0	704.5	701.8	701.9	0.09	0.22	0.02	1.78	0.03
23	830.8	327.5	43.7	91.9	91.7	803.9	801.5	801.6	0.08	0.22	0.02	1.85	0.03
24	926.8	330.7	43.6	91.5	91.3	903.5	901.4	901.5	0.07	0.22	0.02	1.93	0.03
25	352.2	346.8	52.8	112.3	111.9	220.9	212.0	208.1	0.33	0.23	0.07	0.46	0.03
27	489.8	361.8	52.4	110.8	110.5	410.7	406.0	404.1	0.14	0.22	0.03	0.63	0.02
28	571.3	364.3	52.4	110.2	109.9	508.5	504.7	503.3	0.10	0.22	0.02	0.71	0.02
29	659.9	374.0	52.2	109.6	109.3	607.1	603.9	602.7	0.08	0.22	0.02	0.77	0.01
30	750.6	378.6	52.1	109.0	108.8	706.1	703.3	702.3	0.07	0.22	0.02	0.83	0.01
31	844.0	379.4	52.0	108.7	108.5	805.3	802.9	802.1	0.07	0.22	0.01	0.86	0.01
32	938.1	382.9	52.1	108.4	108.2	904.7	902.6	901.8	0.06	0.22	0.01	0.88	0.01
a1	220.8	166.8	23.5	63.1	61.2	187.2	176.7	184.2	0.35	0.22	0.08	6.64	0.50
a2	205.6	165.5	23.6	63.8	62.0	168.1	156.3	164.7	0.37	0.22	0.08	5.89	0.48
a3	191.5	164.5	23.6	64.1	62.6	149.2	135.7	145.4	0.41	0.22	0.09	5.30	0.48
a4	178.0	163.3	23.6	64.3	63.4	130.6	115.0	126.2	0.44	0.22	0.10	4.55	0.45
a5	166.0	161.8	23.7	64.1	64.1	112.6	94.0	107.4	0.48	0.23	0.11	4.07	0.46

Table 5.12: Output parameters for the SUGRA points scanned. All σ are in picobarns.

Set	$\tilde{q}$	$\tilde{g}$	$\tilde{\chi}_1^0$	$\tilde{\chi}_2^0$	$\tilde{\chi}_1^\pm$	$\tilde{\ell}_L$	$\tilde{\nu}$	$\tilde{\ell}_R$	BR→$\ell\ell$ $\tilde{\chi}_2^0$	BR→$\ell\nu$ $\tilde{\chi}_1^\pm$	BR→3ℓ Total	σ	σ·BR
					(GeV/c^2)								
b1	218	230	34.3	79.9	79.4	119.7	102.4	109.6	0.46	0.29	0.13	1.68	0.22
b2	226	229	34.3	79.9	79.2	136.8	122.0	128.1	0.46	0.25	0.12	1.78	0.21
b3	237	232	34.2	79.8	78.9	154.6	141.7	147.0	0.44	0.24	0.10	1.91	0.20
b4	248	233	34.2	79.5	78.5	172.9	161.4	166.1	0.40	0.23	0.09	2.06	0.19
b5	261	233	34.2	79.2	78.2	191.5	181.2	185.5	0.37	0.22	0.08	2.21	0.18
b6	1013	264	33.0	69.8	69.5	1002.1	1000.1	1001.0	0.09	0.22	0.02	6.63	0.13
b7	1508	272	32.8	68.5	68.4	1501.4	1500.1	1500.7	0.07	0.22	0.02	7.39	0.11
b8	2006	275	32.7	67.8	67.8	2001.0	2000.0	2000.5	0.06	0.22	0.01	7.73	0.10
b9	2504	284	32.7	67.6	67.6	2500.8	2500.0	2500.4	0.05	0.22	0.01	7.86	0.09
c1	269	291	44.7	97.4	97.0	128.9	113.0	112.6	0.40	0.36	0.14	0.74	0.10
c2	276	293	44.6	97.4	97.0	144.9	131.0	130.6	0.42	0.29	0.12	0.77	0.09
c3	285	294	44.6	97.4	96.8	161.8	149.4	149.2	0.41	0.26	0.11	0.80	0.08
c4	294	295	44.6	97.3	96.7	179.3	168.3	168.1	0.39	0.24	0.09	0.84	0.08
c5	305	297	44.6	97.2	96.6	197.3	187.4	187.2	0.36	0.23	0.08	0.88	0.07
c6	1023	334	43.6	91.1	90.9	1003.1	1001.2	1001.3	0.07	0.22	0.02	2.01	0.03
c7	1514	344	43.4	90.1	90.0	1502.1	1500.8	1500.9	0.05	0.22	0.01	2.17	0.03
c8	2010	353	43.4	89.7	89.6	2001.5	2000.6	2000.7	0.05	0.22	0.01	2.24	0.02
c9	2508	355	43.5	89.4	89.4	2501.2	2500.4	2500.5	0.04	0.22	0.01	2.25	0.02
d1	310	340	52.9	112.3	112.0	137.4	122.6	115.5	0.36	0.41	0.15	0.39	0.06
d2	316	342	52.9	112.4	112.1	152.5	139.4	133.2	0.39	0.32	0.12	0.40	0.05
d3	324	343	52.9	112.4	112.1	168.6	156.8	151.4	0.39	0.27	0.11	0.41	0.04
d4	332	344	52.9	112.4	112.0	185.5	174.9	170.1	0.38	0.25	0.09	0.43	0.04
d5	342	345	52.9	112.3	112.0	203.0	193.3	189.0	0.35	0.23	0.08	0.44	0.04
d6	1033	384	52.0	108.0	107.8	1004.2	1002.3	1001.6	0.06	0.22	0.01	0.92	0.01
d7	1521	395	52.0	107.2	107.1	1502.8	1501.5	1501.1	0.05	0.22	0.01	0.99	0.01
d8	2015	406	52.1	106.9	106.8	2002.1	2001.1	2000.8	0.04	0.22	0.01	1.03	0.01
e1	2501	168	17.7	37.1	37.1	2500.4	2499.7	2500.3	0.07	0.22	0.02	3482	55.0
e2	2502	201	22.0	45.8	45.8	2500.5	2499.7	2500.3	0.06	0.22	0.01	72.02	1.02
e3	2502	234	26.3	54.5	54.5	2500.6	2499.8	2500.3	0.06	0.22	0.01	22.62	0.29
e4	2504	267	30.6	63.2	63.2	2500.7	2500.0	2500.4	0.05	0.22	0.01	10.81	0.13
e5	2505	295	34.9	71.9	71.9	2500.9	2500.1	2500.4	0.05	0.22	0.01	5.99	0.07
e6	2506	329	39.1	80.7	80.6	2501.0	2500.3	2500.5	0.04	0.22	0.01	3.58	0.03
e7	2508	355	43.5	89.4	89.4	2501.2	2500.4	2500.5	0.04	0.22	0.01	2.25	0.02
e8	2509	383	47.8	98.2	98.1	2501.4	2500.6	2500.6	0.04	0.22	0.01	1.50	0.01
e9	2511	411	52.1	106.7	106.7	2501.6	2500.9	2500.7	0.04	0.22	0.01	1.05	0.01

Table 5.13: Output parameters for the SUGRA points scanned. All σ are in picobarns.

Set	$\tilde{q}$	$\tilde{g}$	$\tilde{\chi}_1^0$	$\tilde{\chi}_2^0$	$\tilde{\chi}_1^\pm$	$\tilde{\ell}_L$	$\tilde{\nu}$	$\tilde{\ell}_R$	BR$\to\ell\ell$ $\tilde{\chi}_2^0$	BR$\to\ell\nu$ $\tilde{\chi}_1^\pm$	BR$\to3\ell$ Total	σ	$\sigma\cdot$BR
					(GeV/c^2)								
f1	147.6	136.6	19.2	57.9	58.9	110.5	91.5	106.8	0.45	0.21	0.09	5.94	0.56
f2	166.0	161.8	23.7	64.1	64.1	112.6	94.0	107.4	0.48	0.23	0.11	4.07	0.46
f3	186.5	189.2	28.0	70.3	69.9	115.1	97.1	108.2	0.49	0.25	0.12	2.82	0.35
f4	207.0	215.0	32.3	76.7	76.2	118.1	100.5	109.1	0.47	0.28	0.13	1.99	0.26
f5	228.8	243.2	36.4	83.3	82.8	121.4	104.4	110.1	0.45	0.30	0.14	1.44	0.20
f6	249.2	268.1	40.5	90.2	89.8	125.0	108.6	111.3	0.42	0.33	0.14	1.03	0.14
f7	269.4	291.9	44.7	97.4	97.0	128.9	113.0	112.6	0.40	0.36	0.14	0.74	0.10
f8	290.6	318.0	48.8	104.8	104.5	133.0	117.7	114.0	0.37	0.38	0.14	0.54	0.08
f9	310.8	340.8	52.9	112.3	112.0	137.4	122.6	115.5	0.36	0.41	0.15	0.39	0.06

Chapter 6

Conclusion

We have searched for evidence of Supersymmetry using the CDF detector and the Fermilab Tevatron. After searching 107 pb^{-1} for three lepton events, we find no evidence for $\tilde{\chi}_1^{\pm}\tilde{\chi}_2^0$ production.

We set limits on $M_{\tilde{\chi}_1^{\pm}}$ and $\sigma_{\tilde{\chi}_1^{\pm}\tilde{\chi}_2^0}\cdot\mathrm{BR}(\tilde{\chi}_1^{\pm}\tilde{\chi}_2^0 \to 3\ell + X)$ in several models. Table 6.1 lists the limits for a general MSSM, Table 6.2 lists the limit for the SU(5)$\times$U(1) supergravity model, and Table 6.3 lists the limits for a general SUGRA model.

In Section 2.5 I introduced the concept of naturalness. In Figure 2.21 we see the naturalness of the $\tilde{\chi}_1^{\pm}$. The limit set by this analysis is well away from the minimum in that plot and begins to approach non-natural (or unlikely) values. Also, if the model assumptions we make are correct, we see that the naturalness of the squark, gluino and slepton masses are starting to move away from their most natural values (see Figure 6.1). We are beginning to challenge SUSY.

It is appropriate to wonder what reach the Tevatron will have during Run II. At high gluino mass the best search mode is $\tilde{\chi}_1^{\pm}\tilde{\chi}_2^0$ or $\tilde{\chi}_1^{\pm}\tilde{\chi}_1^{\pm}$: the production cross section for gluinos and squarks becomes quite small (as seen in Figure 6.2), while the $\tilde{\chi}_1^{\pm}$ and $\tilde{\chi}_2^0$ masses tend to be $\sim 1/3$ the gluino masses. Table 6.4 lists the upper reach for CDF during Run II, for either 1 or 2 fb^{-1}.

Either Supersymmetry will be discovered during Run II at the Tevatron or its viability as a physically acceptable theory will be greatly compromised.
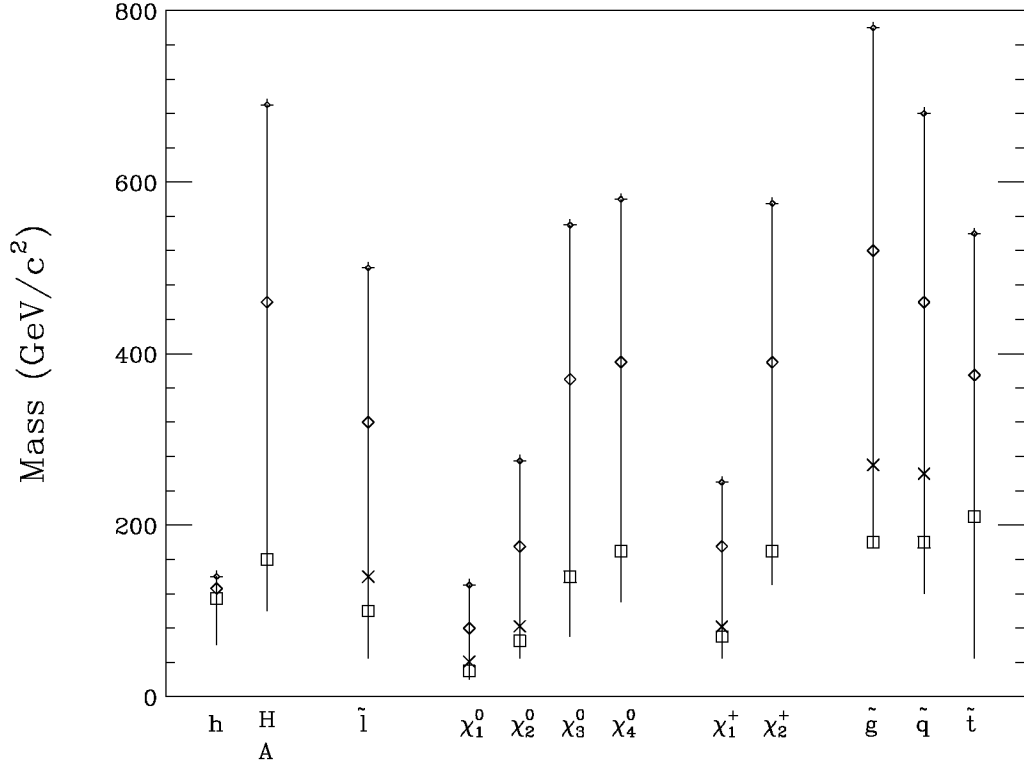
Figure 6.1: The naturalness for a variety of different sparticles. The bottom of each line is the world limit prior to this analysis, the box ($\square$) represents a naturalness of 1, the diamond ($\diamond$) a naturalness of 5 and the top of the line ($+$) a naturalness of 10. The limits from this analysis (primarily for $\widetilde{\chi}_1^\pm$ and $\widetilde{\chi}_2^0$, but also for $\widetilde{\ell}$, $\widetilde{g}$ and $\widetilde{q}$) are represented by the cross ($\times$). We have excluded the most natural values. Adapted from Ref. [25].

Table 6.1: Limits on chargino and neutralino masses within the framework of the SUGRA-inspired MSSM. All masses are in GeV/c^2.

Input Parameters				Limits			
$M_{\tilde{g}}$	$M_{\tilde{q}}$	$\tan\beta$	μ	$M_{\tilde{\chi}_1^{\pm}}$	$M_{\tilde{\chi}_2^0}$	$M_{\tilde{\chi}_1^0}$	$\sigma\cdot\text{BR (pb)}$
220	330	2	-400	68.0	69.0	29.2	0.45
220	264	2	-400	71.0	72.1	32.0	0.40
200	200	2	-200	72.5	73.4	30.7	0.40
240	240	2	-400	76.5	77.1	36.1	0.37
260	260	2	-600	81.5	82.2	38.1	0.34
270	270	2	-800	81.0	81.0	39.3	0.35
260	260	2	-1000	78.5	78.4	37.5	0.36
200	500	2	-400	58.0	59.0	26.4	0.60

Table 6.2: Limits on chargino and neutralino masses within the framework of the SU(5)×U(1) model. All masses are in GeV/c^2. Recall for this model $\tan\beta = 1.4$.

Input Parameters			Limits			
$M_{\tilde{g}}$	$M_{\tilde{q}}$	μ	$M_{\tilde{\chi}_1^{\pm}}$	$M_{\tilde{\chi}_2^0}$	$M_{\tilde{\chi}_1^0}$	$\sigma\cdot\text{BR (pb)}$
373.9	366.3	291.3	81.0	86.7	43.2	0.4

Table 6.3: Limits on chargino and neutralino masses within the framework of SUGRA. All masses are in GeV/c^2. Recall we used $\tan\beta = 2$ and $A = 0$.

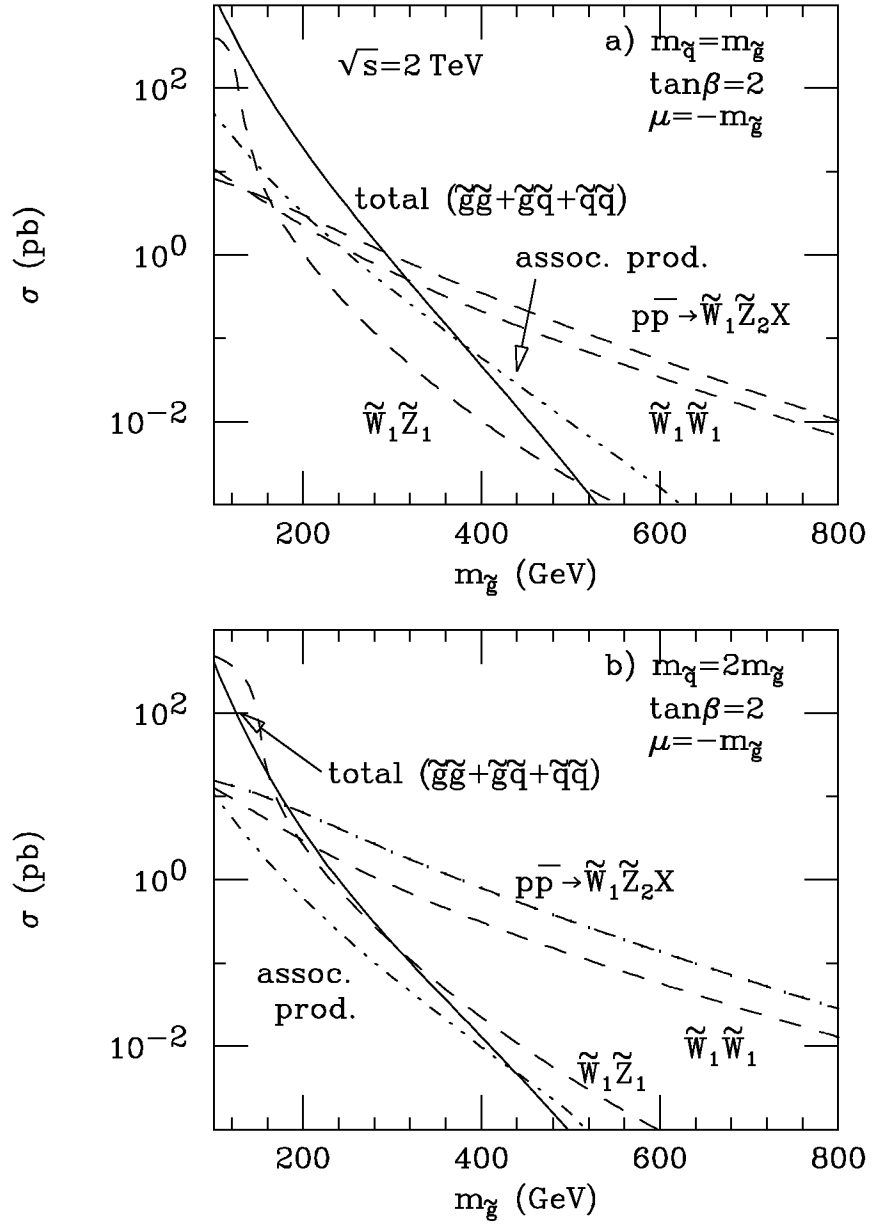| Input parameters		Limits						
m_0	$m_{1/2}$	$M_{\tilde{g}}$	$M_{\tilde{q}}$	μ	$M_{\tilde{\chi}_1^{\pm}}$	$M_{\tilde{\chi}_2^0}$	$M_{\tilde{\chi}_1^0}$	$\sigma\cdot\text{BR (pb)}$
200	50	237.3	168.0	-186.1	62.3	60.3	23.5	0.5

Figure 6.2: Production cross section for a variety of processes at the upgraded Tevatron. Clearly, the best search modes are $\tilde{\chi}_1^{\pm}\tilde{\chi}_2^0$ or $\tilde{\chi}_1^{\pm}\tilde{\chi}_1^{\pm}$. Adapted from Ref. [9].

Table 6.4: Lower limits for several searches using Run II at the Tevatron. For the various gluino and squark searches, OS means searching for opposite sign dilepton + jets, SS is same sign dilepton + jets, 3ℓ is trilepton + jets, and $\not{\!\!E}_T$ is $\not{\!\!E}_T$ + jets. Adapted from Refs. [9] and [50].

Particle	Search Method	Limit (GeV/c^2) 1 fb^{-1}	2 fb^{-1}
$\tilde{\chi}_1^{\pm}\tilde{\chi}_2^0$	$3\ell + \not{\!\!E}_T$	150	210
$\tilde{g}$ and $\tilde{q}$: $m_{\tilde{q}} = m_{\tilde{g}} + 10$ GeV	$\not{\!\!E}_T$	260	
	OS	290	
	SS	320	
	$3\,\ell$	425	
$m_{\tilde{q}} = m_{\tilde{g}} - 10$ GeV	$\not{\!\!E}_T$	265	
	OS	235	
	SS	325	
	$3\,\ell$	440	
$m_{\tilde{q}} = 2m_{\tilde{g}}$	$\not{\!\!E}_T$	200	
	OS	180	
	SS	210	
	$3\,\ell$	260	
$\tilde{t}$	all	125	150
$\tilde{\ell}$	all	100 (for 25 fb^{-1})	

Bibliography

[1] *Webster's New World Dictionary*, 2nd College Edition, 1984.

[2] K. G. Wilson, Phys.Rev.**D10**:2445-2459 (1974); G. Altarelli and G. Parisi, Nucl.Phys. **B126**:298 (1977).

[3] S. L. Glashow, Nucl. Phys. **22**, 579-588, 1961; S. Weinberg, Phys. Rev. Lett. **19**, 1264-66, 1967; A. Salam, in *Elementary Particle Theory*, N. Svartholm, ed. (Stockholm: Almquist and Wiksell, 1968).

[4] F. Abe, *et al.* (The CDF Collaboration), March 1995, Phys. Rev. Lett. **74**:2626-2631,1995.

[5] Particle Data Group, *Review of Particle Physics*, Phys. Rev. **D54**, 1 July 1996.

[6] M. Drees and S. Martin, *Implications of SUSY Model Building*, Report of the DPF Working Group on "Electroweak Symmetry Breaking and Beyond the Standard Model",March 1995, hep-ph/9504324.

[7] See http://www-spires.slac.stanford.edu/find/hep.

[8] M. Drees, *An Introduction to Supersymmetry*, Lectures given at Inauguration Conference of the Asia Pacific Center for Theoretical Physics (APCTP), Seoul, Korea, 4-19 Jun 1996, hep-ph/9611409.

[9] H. Baer, *et. al.*, *Low Energy Supersymmetry Phenomenology*, Report of the DPF Working Group on "Electroweak Symmetry Breaking and Beyond the Standard Model", March 1995, hep-ph/9503479.

[10] J. Lopez, Rept. Prog. Phys. **59**:819-865,1996.

[11] A.H. Chamseddine, R. Arnowitt, and P. Nath, Phys. Rev. Lett. **49**, 970 (1982); R. Barbieri, S. Ferrora, and C.A. Savoy, Phys. Lett. **B119**, 343 (1982); L. Hall, J. Lykken, and S. Weinberg, Phys. Rev. **D27**, 2359 (1983). For a recent review, see R. Arnowitt and P. Nath, "Supersymmetry and Supergravity: Phenomenology and Grand Unification," Proceedings of VIIth J.A. Swieca Summer School, Campos de Jordao, Brazil, 1993 (World Scientific, Singapore, 1994).

[12] R. Phillips and V. Barger, *Collider Physics*, Addison-Wesley (1987).

[13] L.E. Ibañez, C. Lopez, and C. Muoñz, Nucl. Phys. **B256**, 218 (1985); G.G. Ross and R.G. Roberts, Nucl. Phys. **B377**, 571 (1992); R. Arnowitt and P. Nath, Phys. Rev. Lett. **69**, 725 (1992); S. Kelley, J.L. Lopez, D.V. Nanopoulos, H. Pois, and K. Yuan, Nucl. Phys. **B398**, 31 (1993); G.L. Kane, C. Kolda, L. Roszkowski, and J.D. Wells, Phys. Rev. **D49**, 6173 (1994). In this analysis we use formulae in H.Baer *et al.*, Phys. Rev. **D47**, 2739 (1993).

[14] M.Drees and M.Nojiri, Nucl. Phys. **B369**, 54 (1992).

[15] See the references in G.L. Kane, HEPPH-9709318. Invited talk at 5th International Conference on Supersymmetries in Physics (SUSY 97), Philadelphia, PA, 27-31 May 1997.

[16] For example T.S. Kosmas and J.D. Vergados, Phys. Rev. **D55**:1752-1764 (1997).

[17] G. Anderson, private communication.

[18] J. Kubo, M. Mondragon and G. Zoupanos, Nucl.Phys. **B424**:291-307 (1994).

[19] D. Griffiths, *Introduction to Elementary Particles.* John Wiley & Sons, Inc, 1987.

[20] F. Halzen and A. Martin, *Quarks & Leptons: An Introductory Course in Modern Particle Physics*, John Wiley & Sons, Inc., 1984.

[21] F. Abe, *et al.* (The CDF Collaboration), Phys. Rev. Lett. **76**:2006-2010, (1996).

[22] F. Abe, *et al.* (The CDF Collaboration), Phys. Rev. Lett. **75** 1017, 1995. F. Abe, *et al.* (The CDF Collaboration), in preparation.

[23] F. Abe, *et al.*, Phys. Rev. Lett. **76**, 4307 (1996).

[24] G. Anderson and D. Castaño, Phys. Letters **B347**, 300 (1995).

[25] G. Anderson and D. Castaño, Phys. Rev. **D52**, 1693 (1995).

[26] J. Huston, FERMILAB-TM-1909 (1994).

[27] For a description of the original CDF detector, see F. Abe, *et al.*, (The CDF Collaboration), Nucl. Instrum. Methods **A271**, 387 (1988) and the references within.

[28] For a description of the CDF upgrades, see F. Abe, *et al.*, (The CDF Collaboration), Phys. Rev. **D50**, 2966 (1994); D. Amidei, *et al.*, Nucl. Instrum. Methods **A350**, 73 (1994) and the references within.

[29] A. Beretvas, *et. al*, CDF Note 3599 (1995).

[30] F. Abe, *et al.*, (The CDF Collaboration), Phys.Rev. **D50**:2966, 1994.

[31] S. Kuhlmann, *et al.*, CDF Note 413 (1986); CDF Note 282.

[32] J.P. Done *et al.*, CDF Note 4218 (1997).

[33] F. Abe, *et. al*, (The CDF Collaboration), Phys. Rev. **D 52** 2624 (1994).

[34] S. Kopp and C. Grosso-Pilcher, CDF Note 1992 (1993).

[35] M. Krasberg and T. LeCompte, CDF Note 2032 (1993).

[36] H. Baer, F.E. Paige, S.D. Protopopescu, and X. Tata, "Simulating Supersymmetry with ISAJET 7.0/ISASUSY 1.0," Proceedings of Workshop on Physics at Current Accelerators and the Supercollider, eds. J. Hewett, A. White and D. Zeppenfeld (Argonne National Laboratory, 1993).

[37] S. Tether, CDF Note 3566 (1996).

[38] The trigger efficiencies come from a variety of CDF Notes: CDF-2391, CDF-2391, CDF-2367, CDF-2186, CDF-3622, CDF-2435, XCES efficiency from CDF-2795, CDF-3060, CDF-2367, CDF-4017, CDF-2954, CDF-4076, CDF-3622, CDF-2596, CDF-2596, CDF-2367, CDF-2367, CDF-3532, CDF-3532, CDF-2191 and CDF-3028.

[39] B. Tannenbaum, CDF Note 2962 (1995).

[40] Andy Beretvas, private communication.

[41] J.P. Done *et al.*, CDF Note 4182 (1997).

[42] K. Byrum and A.B. Wicklund, CDF Note 3665 (1996). The Level 2 trigger efficiency for CEM_9_SEED_9_SH_7_CFT_9_2_V2 in Run 1A is $\epsilon_{L2} = (92.4 \pm 1.7\ ^{+3.0}_{-4.7})\%$. We shift the Run 1A trigger efficiency curve by 1 GeV and fold with XCES efficiencies (100% at plateau) from CDF Note 2795; As for the Level 1 trigger efficiency, we take the Run 1A result ($\epsilon_{L1} = (99.2 \pm 0.1)\%$) from CDF Note 2391 and shift the curve by 1 GeV for Run IB; As for the Level 3 trigger efficiency for Run IB, we take the Run 1A result ($\epsilon_{L3} = (95.2 \pm 1.5)\%$) from CDF Note 2596; The total efficiency of L1*L2*L3 is $(87.3^{+3.5}_{-4.9}(\text{stat.+syst.}))\%$.

[43] J.P. Done *et al.*, CDF 4017 (1997). The Level 2 trigger efficiency in Run IB is $\epsilon_{L2} = (95.1\pm1.2\pm 0.8)\%$; As for the Level 1 trigger efficiency, we have the Run IB result ($\epsilon_{L1} = (93.1\pm1.1\pm1.0)\%$) from CDF Note 3028; As for the Level 3 trigger efficiency, we take the Run 1A results ($\epsilon_{L3} = (98.4 \pm 0.4 \pm 2.0)\%$) from CDF Note 2596 for Run IB; The total efficiency of L1*L2*L3 is $(87.1\pm2.9(\text{stat.+syst.}))\%$.

[44] B. Tannenbaum and T. Kamon, CDF Note 3538 (1996).

[45] Y. Kato, D.Sc. Dissertation, (1996).

[46] B. Abbott, *et al.*, hep-ex/9705015 (1997).

[47] Glen Cowen, CERN Particle Physics Seminar, 25 February 1997, http://alephwww.cern.ch/-ALPUB/seminar/cowen-172-jam/cowan.html.

[48] J. Lopez, D. Nanopoulos, A. Zichichi, Phys. Rev. **D52**, 4178 (1995) and **D53** 5253 (1996).

[49] H. Baer, *et al* Phys. Rev. D51,1046 (1995) and references within.

[50] R. Blair, *et al* (The CDF II Collaboration), *The CDF II Detector Technical Design Report*, FERMILAB-Pub-96/390-E (1996).

[51] R. Barbieri and G. F. Giudice, Nucl. Phys, **B306**, 63 (1988); J. Ellis, K. Enqvist, D.V. Nanopoulos, and F. Zwirner, Mod. Phys. Lett. **A1**, 57 (1986).

[52] F. Abe, *et. al*, (The CDF Collaboration), Phys. Rev. **D 52** 4784 (1995).